Orbital Evolution of Interplanetary Dust

Stanley F. Dermott[1], Keith Grogan[2], Daniel D. Durda[3], Sumita Jayaraman[4], Thomas J. J. Kehoe[1], Stephen J. Kortenkamp[5,6], Mark C. Wyatt[7]

[1] University of Florida, Gainesville, Florida, USA
[2] NASA Goddard Space Flight Center, Greenbelt, Maryland, USA
[3] Southwest Research Institute, San Antonio, Texas, USA
[4] Vanguard Research Inc., Scotts Valley, California, USA
[5] University of Maryland, College Park, Maryland, USA
[6] Carnegie Institution of Washington, Washington, District of Columbia, USA
[7] University of Edinburgh, Edinburgh, UK

Abstract. The two most important dynamical features of the zodiacal cloud are: (i) the dust bands associated with the major Hirayama asteroid families, and (ii) the circumsolar ring of dust particles in resonant lock with the Earth. Other important dynamical features include the offset of the center of symmetry of the cloud from the Sun, the radial gradient of the ecliptic polar brightness at the Earth, and the warp of the cloud. The dust bands provide the strongest evidence that a substantial and possibly dominant fraction of the cloud originates from asteroids. However, the characteristic diameter of these asteroidal particles is probably several hundred microns and the migration of these large particles towards the inner Solar System due to Poynting-Robertson light drag and their slow passage through secular resonances at the inner edge of the asteroid belt results in large increases in their eccentricities and inclinations. Because of these orbital changes, the dividing line between asteroidal and cometary-type orbits in the inner Solar System is probably not sharp, and it may be difficult to distinguish clearly between asteroidal and cometary particles on dynamical grounds alone.

I. INTRODUCTION

Advances in infrared astronomy have revealed that the structure of the zodiacal cloud is complex and substantially different from the smooth, rotationally symmetric cloud assumed prior to the launch of the IRAS (Infrared Astronomical Satellite) and COBE (Cosmic Background Explorer) spacecraft (Giese et al. 1986). We now know that the Sun is not at the center of symmetry of the cloud (Kelsall et al. 1998; Dermott et al. 1999; Wyatt et al. 1999b), that the cloud contains dust bands originating from the disintegration of asteroids (Low et al. 1984; Dermott et al. 1984), dust trails derived from known comets (Sykes and Walker 1992), and clouds of dust associated with a circumsolar ring of dust particles trapped in resonant lock with the Earth (Dermott et al. 1994a; Reach et al. 1995). These features pose challenging dynamical problems. However,

they are also our best source of information on the sources that supply the cloud. The plan of this review is as follows.

In Section II, we discuss the LDEF (Long Duration Exposure Facility) results on the sizes of the particles accreted by the Earth. These results show very clearly that, in the vicinity of the Earth, the dominant particles in the cloud have characteristic diameters $\sim 10^2\,\mu$m (Love and Brownlee 1993). A similar conclusion was reached by Grün et al. (1985), who reviewed evidence from a variety of other sources including the lunar microcratering record as well as spacecraft micrometeoroid detectors. These particles are not primordial (their lifetimes are $\sim 10^6$ yr) but are replenished from sources that must be either asteroidal or cometary. However, which of these sources is dominant is still a matter of debate. The main purpose of this review is to analyze the constraints on the origins of the particles that are imposed by the dynamics. Section II also contains a brief discussion of the collisional evolution of the particle sizes and of the radiation forces that act on the particle orbits. In Section III, we discuss in detail the variations of the orbital elements of asteroidal and cometary particles due to Poynting-Robertson light drag. Some of these variations arise from gravitational interactions with the planets and these changes determine many of the dynamical features of the cloud. Of particular importance are the long term changes in the eccentricities and inclinations of the particle orbits due to secular perturbations, and the dependence of these changes on particle size.

The most important source of information on the asteroidal contribution to the zodiacal cloud are the IRAS multi-waveband observations of the dust bands. In Section IV, we use these IRAS data to quantify the magnitude of the asteroidal source and to determine the size-frequency distribution of the particles. We do not have any useful way of assessing the direct contribution of cometary material and our only recourses are either to estimate the fraction of the cloud that is asteroidal and ascribe the remainder to comets, or to examine whether there are any features of the cloud that dictate that there must be a significant cometary contribution. COBE provided particularly useful information on the structure of the broad-scale, background cloud. In Section V, we discuss the shape of the cloud, the offset of the center of symmetry from the Sun, the plane of symmetry, and the variation of the ecliptic polar brightness with heliocentric distance. One of the most striking features of the zodiacal cloud revealed by IRAS and confirmed by COBE is the trailing/leading asymmetry which has been accounted for by resonant trapping of dust particles by the Earth (Dermott et al. 1994a). In Section VI, we discuss the origin of this asymmetry and the dynamics of the Earth's resonant ring.

The problem of the origin of the IDPs (Interplanetary Dust Particles) collected in the Earth's atmosphere is obviously related to the origin of the particles in the cloud but there are two other dynamical factors that influence the rate of accretion. In Section VII, we discuss the role of gravitational focusing in the accretion of low-eccentricity asteroidal particles. We also discuss the possible role of the Earth's resonant ring in the accretion process. Finally, we

discuss the variation of the accretion rate with time due to the variation of the Earth's orbital elements.

II. FORCES AND COLLISIONS

A wide range of gravitational and non-gravitational forces act to change the orbits of particles in the zodiacal cloud. At the same time, the particle size distribution evolves due to mutual collisions. Of particular importance for our discussion is the critical diameter, $D_{\rm crit}$, that divides the larger particles in the cloud, those that are collisionally evolved and have lifetimes determined by mutual collisions, from the smaller particles that have lifetimes determined by drag and radiation forces. The summary that follows is concerned largely with the evolution of asteroidal particles and is based on the account given recently by Wyatt et al. (1999b). For a more complete discussion of the collisional evolution of asteroidal and cometary dust see the paper by Grün et al. (1985).

A typical asteroidal dust particle is created by the breakup of a larger "parent" body. This parent body could have been created by the breakup of an even larger body, and the particle itself will most likely end up as a parent body for particles smaller than itself. This "collisional cascade" spans the complete size range of disk material, and the particles that share a common ancestor are said to constitute a "family" of particles. The size distribution that results from this collisional cascade is given by

$$N(D) = \frac{1}{3(3q-1)} \left(\frac{D_0}{D}\right)^{3(q-1)}, \tag{1}$$

where $N(D)$ is the number of asteroids with diameter $> D$, D_0 is a constant, and q is the power law index (Dohnanyi 1969). If $5/3 < q < 2$, then the total area, A, in the cascade population is dominated by contributions from the smallest particles of diameter $\sim D_{\rm min}$, where $D_{\rm min}$ is the lower cutoff of the size distribution, whereas the total volume, V, of the source population is dominated by the contributions from the larger fragments. If we write V in terms of the equivalent diameter, D_e, that is, $V = (\pi/6)D_e^3$, then

$$A = \frac{(\pi/4)D_{\rm min}^2}{(3q-5)} \left(\frac{D_0}{D_{\rm min}}\right)^{3(q-1)} \tag{2}$$

and

$$D_0 = D_e \left[3(2-q)\right]^{1/3} \left(\frac{D_0}{D_{\rm max}}\right)^{2-q}, \tag{3}$$

where $D_{\rm max}$ is the diameter of the largest family fragment in the cascade. For the three major Hirayama families, Eos, Themis and Koronis (Hirayama 1918), $D_e/D_0 \simeq 1.2$ (Dermott et al. 1984).

Dohnanyi's derivation of the above power law assumed an infinite range of sizes. However, in the asteroid belt, the smallest particles are removed by

drag forces and light pressure (as discussed in the following two subsections). Given that these small particles are the bullets that destroy bodies a magnitude larger, their removal could have a profound effect on the size distribution of the larger bodies. Numerical experiments (Davis et al. 1993; Durda and Dermott 1997) have shown that the rapid removal of the smallest particles could result in strong departures from Dohnanyi's simple power law. However, Durda and Dermott (1997) argue that, in the asteroid belt, Poynting-Robertson light drag does not in fact remove the smaller particles on a fast enough timescale to affect the size distribution.

Dohnanyi (1969) also assumed that all particles in the asteroid collision cascade have the same, size-independent impact strength, in which case it can be shown analytically that $q = 1.83$. However, strain-rate effects (Housen and Holsapple 1990) and gravitational overburden of large asteroids (Davis et al. 1985) lead to size-dependent strengths among real asteroids. Durda and Dermott (1997) and Durda et al. (1998) have shown that size-dependent impact strengths can lead to evolved size distributions that deviate from the classic Dohnanyi power law distribution. Observation of the small ($D < 30\,\mathrm{km}$) asteroids in the inner region of the main belt shows that $q = 1.78 \pm 0.02$, indicating some dependence of the strength of asteroids on their size (Durda and Dermott 1997). The distribution of the very largest ($D > 30\,\mathrm{km}$) asteroids also deviates from the Dohnanyi distribution because of the transition from strength-scaling to gravity-scaling for asteroids larger than $\sim 150\,\mathrm{m}$ (Durda et al. 1998), and also because some of the larger asteroids are original and not part of the collisional cascade. Overall, however, the basic collision cascade theory is well-supported by evidence from the larger, observable members of the main belt asteroid population.

The size distribution of the zodiacal cloud's medium-sized ($1\,\mathrm{mm} < D < 3\,\mathrm{km}$) members is also expected to follow Eq. (1), but there is no observational proof of this, since these members are too faint to be seen. However, the proof that the zodiacal cloud's collisional cascade extends from its largest members down to its smallest dust particles is, of course, provided by the existence of the Solar System dust bands that we know are derived from asteroidal collisions (Dermott et al. 1984; Grogan et al. 2001).

Mutual collisions among asteroidal particles are typically not catastrophic: $N(D)$ increases rapidly with decreasing D and so a particle in the main belt is most likely to be broken up by a projectile that has just enough mass (and hence energy) to do so. This in turn means that the collisional fragments have velocities, and hence orbital elements, that are almost identical to those of the original particle; that is, in the absence of other forces, all members of the same family have near-identical orbits. This, of course, is the reason for the close grouping of the orbital elements of the Hirayama family members. It is also the reason why dust bands actually exist and are observable.

II.A. Radiation Forces

In this chapter, we are concerned only with the dynamical effects of solar radiation on micron-sized dust particles, but given the current interest in exozodiacal clouds it is useful to follow Wyatt et al. (1999b) and to generalize all of our equations to any star. In this context, radiation forces are caused by the absorption, scattering, and re-emission of incident photons by the dust particle (refer to Burns et al. 1979, for a thorough description). Radiation pressure is the component of the radiation force that points radially away from the star. It is defined for different size particles by its ratio to the gravitational force, and is denoted by the symbol β. We can write (Gustafson 1994):

$$\beta(D) = F_{\rm rad}/F_{\rm grav} = C_{\rm r}(\sigma/m)\langle Q_{\rm pr}\rangle_{T_*}(L_*/L_\odot)(M_*/M_\odot), \tag{4}$$

where $C_{\rm r} = 7.65 \times 10^{-4}\,{\rm kg\,m^{-2}}$; σ/m is the ratio of the particle's cross-sectional area to its mass (for example, $\sigma/m = 1.5/\rho D$ for spherical particles of density ρ);

$$\langle Q_{\rm pr}\rangle_{T_*} = \frac{\int Q_{\rm pr}(D,\lambda)F_\lambda {\rm d}\lambda}{\int F_\lambda {\rm d}\lambda} \tag{5}$$

is the particle's radiation pressure efficiency averaged over the stellar spectrum, F_λ; T_* is the star's effective temperature; M_* and L_* are the mass and luminosity of the star; and $M_\odot$ and $L_\odot$ are the mass and luminosity of the Sun.

A useful approximation for large particles is that $\langle Q_{\rm pr}\rangle_{T_*} \approx 1$; in which case

$$\beta(D) = (1150/\rho D)(L_*/L_\odot)(M_*/M_\odot), \tag{6}$$

where ρ is measured in ${\rm kg\,m^{-3}}$, and D is in μm. This approximation is valid for astronomical silicate particles in the Solar System with $D \gtrsim 1\,\mu$m (see Fig. 1).

The effect of radiation pressure is equivalent to reducing the mass of the star by a factor $1-\beta$. This means that small daughter fragments created by the breakup of a parent body move on orbits that can be substantially different from that of the parent. The reason for this is that while the positions and velocities of a parent and its daughter fragments are the same at the moment of breakup (apart from a small velocity dispersion), their β are different, and so the daughter fragments move in effective potentials that are different from that in which the parent moves. Daughter fragments created in the breakup of a parent body with $\beta = 0$, and for which the orbital elements at the time of the breakup were semi-major axis a, eccentricity e, inclination I, longitude of ascending node Ω, longitude of pericenter ϖ, and true anomaly f, move in the same orbital plane as the parent, $I' = I$ and $\Omega' = \Omega$, but on orbits with semi-major axes a', eccentricities e', and pericenter orientations ϖ', given by (Burns et al. 1979; Kortenkamp and Dermott 1998a; Wyatt et al. 1999b)

$$a' = a(1-\beta)/[1 - 2\beta(1 + e\cos f)/(1-e^2)], \tag{7}$$

$$e' = (1-\beta)^{-1}\sqrt{(e^2 + 2\beta e\cos f + \beta^2)}, \tag{8}$$

$$\varpi' - \varpi = f - f' = \arctan[\beta \sin f/(\beta\cos f + e)]. \tag{9}$$

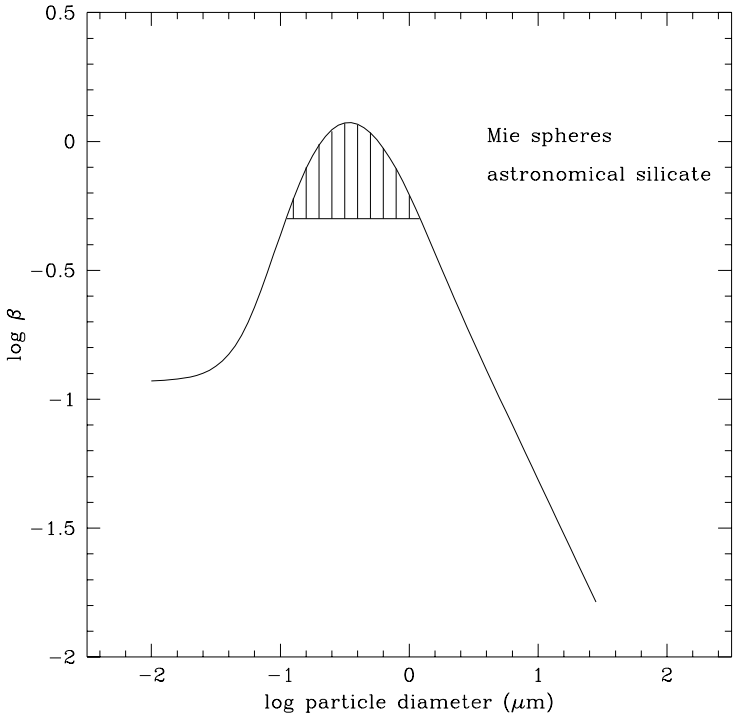

Figure 1. Variation with particle diameter D of the ratio, β, of the forces due to solar radiation and gravity acting on a spherical particle of density 2,500 kg m^{-3} with the optical properties of astronomical silicate calculated using Mie theory. Radiation pressure acts on particles with $\beta > 0.5$ (shown hatched) derived from larger particles moving on near-circular orbits, to blow these small particles out of the Solar System. For $D(\mu\mathrm{m}) \gtrsim 1$, $\beta \approx 1/(2.2D)$.

Analysis of these equations shows that the orbits of the largest fragments, those for which $\beta < 0.1$, are similar to that of the parent. On the other hand, the smallest fragments, those for which $\beta > 0.5(1-e^2)/(1+e\cos f)$, have hyperbolic orbits ($e' > 1$) and are known as "β meteoroids" (Zook and Berg 1975). Since β meteoroids are blown out of the system on the timescale of the orbital period of the parent, the diameter of the particle for which $\beta > 0.5$ essentially defines the lower limit of the collisional cascade. However, as we have assumed here that the parent body is on a nearly circular orbit, this result does not apply to bodies on comet-like orbits. Figure 1 shows that there may also be a population of submicron particles that have $\beta < 0.5$ (Gustafson 1994).

II.B. Poynting-Robertson (P-R) Light Drag

The component of the radiation force tangential to a particle's orbit is called the P-R drag force. This force is also proportional to β. It results in an evolutionary

decrease in both the semi-major axis and the osculating eccentricity of the particle's orbit (Wyatt and Whipple 1950):

$$\dot{a}_{\rm PR} = -(\alpha/a)(2+3e^2)/(1-e^2)^{3/2} = -2\alpha/a + O(e^2), \tag{10}$$

$$\dot{e}_{\rm PR} = -2.5(\alpha/a^2)e/(1-e^2)^{1/2} = -2.5\alpha e/a^2 + O(e^3), \tag{11}$$

where $\alpha = 6.24\times10^{-4}\beta(M_*/M_\odot)\,{\rm AU^2\,yr^{-1}}$. P-R drag therefore causes the orbit of the particle to spiral in towards the star. However, it does not change the plane of the particle's orbit, $\dot{I}_{\rm PR} = \dot{\Omega}_{\rm PR} = 0$; neither does it affect the orientation of the particle's pericenter, $\dot{\varpi}_{\rm PR} = 0$.

For a particle with zero eccentricity, Eq. (10) can be solved to find the time it takes for the particle to spiral in from an astrocentric radial distance r_1 to r_2:

$$t_{\rm PR} = 400(M_\odot/M_*)\left[(r_1/a_\oplus)^2 - (r_2/a_\oplus)^2\right]/\beta, \tag{12}$$

where $t_{\rm PR}$ is given in years and $a_\oplus = 1\,{\rm AU}$ is the semi-major axis of the Earth's orbit. The time taken for an asteroidal particle to migrate from its source region to the Earth is $\propto D$ (Eq. 6, large particle approximation). For a particle of diameter $D = 100\,\mu{\rm m}$, released at a radial distance $r_1 = 3\,{\rm AU}$, $t_{\rm PR} \sim 7\times10^5\,{\rm yr}$. It follows from Eq. (10) that the P-R decay timescale, $t_{\rm PR}$, decreases as the eccentricity of the particle increases. Dividing Eq. (10) by Eq. (11) gives ${\rm d}a/{\rm d}e$, the rate of change of the semi-major axis of a particle with eccentricity, which is clearly independent of β and hence the size of the particle. This leads to the interesting result that the eccentricity distribution of a wave of particles spiraling towards a star, is only dependent, at any given semi-major axis, on the initial distribution of semi-major axes and eccentricities of the particles. Although the time taken for any particular particle to reach the given semi-major axis is dependent on its size.

The effects of the average force due to scattering of incident protons in a stellar wind, which acts in the same way as P-R light drag, should also be added to Eqs. (10)–(12), Gustafson (1994). In the Solar System, this force, known as solar wind drag, is usually taken to be 30% of the P-R light drag force, varying over the 11-year solar cycle from 20% to 40%, thus reducing the timescale in Eq. (12) by about 30%.

II.C. Collisions

The importance of collisions in determining a particle's evolution depends on its collisional lifetime. The collisional lifetime of the particles of diameter $D_{\rm typ}$ that constitute most of a disk's cross-sectional area (that is, those particles that are expected to characterize the disk's mid-IR emission), can be approximated by

$$t_{\rm coll}(D_{\rm typ}, r) = \frac{t_{\rm per}}{4\pi\tau_{\rm eff}(r)}, \tag{13}$$

where r is the astrocentric radial distance and $\tau_{\rm eff}(r)$ is the disk's effective face-on optical depth, which would be equal to the disk's true optical depth if its

particles had unity extinction efficiency (Artymowicz 1997; Wyatt et al. 1999b). The orbital period of the particle in years is given by $t_{\rm per} = \sqrt{(a/a_\oplus)^3 (M_\odot/M_*)}$.

Consider the fragments created in the breakup of an asteroid at a heliocentric distance r. The largest fragments, with $D > D_{\rm crit}$, are broken up by collisions before their orbits have suffered any significant P-R drag evolution, while the smaller fragments, with $D < D_{\rm crit}$, for which the P-R drag evolution is faster, can reach the Sun without a catastrophic collision. By equating the collisional and P-R drag lifetimes given by Eqs. (12) and (13), and using the large particle approximation for β, Eq. (6), Wyatt et al. (1999b) estimate that

$$D_{\rm crit} = \frac{0.23}{\rho \tau_{\rm eff}(r)} \left(\frac{L_*}{L_\odot} \right) \sqrt{\left(\frac{M_\odot}{M_*} \right) \left(\frac{a_\oplus}{r} \right)}, \tag{14}$$

where ρ is measured in kg m^{-3}, and $D_{\rm crit}$ in μm.

Consider the daughter fragments created in the breakup of an "endless" supply of asteroids on orbits with semi-major axis a_s that flow towards the Sun due to P-R drag. If we ignore any further disintegrations of the particles that are involved in the flow, then the orbits of all the particles in a given size range will be distributed between the source and the Sun according to

$$N(a) \propto 1/\dot{a}_{\rm PR} \propto a, \tag{15}$$

where $N(a)\mathrm{d}a$ is the number of orbits with semi-major axes in the range a to $a + \mathrm{d}a$. Thus, the spacing of the orbits increases as the particles approach the Sun and this fact tends to decrease the number density of the particles, defined as the number of particles per unit volume. But given that both the circumferences of the orbits and the vertical extent of the particle distributions also decrease proportionally with decreasing a, it follows that, for particles in near-circular orbits, the number density of these particles, regardless of their size, will increase inversely with heliocentric distance.

However, because the flow rate of the particles is inversely proportional to their diameter, that is, because $\dot{a}_{\rm PR} \propto 1/D$ (see Eqs. 6 and 10), it follows that the size distribution of the particles in the flow region interior to the asteroid belt, must be quite different from that in the source region.

If the collisional processes leading to the size distribution of the large parent bodies, $N_s(D)$, still holds for the production of the P-R drag affected particles, then the size distribution in the flow region is given by:

$$N(D) \propto N_s(D)/\dot{a}_{\rm PR} \propto N_s(D) D. \tag{16}$$

Thus, if $N_s(D)$ is given by Eq. (1) with $q = 11/6$, then the cross-sectional area of a disk's smaller, P-R drag affected particles is concentrated in the largest of these small particles, while the cross-sectional area of the particles that are large enough to be unaffected by P-R drag ($D > D_{\rm crit}$) is concentrated in the smallest of these larger particles. The result is that most of a disk's cross-sectional area is expected to be concentrated in particles with $D_{\rm typ} \approx D_{\rm crit}$, justifying the use of Eq. (13) for the collisional lifetime of these particles.

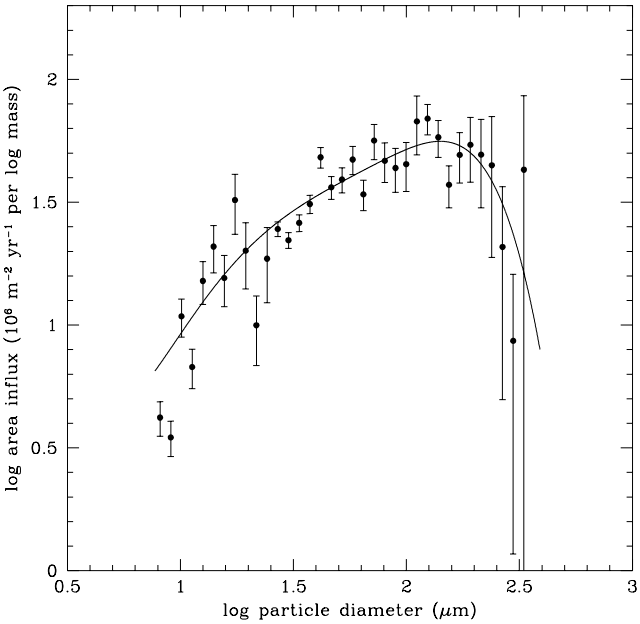

Figure 2. Incremental area of particles accreted annually by the Earth as a function of particle diameter. The bold line is the polynomial derived by Love and Brownlee (1993) from the cratering record on LDEF (Long Duration Exposure Facility). The total area of the accreted particles is dominated by particles with diameters between 60 μm and 200 μm.

Observations of the mean polar brightness of the zodiacal cloud at 1 AU (see Fig. 19) can be used to estimate (the results are somewhat model dependent) that, near the Earth, the effective, normal optical depth is $\sim 5 \times 10^{-8}$. If, as we believe, these zodiacal particles originated in the asteroid belt and migrated to 1 AU due to the P-R drag, then the zodiacal cloud's volume density should vary $\sim 1/r$ and its effective optical depth in the asteroid belt should be similar to that at 1 AU. Assuming the zodiacal cloud particles to have a density 2,500 kg m^{-3}, the cross-sectional area of material in the asteroid belt should be concentrated in particles with $D_{\rm typ} \sim 10^3$ μm for which the collisional lifetime, and the P-R drag lifetime, are $\sim 10^7$ yr.

However, because the collisional and P-R lifetimes are similar, we must expect many of these large particles to be broken up by collisions before they reach the inner Solar System; in which case we must expect the cross-sectional area of material at 1 AU to be concentrated in particles smaller than that in the asteroid belt. This is in agreement with the LDEF observations of Love and Brownlee (1993) and other evidence (see the review by Grün et al. 1985) that shows the cross-sectional area distribution at 1 AU to peak for particles with $D \sim 10^2$ μm (see Fig. 2).

The analysis of the collisional lifetimes of Wyatt et al. (1999b) also predicts that the collisional lifetime of the large bodies in the asteroid belt should be $\sim 10^9\sqrt{D}\,\mathrm{yr}$, where D is in km. Since the Solar System is 4.5×10^9 years old, this implies that the population of asteroids larger than $\sim 20\,\mathrm{km}$ should be progressively dominated by primordial objects; this is in agreement with the observed size distribution of these asteroids — see Fig. 15.

Analysis of the collision rates of objects in the Kuiper Belt (Stern 1995) shows that a collisional cascade should exist there too; there is also evidence to suggest that the Kuiper Belt was once more massive than it is today (Jewitt 1999), meaning that in the past collisions would have played a much larger role in determining its structure than they do today, maybe even causing the supposed mass loss (Stern and Colwell 1997). The size distribution of the observed Kuiper Belt objects appears to be slightly steeper than that in the inner Solar System ($q > 11/6$, Jewitt 1999), while observations have been unable, as yet, to determine its dust distribution (Backman et al. 1995; Gurnett et al. 1997).

The migration of small dust grains from the Kuiper Belt has been investigated by Liou et al. (1996), who discovered that only grains with diameter $\sim 1\,\mu\mathrm{m}$ survived collisions with interstellar dust particles to reach the inner Solar System. As the P-R drag lifetime for dust grains with diameter $\sim 10^2\,\mu\mathrm{m}$ is significantly longer, it is questionable whether such large grains could reach the inner Solar System without suffering some disruption due to mutual collisions with other Kuiper Belt dust grains or with interstellar dust particles. An investigation by Grogan et al. (1996) concluded that interstellar dust particles themselves provide only a minor contribution to the zodiacal cloud. In this chapter, we therefore focus on the orbital evolution of asteroidal and cometary dust particles with diameters in the range 1 to $10^3\,\mu\mathrm{m}$. The dominant non-gravitational forces acting on these particles in the inner Solar System are radiation pressure, P-R drag and solar wind drag. Particles smaller than this are affected by the Lorentz force, which can also become important for larger dust particles in the outer Solar System (Leinert and Grün 1990). Whereas meter-sized bodies are acted upon by the Yarkovsky effect which, although not directly relevant to the dynamical behaviour of micron-sized dust particles, can lead to significant changes in the orbital distribution of their source bodies (Bottke et al. 2000). These effects are beyond the scope of the discussion presented here.

III. ORBITAL EVOLUTION

The orbital evolution of a given dust particle in the cloud will also be affected by both secular (long-period), resonant, and short-period gravitational perturbations imposed by the planets. Secular perturbations give rise to long term variations in a particle's orbit (as discussed below) and short-period perturbations can lead to gravitational scattering. A resonant perturbation arises when two periods or frequencies are in a simple numerical ratio and can lead to large changes in a particle's orbit. A mean motion resonance occurs when

such a relationship exists between the orbital periods of two bodies (this type of resonance is discussed further in Section VI). In the case of secular resonance, the relevant frequencies are the rates of change of the proper longitude of pericenter ($\dot{\varpi}_{\rm p} = A$) or proper longitude of ascending node ($\dot{\Omega}_{\rm p} = -A$) of the particle, and one of the eigenfrequencies of the planetary system (g_k or f_k respectively, see Eqs. 27 and 28 below). In order to determine the secular evolution of asteroidal dust particles (i.e., particles in low eccentricity and inclination orbits), low order secular perturbation theory may be employed (e.g., Brouwer and Clemence 1961; Dermott and Nicholson 1986; Murray and Dermott 1999; Wyatt et al. 1999b); as the secular evolution of the particle's complex eccentricity, z, and complex inclination, y, are decoupled (see Eqs. 21 and 22). This low order theory is not, however, suitable for determining the secular evolution of cometary dust particle orbits with moderate to high eccentricities or inclinations; as above a certain threshold value the secular evolution of the particle's complex eccentricity and inclination are no longer decoupled. These threshold values for eccentricity, e, and inclination, I, have not yet been accurately determined, but our investigations indicate that a maximum e and $\sin I$ of ~ 0.2 may be adopted.

The gravitational perturbations imposed on a particle's orbit by a planetary system containing $N_{\rm pl}$ bodies with masses M_j, orbiting a central star of mass $M_\star$, can be described by the particle's disturbing function, R. This function can be decomposed into the sum of many terms, and those which do not depend on the mean longitudes of either the particle or the planets (i.e., long-period terms) can be identified as contributing to the secular perturbations, $R_{\rm sec}$. To second order in the eccentricities, e, and inclinations, I,

$$R_{\rm sec} = na^2 \left[\frac{1}{2} A \left(e^2 - I^2 \right) + \sum_{j=1}^{N_{\rm pl}} A_j e e_j \cos\left(\varpi - \varpi_j\right) + \sum_{j=1}^{N_{\rm pl}} B_j I I_j \cos\left(\Omega - \Omega_j\right) \right], \tag{17}$$

where ϖ is the longitude of pericenter, Ω is the longitude of ascending node, n is the mean motion of the particle (accounting for the effect of radiation pressure), and

$$A = +\frac{n}{4(1-\beta)} \sum_{j=1}^{N_{\rm pl}} \left(\frac{M_j}{M_\star} \right) \alpha_j \bar{\alpha}_j b_{3/2}^{(1)}(\alpha_j), \tag{18}$$

$$A_j = -\frac{n}{4(1-\beta)} \left(\frac{M_j}{M_\star} \right) \alpha_j \bar{\alpha}_j b_{3/2}^{(2)}(\alpha_j), \tag{19}$$

$$B_j = +\frac{n}{4(1-\beta)} \left(\frac{M_j}{M_\star} \right) \alpha_j \bar{\alpha}_j b_{3/2}^{(1)}(\alpha_j), \tag{20}$$

where $\alpha_j = a_j/a$ and $\bar{\alpha}_j = 1$ for $a_j < a$; $\alpha_j = \bar{\alpha}_j = a/a_j$ for $a_j > a$; a is the semi-major axis, and $b_{3/2}^{(s)}(\alpha_j)$ are the Laplace coefficients ($s = 1, 2$). A, A_j and

B_j are in units of radian s^{-1}, R_{sec} is in units of $m^2\,s^{-2}$; quantities subscripted j refer to the jth planet and unsubscripted quantities refer to the particle.

The effects of these secular perturbations are such that the semi-major axis remains constant while the eccentricity and inclination vary in a manner coupled with the variations of its longitude of pericenter and ascending node, described by the complex eccentricity z and complex inclination y,

$$z = e \exp i\varpi, \tag{21}$$

$$y = I \exp i\Omega. \tag{22}$$

Lagrange's planetary equations then give the eccentricity and inclination variations due to secular perturbations as

$$\dot{z}_{sec} = +iAz + i\sum_{j=1}^{N_{pl}} A_j z_j, \tag{23}$$

$$\dot{y}_{sec} = -iAy + i\sum_{j=1}^{N_{pl}} B_j y_j, \tag{24}$$

where z_j and y_j are the complex eccentricities and inclinations of the perturbers, which vary over time, t, according to

$$z_j(t) = \sum_{k=1}^{N_{pl}} e_{jk} \exp i(g_k t + \zeta_k), \tag{25}$$

$$y_j(t) = \sum_{k=1}^{N_{pl}} I_{jk} \exp i(f_k t + \gamma_k), \tag{26}$$

where g_k and f_k are the eigenfrequencies of the perturber system, the coefficients e_{jk} and I_{jk} are the corresponding eigenvectors, and ζ_k and γ_k are constants dependent on the initial conditions of the perturber system.

The solution of Eqs. (23) and (24), giving the secular evolution of the particle's instantaneous complex eccentricity and inclination (the osculating elements) can be decomposed into two distinct time-varying elements, the forced elements and the proper elements, to be added vectorially in the complex plane:

$$\begin{aligned} z(t) &= z_f(t) + z_p(t) \\ &= \sum_{k=1}^{N_{pl}} \left[\frac{\sum_{j=1}^{N_{pl}} A_j e_{jk}}{g_k - A} \right] \exp i(g_k t + \zeta_k) + e_p \exp i(+At + \zeta_0), \end{aligned} \tag{27}$$

$$\begin{aligned} y(t) &= y_f(t) + y_p(t) \\ &= \sum_{k=1}^{N_{pl}} \left[\frac{\sum_{j=1}^{N_{pl}} B_j I_{jk}}{f_k + A} \right] \exp i(f_k t + \gamma_k) + I_p \exp i(-At + \gamma_0), \end{aligned} \tag{28}$$

where e_p, ζ_0 and I_p, γ_0 are determined by the initial conditions of the particle.

These equations have simple physical and geometrical interpretations. A particle's forced elements, $z_{\rm f}$ and $y_{\rm f}$, depend only on the orbits of the perturbers in the system (that have a slow secular evolution, Eqs. 25 and 26), as well as on the particle's semi-major axis (which has no secular evolution). Thus, at a time t_0, a particle that is on an orbit with a semi-major axis a, has forced elements imposed on its orbit by the perturbers in the system that are defined by $z_{\rm f}(a,t_0)$ and $y_{\rm f}(a,t_0)$. The contribution of the particle's proper elements to its osculating elements, $z(t_0)$ and $y(t_0)$, is then given by: $z_{\rm p}(t_0) = z(t_0) - z_{\rm f}(a,t_0)$ and $y_{\rm p}(t_0) = y(t_0) - y_{\rm f}(a,t_0)$; thus defining the particle's proper eccentricity, $e_{\rm p}$, and proper inclination, $I_{\rm p}$, which are its fundamental orbital elements (i.e., those that the particle would have if there were no perturbers in the system), as well as the orientation parameters ζ_0 and γ_0. Since both the forced elements, and the osculating elements, of collisional fragments are similar to those of their parent (apart from fragments with $\beta > 0.1$, see Eqs. 7–9), particles from the same family have almost the same proper elements, $e_{\rm p}$ and $I_{\rm p}$.

The evolution of a particle's proper elements is straight-forward — they precess around circles of fixed radius, $e_{\rm p}$ and $I_{\rm p}$, at a constant rate, A, counterclockwise for $z_{\rm p}$, clockwise for $y_{\rm p}$. The secular precession timescale depends only on the semi-major axis of the particle's orbit:

$$t_{\rm sec} = 2\pi / A t_{\rm year}, \tag{29}$$

where $t_{\rm sec}$ is given in years, $t_{\rm year}$ is one year measured in seconds, and A is given by Eq. (18); secular perturbations produce long period variations in a particle's orbital elements (e.g., $t_{\rm sec} \sim 10^5$ yr in the asteroid belt). The centers of the circles that the proper elements precess around are the forced elements (Fig. 3).

Now consider the family of collisional fragments originating from a primordial body, the orbital elements of which were described by a, $e_{\rm p}$, and $I_{\rm p}$. Here we consider only fragments that are unaffected by Poynting-Robertson drag, i.e. the largest particles in the distribution. The orbital elements of the largest fragments, those with $\beta < 0.1$, created in the breakup of the primordial body are initially very close to those of the primordial body; they do not have identical orbits due to the velocity dispersion imparted to the fragments in the collision. The forced elements imposed on the orbits of all of these collisional fragments are similar to those imposed on the primordial body (as their semi-major axes are almost the same). The secular evolution of their proper eccentricities and inclinations is to precess about the forced elements (which are also varying with time), but at slightly different rates (due to their slightly different semi-major axes). A similar argument applies for all particles created by the collisional breakup of these fragments. Thus, after a few precession timescales, the complex eccentricities and complex inclinations of the collisional fragments of this family lie evenly distributed around circles that are centered on $z_{\rm f}(a,t)$ and $y_{\rm f}(a,t)$, and that have radii of $e_{\rm p}$ and $I_{\rm p}$ (e.g., their complex eccentricities lie on the circle shown in Fig. 21 (left)), while their semi-major axes are all still

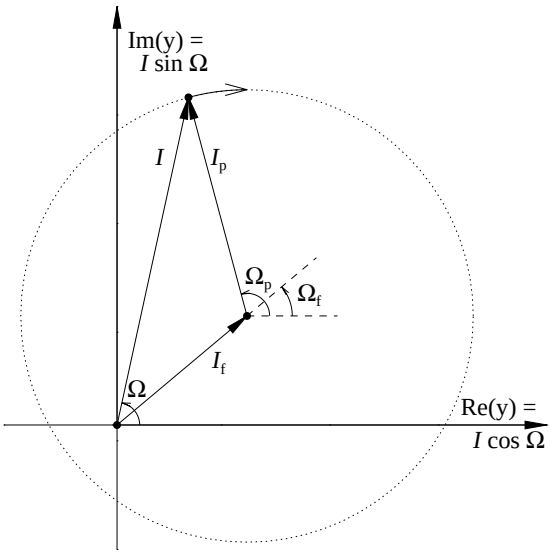

Figure 3. Schematic showing the vectorial combination of the proper and forced inclinations (I_p, I_f) and their ascending nodes (Ω_p, Ω_f) to give the osculating inclination and node (I, Ω). Reprinted with permission from Grogan et al. (2001).

close to a. This is seen to be the case in the asteroid belt: there are families of asteroids that have similar a, e_p, and I_p, that are the collisional fragments resulting from the breakup of a much larger asteroid (Hirayama 1918).

III.A. P-R Drag Affected Orbits

The solution given by Eqs. (27) and (28) accounts for the fact that small particles see a less massive star due to the action of radiation pressure, but not for the P-R drag evolution of their orbits. To find the secular evolution of the orbital elements of a particle that is affected by P-R drag, the equations governing the evolution of its complex eccentricity and inclination (Eqs. 23 and 24), must both be solved in conjunction with the P-R drag evolution of its semi-major axis and eccentricity (Eqs. 10 and 11). While the solution given by Eqs. (27) and (28) is no longer applicable, the decomposition of the particle's complex eccentricity and complex inclination into forced and proper elements, and the physical meaning of these elements, is still valid; however, each of these elements now depends on the particle's dynamical history.

Consider the P-R drag affected particles created by the breakup of an asteroid family group. Immediately after they are created, the osculating orbital elements of these particles are similar to those of the rest of the family; i.e., they have similar semi-major axes, and complex eccentricities and complex inclinations that are uniformly distributed in these planes around circles of radii approximately equal to the proper elements of the family, e_p and I_p. The

dynamical evolution of a wave of these particles, i.e., those that were created at the same time, can be followed by numerical integration to ascertain how the orbital elements of the particles in the wave vary as their semi-major axes decrease due to P-R drag; this is the "particle in a circle" method (Dermott et al. 1992). The complex eccentricities and complex inclinations of a wave of particles originating in the asteroid belt remain on circles, and the wave's semi-major axis, $a_{\rm wave}$, decreases: its effective proper eccentricity (the radius of the wave's circle in the complex eccentricity plane) decreases $\propto e_{\rm p}(a_{\rm wave}/a)^{5/4}$; its effective proper inclination (the radius of the wave's circle in the complex inclination plane) remains constant at $I_{\rm p}$; the distributions of the particles' $\varpi_{\rm p}$ and $\Omega_{\rm p}$ remain random; while its effective forced elements (the centers of the circles in the complex eccentricity and complex inclination planes) have a more complicated variation. Figure 4 shows this behavior in the variation of the inclination distribution of a wave of 40 μm diameter dust particles derived from the Eos family. The radius of the circle represents the proper inclination $I_{\rm p}$ which remains unchanged until the mean semi-major axis of the wave approaches Earth where many of the particles are gravitationally scattered.

Thus, the orbital element distributions, $n(z)$ and $n(y)$, of P-R drag affected particles are like that of the large particles, in that they are the vector addition of forced elements, $z_{\rm f}$ and $y_{\rm f}$, to symmetrical proper element distributions; however, their forced and proper elements are different for particles from different families, as well as being different for particles of different sizes and with different orbital semi-major axes. The presence of forced elements, and their variation, can lead to asymmetries in the large-scale distribution of dust particle orbits that can be detected observationally (see Sections IV and V for details) to provide information about the perturbers in the system, as well as the properties of the dust particles themselves.

III.B. Numerical Simulations

We have developed a unique integration code specifically designed for evolving the orbits of large populations of dust particles under the effects of radiation pressure, P-R drag and solar wind drag, as well as point-mass gravitational forces. To achieve this, we have applied the dissipative mapping technique (Malhotra 1994) to the specific problem of deriving a MVS (Mixed Variable Symplectic) type integration code (Wisdom and Holman 1991) that also incorporates the effects of these non-gravitational forces (Burns et al. 1979). The development and testing of this dissipative code, significantly faster than more conventional integration techniques, is described in detail elsewhere (Kehoe 1999; Kehoe et al. 2001a). We have employed the code to evolve representative samples of asteroidal dust particles forward in time to the present epoch, along with the planets Jupiter, Saturn, Uranus, and Neptune, from a number of different epochs in the past (Kehoe et al. 2001b). As the timescale for a dust particle orbit to decay under the effect of P-R and solar wind drag is dependent on the particle size (Eqs. 6 and 12), each set of past epochs chosen was dependent on the size of the dust particles considered, and a separate set

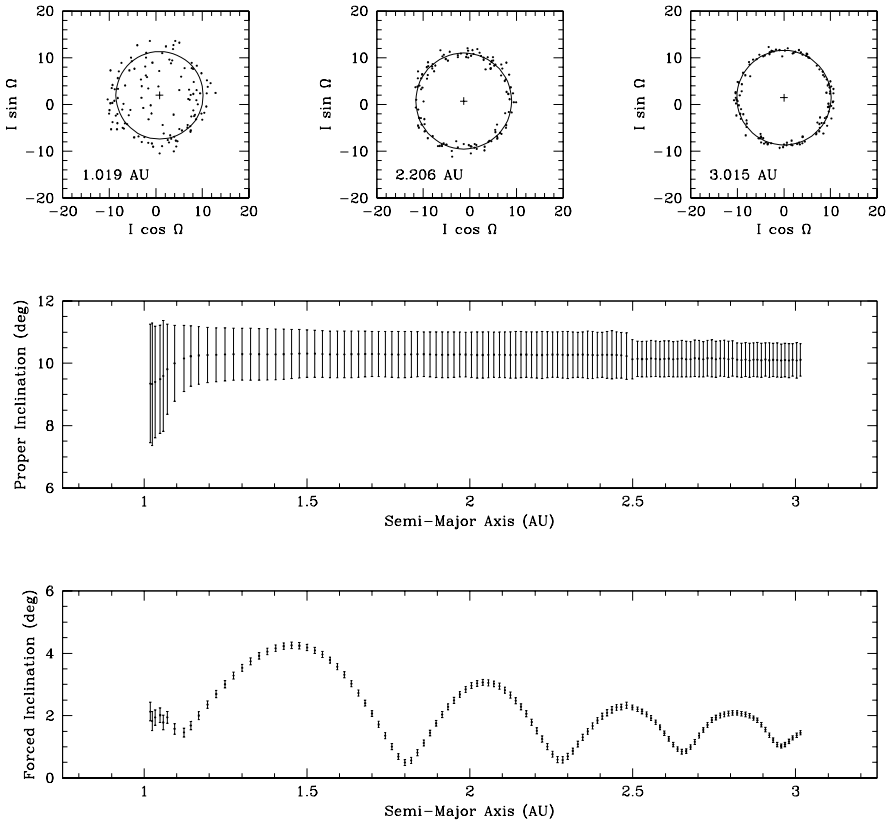

Figure 4. Variation of the inclination distribution of a wave of 40 μm diameter dust particles derived from the Eos family. The particles were released 2×10^5 years ago with a mean semi-major axis of $a = 3.015$ AU and migrated from the asteroid belt toward the Sun due to the action of drag forces. The mean semi-major axis of the particles in the wave reached $a = 1$ AU at the present time. The variation in the "center of mass" (marked by a cross in the upper three panels) corresponds to the variations of the forced elements, $I_{\rm f}$ and $\Omega_{\rm f}$, of the particles. The radius of the circle represents the proper inclination, $I_{\rm p}$ which remains unchanged until the mean semi-major axis of the wave approaches Earth where many of the particles are gravitationally scattered. Note that the forced elements are calculated at different times in the past (Grogan et al. 2001).

of integrations had to be carried out for each different particle size. Up to 80 past epochs were selected for each particle size, in order to provide a comprehensive picture of the forced element distribution of asteroidal dust particles across a wide range of semi-major axis values in the inner Solar System at the present time. Here we consider asteroidal dust particles (originating in this case from the Eos family, although this is not critical) composed of astronomical

silicate of density 2,500 kg m^{-3} with diameters 10, 100 and 200 μm, for which we calculated β values (the ratio of radiation pressure to solar gravity, Eq. 4) of 0.04871, 0.00446 and 0.00221 respectively, using Mie theory. The longest integrations performed for the 10, 100 and 200 μm diameter dust particles were for timescales of 0.06, 0.6 and 1.2 Myr, respectively.

To obtain initial orbital element distributions for our forward integrations we first employed a standard MVS integration code (incorporating point-mass gravitational forces only) to evolve Eos family asteroids, along with the gas giant planets, backwards in time from the present. Initial osculating orbital elements for 444 Eos family asteroids were obtained from The Asteroid Orbital Element Database (Bowell 1997) for the epoch of Julian Date 2450700.5, using the family classification of Zappalà et al. (1995). Osculating orbital elements for the planets were obtained for the same epoch using the data from Standish et al. (1992). Using the particle on a circle method we then generated initial osculating orbital elements for 124 dust particles, representative of the whole Eos asteroid family, at each of the past epochs required.

The results of the integrations presented in Fig. 5 represent a total of over 4 months CPU time running on a variety of Pentium processors. All orbital elements are heliocentric and given with respect to the mean ecliptic and equinox of the standard J2000 reference frame. In the region of the main asteroid belt (between 2.5 and 3 AU), the forced elements of the large particles display similar behaviour to that of the small particles. That is, their forced elements are locked onto Jupiter's osculating elements such that

$$z_{\rm f} \approx \left[b^2_{3/2}(\alpha_j)/b^1_{3/2}(\alpha_j)\right] e_j \exp i\tilde{\omega}_j, \tag{30}$$

$$y_{\rm f} \approx I_j \exp i\Omega_j. \tag{31}$$

The low dispersion of the inclinations and nodes in this region of the main belt, regardless of particle size, is the fundamental reason why dust bands are observed at these heliocentric distances. However, as the large dust particles encounter the ν_{16} secular resonance at the inner edge of the asteroid belt (at about 2 AU), the effect of the resonance disperses their forced inclinations and nodes, diffusing the dust band particles into the broad-scale zodiacal background. The ν_6 secular resonance (also at about 2 AU) produces analogous behaviour in the forced eccentricities and longitudes of pericenter of the dust particles. The effects of these secular resonances are more pronounced for the large dust particles because they are acted on by the resonances for longer periods of time. The orbital element distributions of large asteroidal dust particles produced by intra-family collisional attrition therefore lose their characteristic family signatures in the inner region of the main belt and become indistinguishable from the general background cloud of zodiacal dust. We also expect that as the dust particles spiral in further towards the Sun, gravitational scattering by the terrestrial planets will act to disperse the particles even more. This effect should be particularly marked for the more slowly evolving large dust particles as the probability of a close planetary encounter is greater. However,

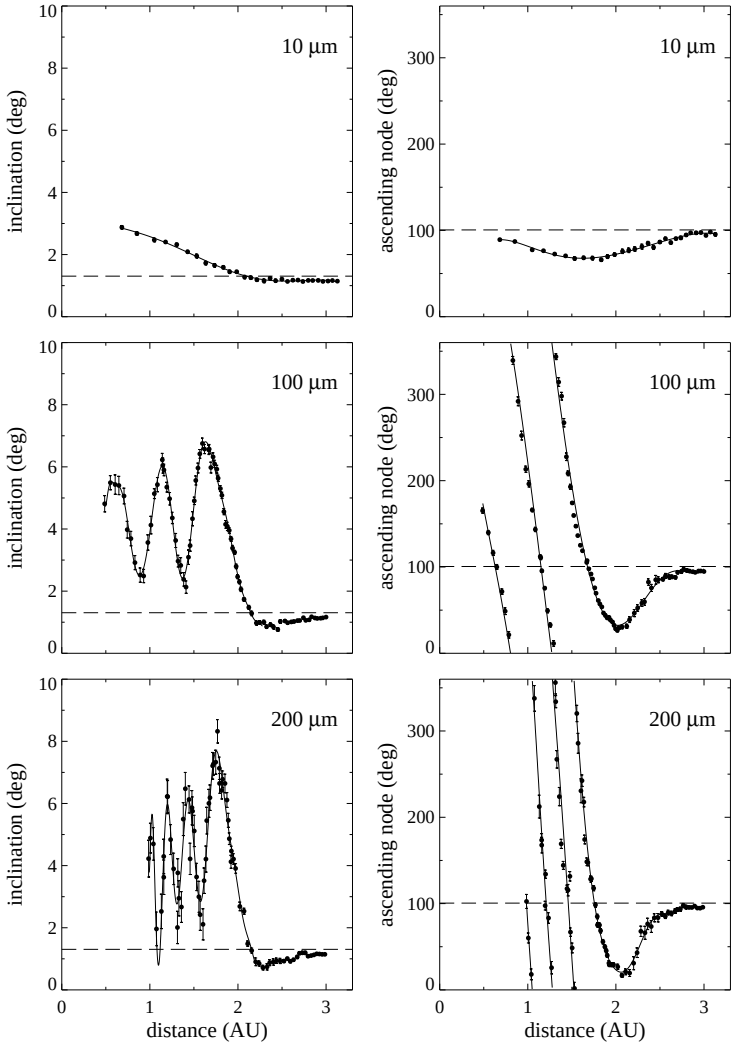

Figure 5(a). Variation of the forced inclination I_f (left), and the forced longitude of ascending node Ω_f (right), with heliocentric distance for Eos family dust particles at the present epoch (Julian Date 2450700.5). The dashed lines show the present osculating inclination (left) and osculating longitude of ascending node (right) for Jupiter (Kehoe et al. 2001b).

this result can not be ascertained from the integrations described above as the terrestrial planets have not been included here, but will be added in future models. The action of secular resonances also means that large asteroidal dust particles in the inner Solar System may have orbits with significant eccentricities and inclinations, comparable to some cometary orbits.

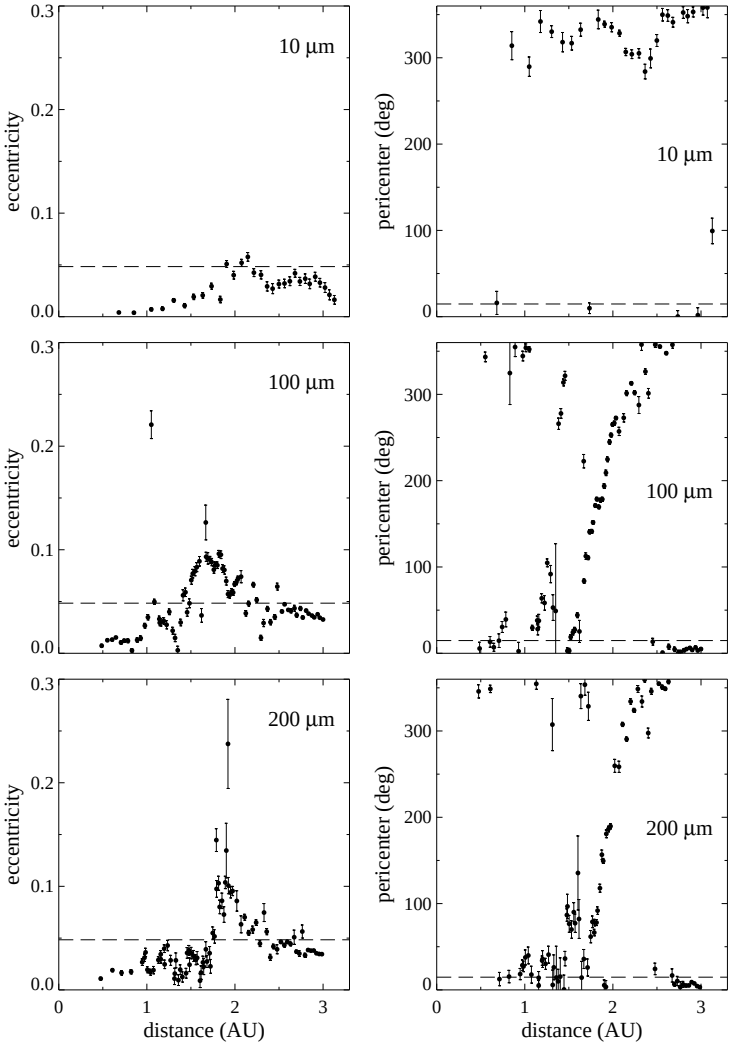

Figure 5(b). Variation of the forced eccentricity e_f (left), and the forced longitude of pericenter ϖ_f (right), with heliocentric distance for Eos family dust particles at the present epoch (Julian Date 2450700.5). The dashed lines show the present osculating eccentricity (left) and osculating longitude of pericenter (right) for Jupiter.

In the future we will extend our knowledge of asteroidal dust particle dynamics to a wider range of particle sizes, and address the main belt (non-family) contribution as well as the dust band (family) component on the way to our ultimate goal of providing a physically motivated, global model for the zodiacal emission. The dynamics of cometary material is a separate issue, we discuss this in Section III.D.

III.C. SIMUL - Visualizing the Orbital Distribution

The knowledge of the orbital distribution of a population of interplanetary dust particles demands some mechanism by which these orbits can be visualized, so that they can be compared to observational data. We have developed a FORTRAN algorithm, SIMUL, for this purpose (Dermott et al. 1988a).

The basic ideas and assumptions behind SIMUL are as follows:

1. A cloud is represented by a large number of dust particle orbits. The total cross-sectional area of the cloud is divided equally among all the orbits.
2. The orbital elements of the dust particle orbits in the cloud can be decomposed into proper and forced vectorial components. When inclination and eccentricity are low, as is typically the case for asteroidal type orbits, at any given time the forced elements are independent of the proper elements and depend only on the semi-major axis and the particle size.
3. As a first approximation, the dust particles in the cloud produced by asteroid families have the same mean proper elements as those of the parent bodies, although the gaussian distribution of these elements is a free parameter.
4. The forced elements as a function of semi-major axis and size are calculated using secular perturbation theory via direct numerical integrations, as outlined above.
5. The semi-major axis of each orbit is chosen randomly from a given radial distribution, and the remainder of the orbital elements are sampled from the distributions found from the numerical integrations.
6. Along each of the orbits, particles are distributed according to Kepler's Law. Once the spatial distribution of the orbits is specified, space is divided into a sufficiently large number of ordered cells and then every orbit is investigated for all the possible cross-sectional area contributions to each of the space cells. The model generates a large three-dimensional array which serves to describe the spatial distribution of the effective cross-sectional area.
7. The viewing geometry of any telescope can be reproduced exactly by calculating the Sun-Earth distance and ecliptic longitude of Earth at the observing time and setting up appropriate coordinate systems. In this way, IRAS-type brightness profiles can be created and compared with the observed profiles.

Although waves of only $\sim 10^2$ individual dust particles have been evolved to produce the forced elements shown in Fig. 5, the distributions are used to populate SIMUL models with $\sim 10^8$ individual orbits. These smooth models of individual components of the cloud for each particle size (which we can then weight according to any given form of size distribution), can then be compared directly with observational data. In this way we ensure that the effects of secular perturbations are fully incorporated into the models. We will discuss how we have produced accurate models for the Solar System dust bands, and

how we have used these models to predict the asteroidal contribution to the zodiacal cloud in Section IV.

III.D. Cometary Particles

The high eccentricity of typical cometary orbits renders them unsuitable for study using the particle in a circle method. Following earlier work by Liou et al. (1995), we have therefore performed direct numerical integrations of a representative sample of cometary orbits in order to determine the orbital evolution of the cometary population of the zodiacal cloud (Kortenkamp and Dermott 1998a). The initial distribution of $10\,\mu$m cometary dust particles is generated from a set of orbital elements for 175 short-period Jupiter family comets. This is a subset of the MPC catalog (Marsden 1995). As of December 1995, this set represented most of the known short-period Jupiter family comets with established orbits. Because we have fewer cometary than asteroidal parent bodies we use Eqs. (7) and (8) to generate a set of 50 dust particle orbits from each cometary orbit. We randomly distributed ϖ, Ω, and the mean anomaly, λ, between 0° and 360°. Because most of these cometary dust particles are Jupiter-crossing one suspects that their orbital evolution is strongly influenced by Jupiter, at least initially. Liou and Zook (1996) have shown that some dust particles originating from the short-period comet Temple 2 (one of our 175 comets) can be injected directly into the 1:2 interior mean motion resonance with Jupiter near 3.2 AU. Some of the particles in their study remained trapped in this resonance for thousands of years and had their eccentricities significantly reduced by the resonant forces. Our primary concern in the handling of the cometary dust particles was to accurately account for this effect.

We used the RADAU fifteenth-order integrator program of Everhart (1985) with variable time steps taken at Gauss-Radau spacing to investigate the dynamical evolution of cometary particles. All of our numerical simulations with RADAU include gravitational interactions with seven planets (Mercury and Pluto are excluded) and include the effects of radiation pressure, P-R drag, and solar wind drag. We numerically evolved the cometary dust particles with RADAU until their orbits had decayed into the Sun or were ejected from the Solar System. Some dust particles decayed into the Sun in less than 30,000 years. Other dust particles that were trapped in the Jovian mean motion resonances (trapping for some lasted as long as 100,000 years) required nearly 150,000 years of integration before decaying into the Sun. Figure 6 gives ten examples of the wide range of evolutionary paths we found for these cometary dust particles. In the course of our study we scrutinized the evolution of 7,114 cometary dust particles with initial semi-major axis $a \leq 6$ AU. We found that 1,330 particles ($\sim 20\%$) were trapped in various mean motion resonances with Jupiter. The remaining 5,784 particles evolved into the inner Solar System without having been previously trapped in mean motion resonances with Jupiter. Typically this trapping leads to a decrease in the dust particle's orbital eccentricity (see discussion following Eq. 34). Eventually the trapped dust particles escape from the resonances and P-R light drag and solar wind drag then cause their orbits

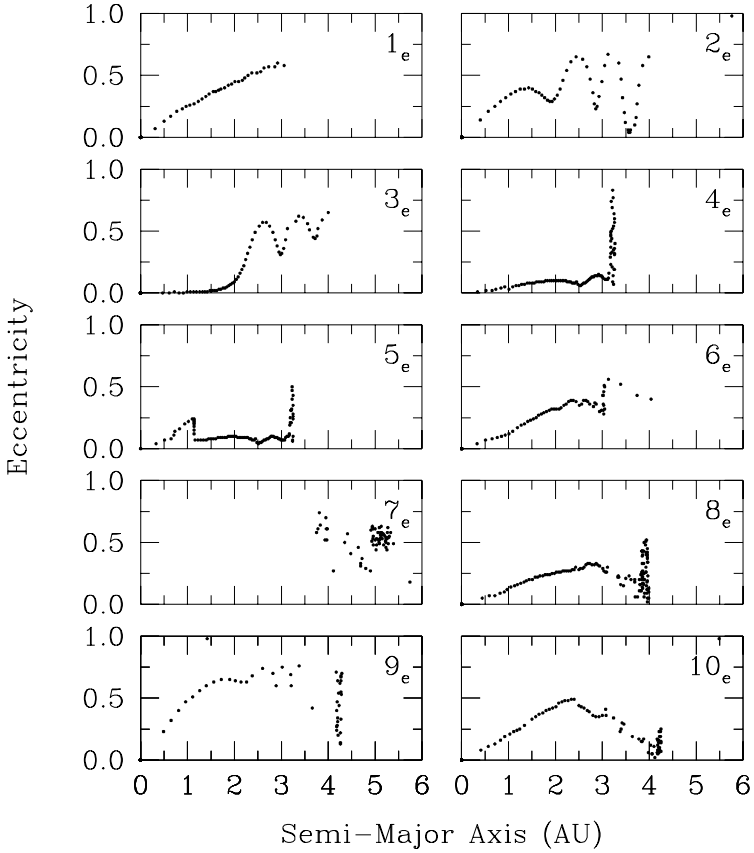

Figure 6. Ten examples showing the diversity of the evolutionary paths followed by cometary dust particles. Points are plotted every 1,000 years and the evolution typically proceeds towards smaller semi-major axes, with the exception of Example 7 (Kortenkamp and Dermott 1998a).

to decay through the inner Solar System. Figure 7 shows the Earth-crossing eccentricity and inclination (top two panels) of both the previously trapped set, and the set that were not previously trapped. The significantly lower eccentricity and slightly lower inclination of the previously trapped set results in lower atmospheric entry velocities (third panel) and a higher average spatial density at 1 AU, which directly translates into a higher capture rate (bottom panel). The cometary dust particles that were previously trapped are about ten times more likely to be captured by Earth than those that were not previously trapped. Because 20% of the total population was trapped this indicates that the ratio of previously trapped to untrapped cometary IDPs in the atmosphere may be as high as 2/1. This is of particular importance when one considers the practice of classifying collected IDPs as asteroidal or cometary based upon

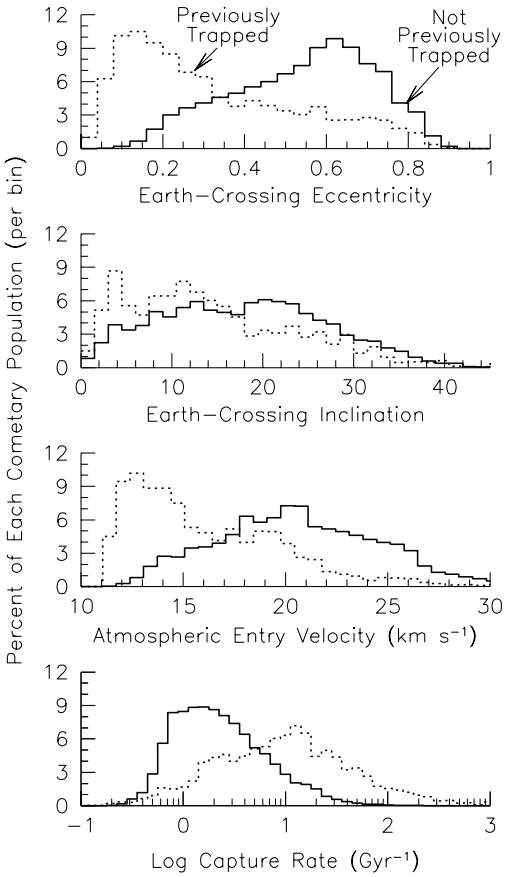

Figure 7. Comparison of two populations of Earth-crossing cometary dust particles — those that were previously trapped in mean motion resonances with Jupiter (dashed lines) and those not previously trapped (solid lines). The top two panels show the Earth-crossing eccentricity and inclination. The third panel shows the atmospheric entry velocity (${v_{\rm atm}}^2 = {v_{\rm e}}^2 + {v_0}^2$, where $v_{\rm e}$ is the escape velocity of Earth and v_0 is the encounter velocity). Dust particles in the previously trapped set have low entry velocities that are indistinguishable from entry velocities of typical asteroidal dust particles. The bottom panel shows the capture rate as given by Eq. (38). Dust particles that were previously trapped have a capture rate about 10 times higher than dust particles that were not previously trapped. Reprinted from Kortenkamp et al. (2001) with kind permission from Kluwer Academic Publishers.

their inferred atmospheric entry velocities (Flynn 1989). In fact, cometary dust particles that were previously trapped in mean motion resonances with Jupiter will have atmospheric entry velocities indistinguishable from typical asteroidal dust particles.

Once we have obtained a satisfactory cometary particle distribution we will generate a SIMUL model and use it to constrain the relative contribution of cometary and asteroidal material in the cloud. Preliminary work on this problem was discussed by Liou et al. (1995). Much work remains to be done: we must investigate a much wider range of cometary particle sizes, and then face the prospect of combining the results into some form of size distribution. Until we complete this work we must continue to extract as much information from the more tractable dynamics of the asteroidal material, and attribute the remainder of the zodiacal signal by default to cometary emission.

IV. DUST BANDS

One of the most basic of all zodiacal cloud questions, namely: "What is the relative contribution of asteroidal and cometary material?", remains perhaps the most difficult to answer. The problem is that we have little information on the dust production rates from the various sources, and even armed with this knowledge we would still be faced with unraveling the complex dynamical processes to which the particles are subject over their lifetime. Mapping of the zodiacal brightness distribution is simply not enough to constrain the problem. The Solar System dust bands (Low et al. 1984) are of fundamental importance in this regard because they are discrete features which have been unambiguously related to the breakup of asteroidal material. In particular, we argue that they are associated with the collisional debris of the Hirayama asteroid families (Dermott et al. 1984; Sykes and Greenberg 1986; Grogan et al. 1997; Reach et al. 1997) and as such they represent a unique observational constraint on the contribution of asteroidal material to the cloud.

Figure 8 shows an IRAS brightness profile of the cloud, along with the results of passing the profile through a fast Fourier filter to isolate the near-ecliptic dust band features. They appear as "shoulders" superimposed on the background emission at $\pm 10^\circ$, and a "cap" near the ecliptic plane. A dust band is a toroidal distribution of asteroidal dust particles with both common proper inclinations and common forced inclinations and nodes. The particles' common proper inclination derives from their common source in a given asteroid family, and their common forced inclinations and nodes result from the dominant perturbing force of Jupiter in the asteroid belt (as discussed in Section III). After a collisional event within an asteroid family, secular perturbations act to distribute the proper longitudes of ascending node of the particles around the sky on a timescale of order 10^5 years (Eq. 29). Since particles in inclined orbits spend a disproportionate amount of time at the extremes of their vertical harmonic oscillations, a set of such orbits with randomly distributed proper nodes will give rise to two apparent bands of particles symmetrically placed above and below the mean plane of the system (Neugebauer et al. 1984). This gives a natural explanation for the shoulders on the IRAS profiles at approximately $\pm 10^\circ$. Similarly, the central cap may be simply explained as a low inclination dust band. Any dispersion in the proper inclinations of the dust particles will

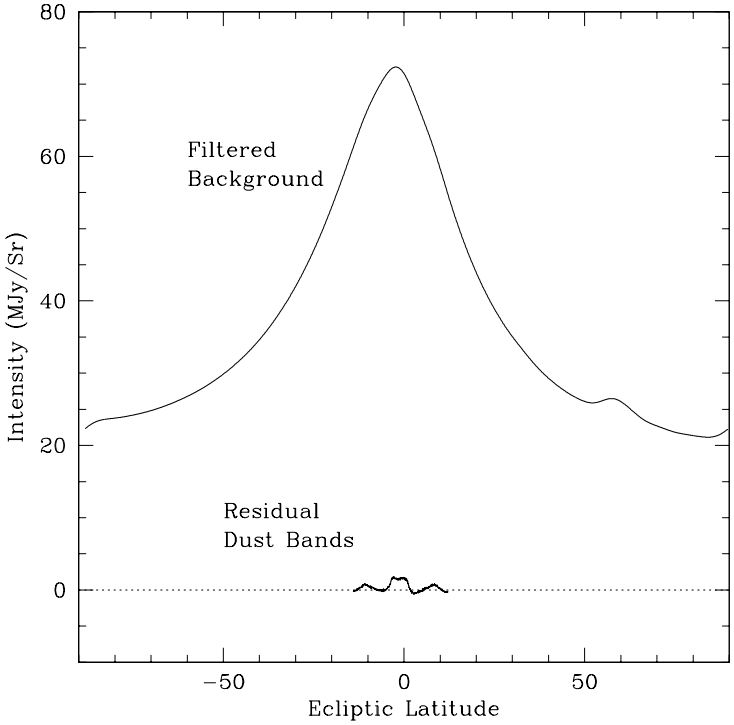

Figure 8. IRAS observation of the zodiacal cloud in the 25 μm infrared wave band. This observation was made at 90° solar elongation (the angle between the telescope pointing direction and the Earth-Sun line) in the direction leading Earth in its orbit when the planet was at an ecliptic longitude of 293°. The dust bands can be seen as projecting "shoulders" near latitudes of ±10° and 0°. The structure around 60° latitude is due to dust in the plane of the Galaxy. By applying a Fourier filter to the IRAS observation, a smooth background profile is separated from the high frequency dust band profile (shown at bottom). This filtered high frequency dust band profile is merely a residual representing the "tip of the iceberg" in terms of the dust band material in the zodiacal cloud (Dermott et al. 1994b; Grogan et al. 1997; Kortenkamp and Dermott 1998a).

lead to the dust band profile appearing broader, with the peak intensity shifted to a lower latitude (Dermott et al. 1990; Grogan et al. 1997).

Particles in cometary type orbits have high orbital eccentricities, and secular gravitational perturbations due to the planets produce large variations in these eccentricities, which are in turn coupled to variations in their inclinations (Liou et al. 1995). Therefore even if a group of cometary type orbits initially had identical inclinations, secular perturbations would disperse those inclinations over a wide range on a timescale of a few precession periods, showing that it is impossible for a comet to produce a well defined dust band.

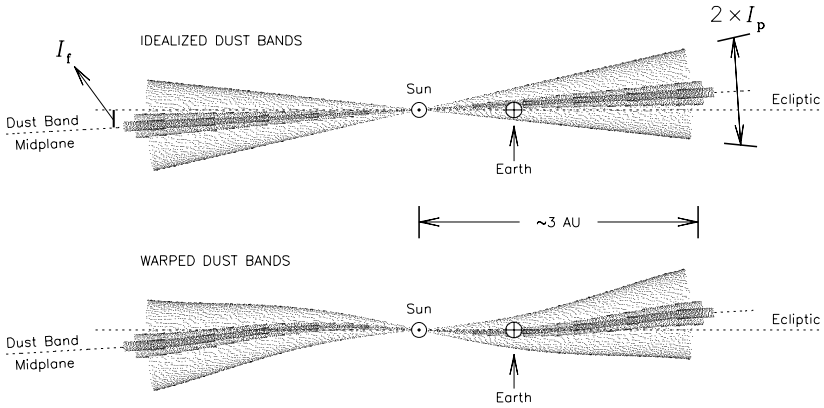

Figure 9. (Top) Cross-sections of *idealized* dust bands. Dust particles are produced by the gradual comminution of asteroid families and decay toward the Sun under the influence of drag forces. The narrow Themis and Koronis dust bands are embedded within the wider Eos dust band. The angular width of each dust band is twice the proper inclination (I_p) of its parental asteroid family. The midplane of the dust bands is inclined to the ecliptic by the forced inclination (I_f). Earth ($\oplus$) orbits the Sun within the dust bands. The spatial density of dust particles is enhanced near their extremes in latitude, which results in the "bands" of emission that were observed by the Infrared Astronomical Satellite (see Fig. 8). (Bottom) The real dust bands have warped midplanes due to variation in the forced inclination (I_f). The forced inclination is dependent on time, the semi-major axis of the decaying dust particle orbits, and on the diameter of the dust particle (see Fig. 5a). For clarity this diagram illustrates the warp obtained for a single size particle distribution at a fixed epoch. Reprinted from Kortenkamp et al. (2001) with kind permission from Kluwer Academic Publishers.

Figure 9 shows a schematic diagram of a cross-section through a dust band. The idealized dust band in the top panel has a constant forced inclination which dictates the inclination of the dust band to the ecliptic. In reality the dust bands have warped midplanes due to the variation in the forced inclination as a function of heliocentric distance, which we sketch in the lower panel. As we will discuss later, even this is a simplified picture as the forced inclinations are also a function of particle size and time, and interior to 2 AU the dispersion in the forced elements is large enough to completely degrade the integrity of the dust band structure. Figure 10 suggests the association of the dust bands with the major Hirayama asteroid families, showing the number of asteroids as a function of proper inclination with absolute visual magnitude $H < 11$. The family asteroid members are dominated by groups near 2° (Themis and Koronis) and 10° (Eos).

Dust band structures are not observed independently from the rest of the zodiacal cloud. The IRAS observations consist of a series of line of sight

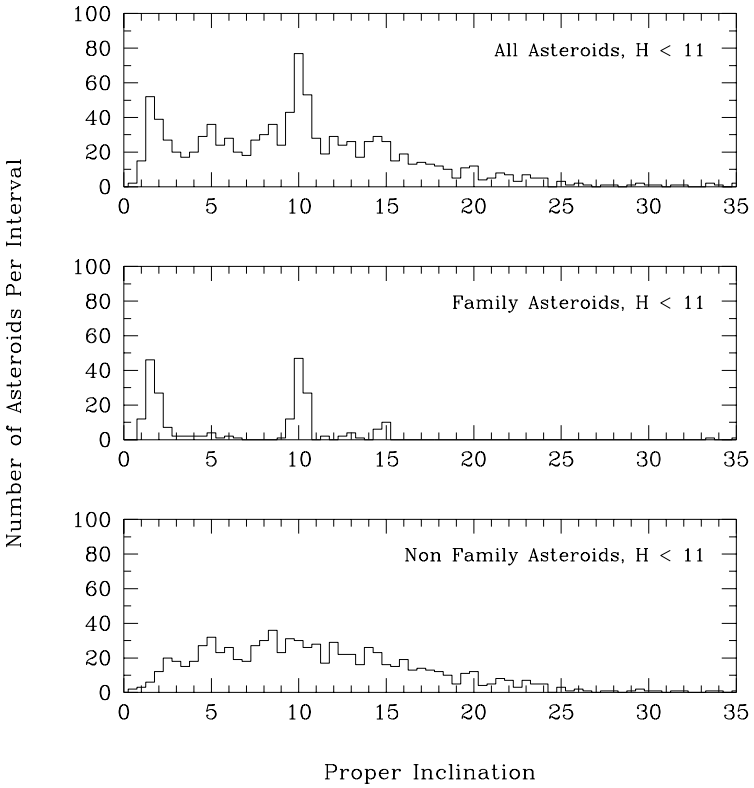

Figure 10. Histogram showing the number of asteroids versus proper inclination, $I_{\rm p}$, for all asteroids with absolute visual magnitude $H < 11$. (Top) All 1,053 asteroids in the set. (Middle and Bottom) Asteroids associated with families and not associated with families, respectively. (Middle) The enhancement near 2° is due to the Themis and Koronis families and the enhancement near 10° is due to the Eos family. The next largest family, Maria, can be seen near 15° (Kortenkamp and Dermott 1998a).

brightness profiles taken through the zodiacal cloud as a whole and to study the bands they must somehow be isolated from the remainder of the cloud. Various techniques have been employed in the literature for this purpose: box-car averaging (Sykes 1990), background subtraction (Reach 1992; Jones and Rowan-Robinson 1993) and Fourier analysis (Dermott et al. 1986; Sykes 1988; Grogan et al. 1997; Reach et al. 1997). The important point is that isolating the dust bands is an arbitrary process. Two different techniques will produce two different sets of dust band residuals. Making the assumption that the residuals obtained from any of these processes gives the complete dust band structures is simply incorrect, because in any filtering process, the low-frequency component of the dust band structures will be indistinguishable from the low-frequency background zodiacal cloud, and the high frequency residuals will be merely the

"tip of the iceberg". We have developed an iterative process (Dermott et al. 1994b; Grogan et al. 1997) to estimate the low-frequency component of the dust band using a combination of the observations and our dust band models. By using the same filter in the modeling process that we use to define the observed dust bands, and iterating, we are able to bypass the arbitrary divide associated with the filter, and extract the underlying low-frequency component of the dust bands which other techniques are unable to retrieve. This is essential in revealing the true extent to which asteroidal dust contributes to the cloud.

IV.A. IRAS Observations

The viewing geometry of the IRAS spacecraft was ideal for the study of the zodiacal cloud. The Medium Resolution ($2'$ in scan) Zodiacal Observational History File (ZOHF) consists of 5,757 sky brightness profiles, each providing a detailed view of the pole-to-pole cloud structure in a given line of sight defined by the ecliptic longitude of Earth, $\lambda_\oplus$, and the solar elongation angle, with most scans being taken at around 90° solar elongation. The changes in shape and amplitude of the dust band residuals from profile to profile are caused by a combination of the complex three-dimensional structure of the dust bands themselves and also the observing geometry of the IRAS satellite. The two primary causes for a change in the line of sight are: (i) the solar elongation angle, and (ii) the longitude of Earth. The changes due to these two parameters can be taken as independent to first order, allowing a quantitative parameter to be associated with each. Changes in elongation angle produce a parallax effect: there is a change in the effective distance to the bands, and hence in their observed peak latitude. For small changes in elongation angle the effect can be assumed to be linear. Characterizing the manner in which the brightness profiles change with elongation angle and longitude of Earth enables the thousands of individual IRAS scans to be reduced to a few representative profiles normalized to 90° solar elongation spaced around the sky in both trailing and leading directions, with an enhancement in the signal to noise ratio of more than an order of magnitude. Figure 11 plots the mean North/South peak latitude of the "ten degree" band for the normalized $25\,\mu$m scans. The sinusoidal variation indicates that the plane of symmetry of the bands, the plane about which on average the proper inclinations of the particles precess, is inclined to the ecliptic. This tilt of the plane of symmetry is due to the secular perturbations of the planets (discussed in Section III), and its orientation depends on the forced elements imposed on the dust particles. When viewed from Earth such a plane would appear as a sine curve, its amplitude equal to the inclination, $I_{\rm f}$, of the plane with respect to the ecliptic (see Fig. 9). Also, the displacement from the ecliptic will be equal in the trailing and leading directions at the ascending and descending nodes. These values are taken from Fig. 11 and listed in Table 1. Notice that for the dust band particles, the forced inclination and node are close to Jupiter's inclination and node and quite different from that of the zodiacal background cloud, strong evidence for the fact that this material is located in the asteroid belt and dominated by Jupiter's influence.

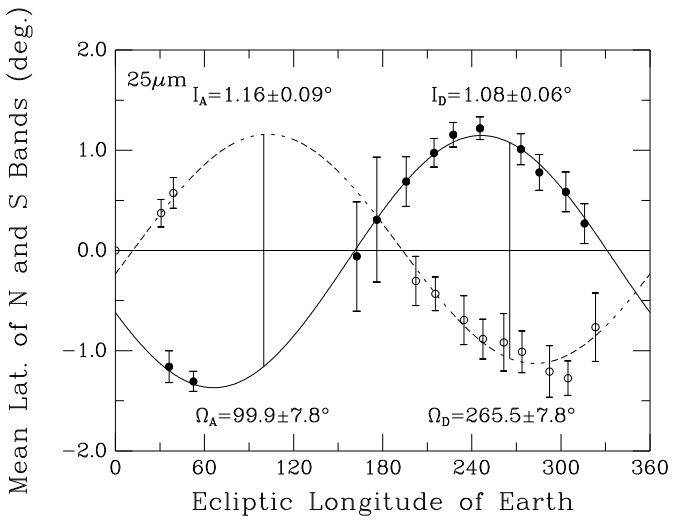

Figure 11. Variation of the latitudes of the median points separating the North and South "ten degree" bands seen by IRAS at an elongation angle of 90° in the leading (open circles) and trailing (filled circles) directions. The vertical lines, where the North and South latitudes of the midpoints are equal and opposite, are associated with the ascending and descending nodes with respect to the ecliptic (Grogan et al. 2001).

IV.B. Modeling the Dust Bands

Our approach to providing a physical model for the various components of the zodiacal cloud, including the dust bands, is essentially a two-step process. (1) Given a postulated source of particles, we describe the orbital evolution of these particles, due to Poynting-Robertson and solar wind drag, using equations of motion that also include the effects of radiation pressure and planetary gravitational perturbations. (2) Once the dust particle orbits have been specified along these lines, the distribution is visualized in three dimensions via the FORTRAN code SIMUL (Dermott et al. 1988a; Grogan et al. 1997), taking into account the thermal and optical properties of the particles and their variation with particle size. The viewing geometry of any telescope can be reproduced exactly by calculating the Sun-Earth distance and ecliptic longitude of Earth at the observing time and setting up appropriate coordinate systems. In this way, IRAS-type brightness profiles can be created and compared with the observed profiles.

This approach differs from that found elsewhere in the literature. Taking the analysis of the dust bands as an example, other authors (Sykes and Greenberg 1986; Sykes 1990; Reach 1992; Reach et al. 1997) employ simple empirical formulations for their three-dimensional structure. Interpretation of the dust band observations relies on the assumption that the spatial distribution

TABLE I.
Orientation of planes of symmetry with respect to the ecliptic (25 μm waveband).

Structural Feature	Ascending Node		Descending Node	
	Inclination	Node	Inclination	Node
Jupiter	1.31°	100.0°	1.31°	280.0°
Eos family	1.19°	97.1°	1.19°	277.1°
Themis family	1.22°	97.8°	1.22°	277.8°
Ten degree bands	1.16±0.09°	99.9±7.8°	1.08±0.06°	265.5±7.8°
Zodiacal Cloud (Ecliptic)	1.49±0.07°	58.4±2.3°	1.59±0.07°	232.8±2.3°

of material can be explained by various combinations of gaussians and power laws in which particles "migrate" into the inner Solar System from the source regions as expected by P-R drag (orbital inclinations remain constant). However no actual orbital evolution is performed, and the effects of secular perturbations on the dust particles are therefore ignored. The results of our numerical integrations show that such secular perturbations are highly significant, particularly for the larger particles (see Section III).

The availability of cheap, fast processors has recently allowed us to extend our numerical investigation of the dynamical history of dust particles to much larger sizes and enhance our previous models of the dust bands (Grogan et al. 1997) to include a size-frequency distribution (Grogan et al. 2001), rather than being restricted to particles of a single size. This is critical in our efforts to provide a model of the dust bands that can match the IRAS observations in multiple wavebands. Particles ranging in size from 1 to 100 μm are included, each of which we assume to be a Mie sphere composed of astronomical silicate (Draine and Lee 1984). We realize that particles larger than 100 μm in diameter will exist in the zodiacal cloud, but we have yet to obtain the complete dynamical history of these particles. We continue to work on the dynamics of particles up to and beyond 500 μm (some results are shown in Figs. 4 and 5), but in this regime we will have to start incorporating the effects of particle-particle collisions as the P-R drag timescales become longer than the collisional lifetimes. In addition, the nature of the size distribution will be a complex function of dust production rates, P-R drag rates, collisional lifetimes and the nature of particle-particle collisions and will, presumably, be some function of heliocentric distance.

The situation is further complicated by the fact that even if the debris of an asteroidal collision could be described by a power law, the size-frequency index q will reflect the characteristics of the parent. The equilibrium size distribution of the collisional cascade originating from a single asteroid has been shown to be a function of the impact strength of that asteroid (Durda and Dermott 1997). Thus, it is possible for the value of q associated with a given family to

TABLE II.

Dust band model parameters — proper elements and cross-sectional areas. The material originating from each family is distributed into the inner Solar System as far as 2 AU according to a $1/r$ P-R drag distribution (Grogan et al. 2001).

Asteroid family	a, Δa (AU)	e, Δe	I, ΔI (°)	Area (10^9 km^2)
Eos	3.015, 0.012	0.076, 0.009	9.35, 1.5	4.0
Themis	3.148, 0.035	0.155, 0.013	1.43, 0.32	0.35
Koronis	2.876, 0.026	0.047, 0.006	2.11, 0.09	0.35

be different from that of other families and different from the value for the background cloud. In the case of a "rubble-pile" (Davis et al. 1989), the value of q associated with the initial disruption may be significantly higher than that associated with the disruption of a solid, coherent asteroid. This provides us with further motivation to relate the dust bands to given parent bodies in the main belt. However, as a first step in answering the fundamental question of the extent to which large and small particles contribute to the dust band emission, we model the size-frequency distribution as a single power law. We will refine this assumption in the future when we have a better understanding of the role of the complicating factors outlined above.

The dust band model parameters input to SIMUL are listed in Table 2. For a given size-frequency index q, the total surface area of material associated with the model bands is adjusted until the amplitudes of the 25 μm model dust bands matches the 25 μm observations; q can then be varied until a single model provides a match in amplitude to the 12, 25 and 60 μm observations simultaneously. Figure 12 shows the best results of our modeling, comparing the dust band observations (solid curves) to the dust band models (dotted curves) in the 12, 25 and 60 μm wavebands. The models were constructed as described above, and have a size-frequency index q equal to 1.43. Large particles dominate this distribution. The amplitudes in all wavebands are well matched, and the shapes of the dust band models describe the variation in shape of the observations around the sky very well.

In essence, the wavebands act as filters through which different particle sizes in the cloud are seen. For a distribution in which the small particles dominate the total surface area ($q > 5/3$, Dohnanyi 1969), the 12 μm waveband preferentially detects emission from the smaller particles, and the 60 μm waveband preferentially detects emission from the larger particles. When q is too high, too many small particles are included in the model, and the amplitudes of the 12 μm models are too large. In addition, too few large particles are included and the amplitudes of the 60 μm models are too small. For a distribution in which large particles dominate ($q < 5/3$), it becomes difficult to discriminate the exact value of q since the particles in the distribution radiate like grey bodies (Gustafson 1994).

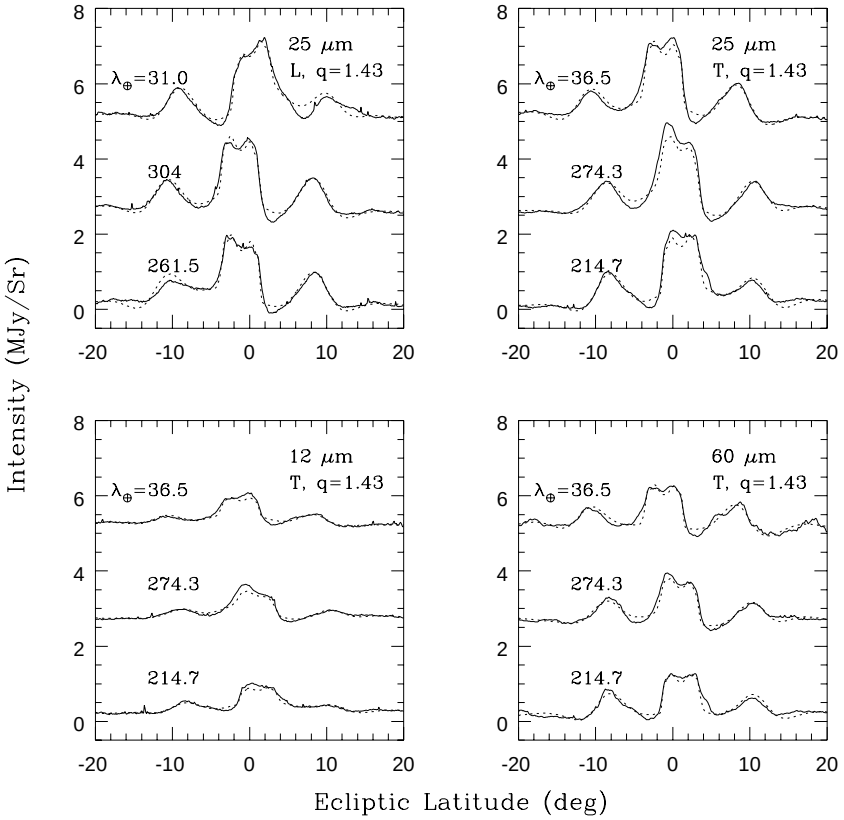

Figure 12. Filtered IRAS dust band profiles (solid lines) in three wavebands are compared with models with a size-frequency distribution, $q = 1.43$. All profiles were made at 90° solar elongation angle in a direction either leading (L) or trailing (T) the Earth in its orbit. The model dust bands (dashed curves) were constructed using particles from the Themis and Koronis families for the central band pair and from the Eos family for the 10° band pair. A dispersion of 1.5° was imposed on the proper inclination of the Eos material in this model and all of the material was confined to the asteroid belt ($2.0\,\mathrm{AU} < a < 3.1\,\mathrm{AU}$). The low value of $q(< 1.66)$ implies that the dominant particles are large (diameters $\lesssim 10^3\,\mu$m). Adapted with permission from Grogan et al. (2001).

A clear result from our modeling is that a high size-frequency index q, in which small particles dominate, fails to account for the observations of the Solar System dust bands. This index has to be reduced to the point where large particles dominate the distribution, and we place an upper limit of $q = 1.4$. This is consistent with the cratering record on the LDEF satellite (Love and Brownlee 1993) which suggests a q of approximately 1.15 at Earth and a peak in the particle diameter at around 100–200 μm. Since the Fourier filter

preferentially isolates material exterior to the 2 AU secular resonance (in the inner Solar System the dust band material is dispersed into the background cloud due to the action of secular resonances), our results are more indicative of the size-frequency index of dust in the asteroid belt.

IV.C. The Importance of Secular Perturbations

The origin of the large dispersion in proper inclination (1.5°) required to successfully model the ten degree band (see Table 2), in rough agreement with the 1.4° found by Sykes (1990) and the 2° found by Reach et al. (1997), remains unclear, although the most likely source of the dispersion is simply the action of the secular resonance at 2 AU. However, this leaves open the question of why a large dispersion is required to model the ten degree band, and only the small dispersion of the Themis and Koronis families is required to successfully reproduce the central band observations. One answer may be that the emission associated with the central band is due to relatively recent collisions within these families. Figure 13 shows the variation with time of the total cross-sectional area associated with the main belt and describes the stochastic breakup of asteroidal fragments. This numerical approach to describing the collisional evolution of the asteroid belt is detailed by Durda and Dermott (1997). The initial main belt mass is taken to be approximately three times greater than the present mass (Durda et al. 1998); this population evolves after 4.5 Gyr to resemble the current main belt. The calculation is performed for particles from 100 μm through the largest asteroidal sizes, with a fragmentation index $q = 1.90$. The dust production rate in the main asteroid belt becomes more stochastic with time following a relatively smooth decrease in area as the small particles created directly from the breakup of the parent body are destroyed. The "spikes" in the dust production are due to the breakup of small to intermediate size asteroids. Therefore while the observable volume of a family may decay at a fairly constant and well-defined rate, the total area of dust associated with the family during that time may fluctuate by an order of magnitude or more.

As the particles move out of the asteroid belt the action of secular resonance disperses them into the background cloud. The integrity of the dust band is lost as the forced inclinations increase and the forced nodes are spread around the sky (Fig. 5a), an effect which is more marked as the particle size increases. We find that models confining the material to the asteroid belt (exterior to 2 AU) match the observations very well. In the future, our models will populate the inner Solar System as well as the main belt region, and the dust bands will disperse naturally into the background cloud. To do this properly we will have to: (i) investigate the dynamical history of a much greater range of particle sizes than we have considered so far in order to properly account for their behavior at the 2 AU secular resonance; and (ii) take into account collisional processes, as larger particles will have shorter collisional lifetimes compared to their P-R drag lifetimes and will therefore not penetrate as far into the inner Solar System.

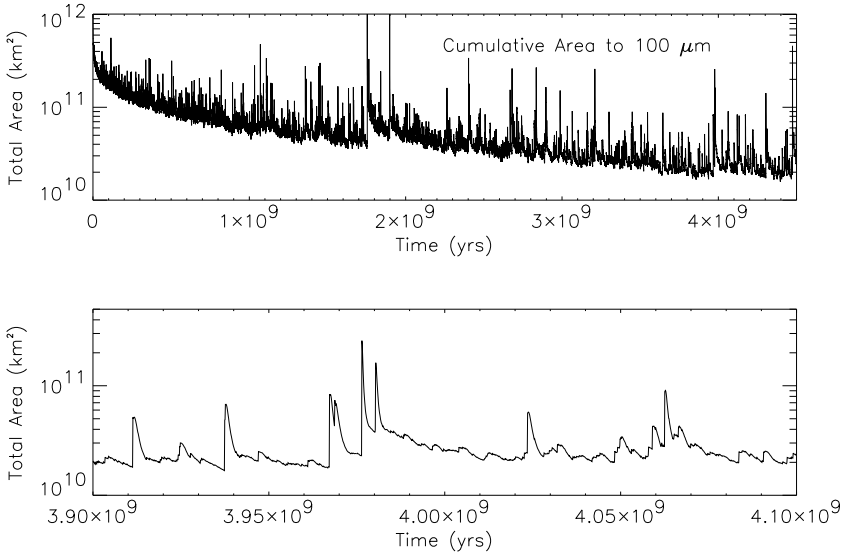

Figure 13. Variation with time of the total cross-sectional area of dust associated with the breakup of an asteroid that was big enough to supply all the observed collision products of the belt. A size-frequency distribution q of 1.9 was assumed for the initial breakup of each asteroid and this accounts for the heights of the "spikes" in the plots (Grogan et al. 2001; adapted from Durda and Dermott 1997).

However, we can obtain an estimate for the dust band contribution to the zodiacal cloud as a whole by simply extending our best fit dust band models to populate the inner Solar System. The distribution of orbits obtained in this manner will not be exactly correct, due to our insufficient treatment of the secular resonance, but will still be reasonably accurate in terms of the total surface area associated with the dust bands. Figure 14 compares the thermal emission obtained from this raw dust band model to the corresponding IRAS profile in the 25 μm waveband. The result is shown for inner Solar System distributions of material corresponding to $1/r^{\gamma}$ where $\gamma = 1.0$, as expected for a system evolved by P-R drag, and $\gamma = 1.3$ as predicted in parametric models of the zodiacal cloud, most recently by Kelsall et al. (1998). The dust bands appear to contribute approximately 30% to the total thermal emission. Also shown is the amplitude of the dust band material confined to the main belt (exterior to 2 AU), which represents the component of the dust band material isolated by the fast Fourier filter. This indicates that approximately 4% of the in-ecliptic infrared emission from the zodiacal cloud is produced by dust band particles that orbit exterior to 2 AU, and also clearly demonstrates the extent to which the dust band contribution is underestimated if it is assumed that the filtered dust band observations represent the entirety of the dust band component of the cloud.

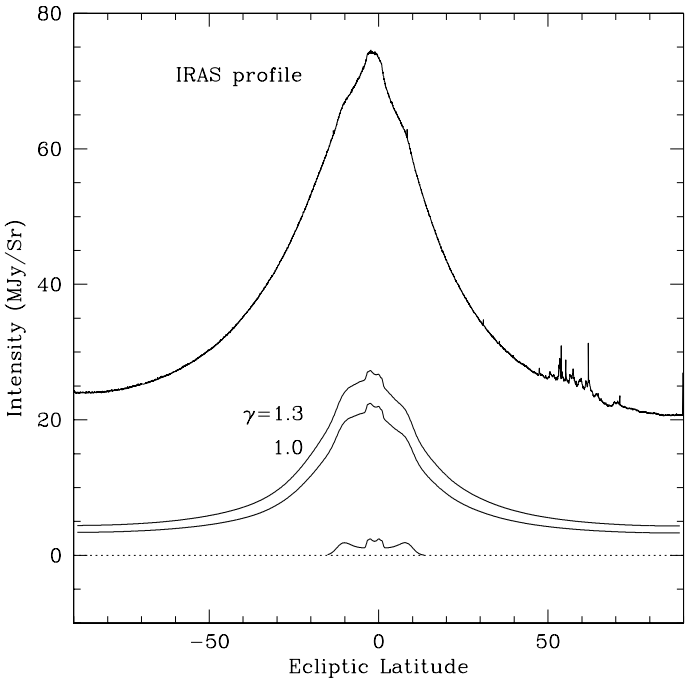

Figure 14. Contribution to the unfiltered IRAS 25 μm wave band observation shown at the top due to three simulated unfiltered profiles taken through three different dust band models. Each of the models was constructed using particles from only three asteroid families: Eos, Themis and Koronis. The model with the smallest amplitude refers to material confined to the asteroid belt. The other two models (labeled $\gamma = 1.0$ and $\gamma = 1.3$) contain, in addition, asteroidal material that has migrated towards the Sun due to Poynting-Robertson light drag (Grogan et al. 2001).

Figure 15 shows the ratio of areas of material associated with the entire main belt asteroid population and all families, for asteroid diameters greater than 1 km. The best fit lines have a slope corresponding to a size-frequency index $q = 1.795$. This diagram can be used to estimate the total contribution of main belt asteroid collisions to the dust in the zodiacal cloud, by extrapolating the observed size distributions of larger asteroids in both populations assuming a collisional equilibrium power law size distribution. The result is that the main belt asteroid population contributes approximately three times the dust area of the Hirayama families alone, and the total asteroidal contribution to the zodiacal cloud could account for almost the entirety of the interplanetary dust complex (Grogan et al. 2001). In reality, evolved size distributions are more complex than simple power laws (Durda et al. 1998) and the size distribution of individual asteroid families likely preserve some signatures of the original fragmentation events from which they were formed. However, small dust-size

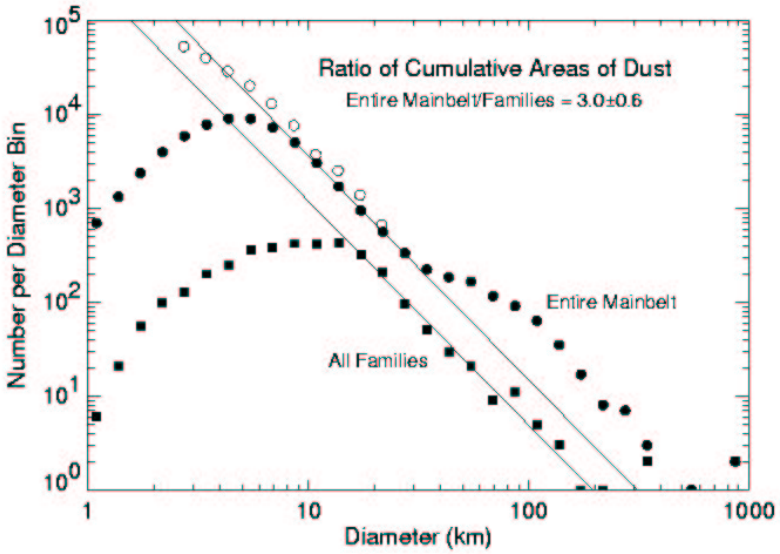

Figure 15. Diameter-frequency diagram for the main belt asteroid population, obtained by combining data from the catalogued population and McDonald/Palomar-Leiden surveys (MDS/PLS). Open points represent counts for which the PLS data had to be corrected for incompleteness. These were not included in the least-squares fits to the linear portion of the distribution. The ratio of the area of dust associated with the entire main belt asteroid population to that of the asteroid families alone was calculated to be 3.0 ± 0.6 (Grogan et al. 2001; updated from Durda and Dermott 1997).

particles and their immediate parent bodies have collisional lifetimes in the main belt that are considerably shorter than the age of the Solar System or the major asteroid families. Thus the dust size distributions associated with both the background main belt and family asteroids may well be considered to have achieved an equilibrium state, with total areas related to the equivalent volumes of the original source bodies in each population. However, to arrive at a more quantitative solution we need to apply our methods to the main belt asteroid population in the same way we have investigated the dust bands. This is an ongoing investigation.

IV.D. Equilibrium vs. Non-Equilibrium

Figure 16 shows the members of the Eos asteroid family in (e, I) space as determined by the hierarchical clustering method (Zappalà et al. 1995). Shown on this diagram is the position of the mean proper inclination of the ten degree band model. The consequence is that the ten degree dust band material is not tracing the orbital element space of the Eos family as a whole, as would perhaps be expected from the equilibrium model (Dermott et al. 1984) in which

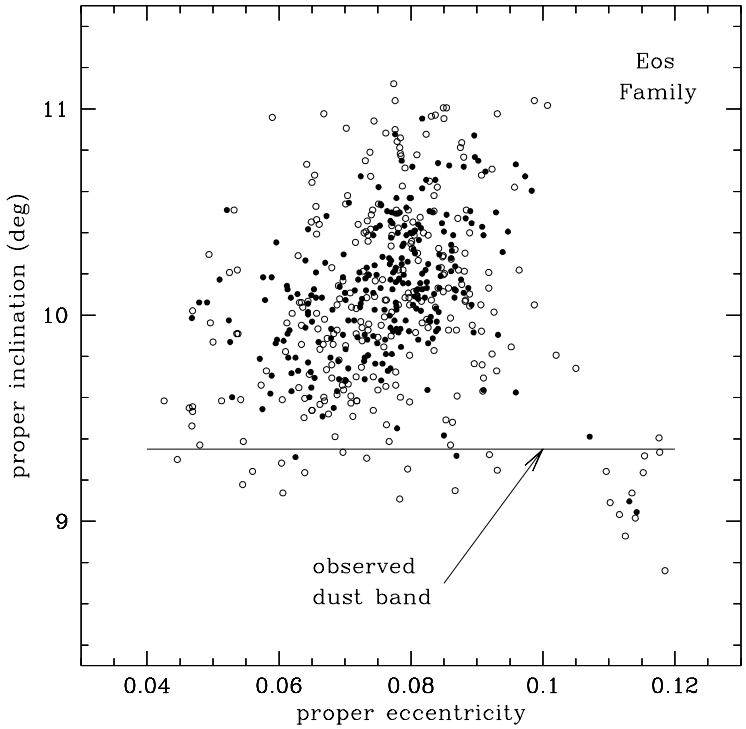

Figure 16. Proper inclination, I_p, and proper eccentricity, e_p, of asteroids in the Eos family. Asteroids with diameters > 15 km are shown with filled circles. Our model dust band that best fits the observed "ten degree" band has a proper inclination of $9.35°$, well below the mean of the Eos family (Grogan et al. 2001).

the dust bands represent the continual grinding down of family asteroids. On the surface this appears to be evidence for a catastrophic (non-equilibrium) origin for the band (Sykes and Greenberg 1986), the dust bands being produced from the disruption of random main belt asteroids. But our results have shown that the structure of a dust band, shaped from the dynamical history of its constituent particles of varying sizes, is much more complex than previously thought. Two important points should be kept in mind here: (i) the action of the secular resonances serves to disperse the inclinations and nodes of the particles (as demonstrated in Section III); and (ii) the grinding down of an asteroid family, as we have modeled and shown in Fig. 13, is a stochastic process. With regard to the first point, the observed latitude of the dust band will decrease as the dispersion of the particle's inclinations and nodes increases. This effect has not yet been fully characterized. The second point leads us to conclude that spikes in the dust production rate correspond to the breakup of individual asteroids, and can therefore originate from any asteroid within the family. The dust band associated with the family, produced by the fresh

injection of material from the most recent fragmentation, may therefore shift in latitude over time to reflect the orbital characteristics of its parent.

Our modeling predicts the amount of cross-sectional area required to produce the dust bands. Can this amount be provided by a relatively small (15 km) asteroid? Figure 17 shows the cumulative surface area as a function of different size-frequency distribution indices for the Eos, Themis and Koronis families and also a single 15 km diameter asteroid. At first this appears to contradict our result that a low q of at most 1.4 is needed to model the dust bands. However, the diagram as set up is indicative of the disruption process, such that the size-frequency distribution is constant from the source body all the way down to the smallest particles. Our result reflects the size distribution imposed by the combination of the dust production, P-R drag flow, and particle-particle collisions. The diagram does suggest that for a single asteroid to be responsible for the ten degree dust band, the size-frequency index of the collisional debris would initially have needed to be extremely high, well over 1.90, to produce the surface area required to match the observations. Perhaps if the initial parent body was a rubble-pile (Davis et al. 1989) rather than a single body, more small material and therefore a high q distribution would be produced. Again, the question is difficult to answer because the problem is poorly constrained, in this case because we have little information on the disruption process.

V. BACKGROUND CLOUD

We showed in the previous section how using a Fourier filter can separate the high-frequency dust band residuals from the smooth, low-frequency "background cloud" (Fig. 8). The dust bands are of great interest because they are features that have been attributed with confidence to main belt asteroids. But it is clear that the background cloud provides the majority of the zodiacal emission (albeit including significant low-frequency components from the dust bands and Earth's resonant ring), and much can be learnt from a study of its structure, especially since the observing geometry changes throughout the year as the Earth moves around its elliptical orbit. Mid-IR geocentric satellite observations (such as the IRAS and COBE observations) clearly show that the cloud is inclined to the ecliptic, that its axis of rotational symmetry is offset from the Sun, and that it is warped. Here we will discuss these observations and their dynamical consequences.

V.A. Tilt, Warp and Offset

Figure 18 shows how the plane of symmetry of the background cloud may be found. The two curves represent the variation of the latitude of peak brightness of the background cloud with ecliptic longitude of Earth, in directions both trailing and leading the Earth at 90° solar elongation. If the plane of symmetry of the cloud was the ecliptic, the latitude of peak brightness would remain constant and in the ecliptic plane. However, the observations give a sinusoidal variation. The points at which the latitudes of peak intensity are equal and

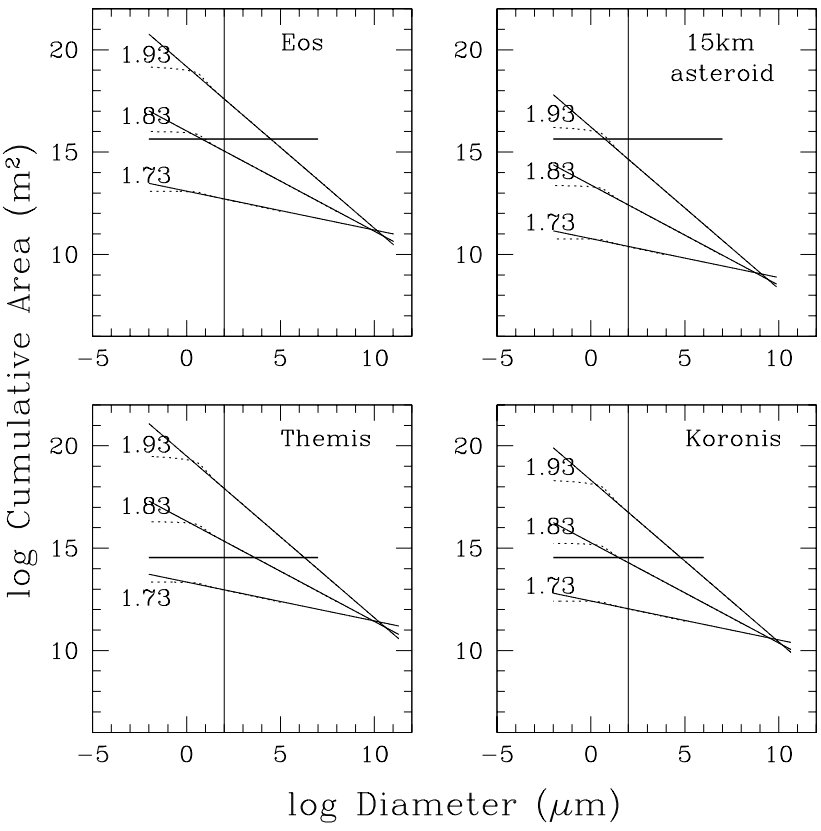

Figure 17. Cumulative area of dust associated with the Zappalà et al. (1995) Eos, Koronis and Themis families for three values of the size-frequency index q. The solid lines represent the geometrical area, while the broken lines are the cross-sectional area of emission calculated for spheres of astronomical silicate of density 2,500 kg m^{-3} calculated using Mie theory. In each panel, the cumulative area of dust from each family (Table 2) needed to model the IRAS observations of the dust bands is represented by a heavy, horizontal line. A vertical line corresponding to a diameter of 100 μm is shown for reference. We also show the area of dust associated with the breakup of a 15 km diameter asteroid. If the "ten degree" band was formed from the disruption of such an asteroid, the size-frequency index q of the collisional debris would have had to be very high, well over 1.90, to account for the amplitude of the band in the IRAS observations (Grogan et al. 2001).

opposite in the leading and trailing directions give the nodes of the cloud; the magnitude of the latitude at these points gives the inclination of the cloud with respect to the ecliptic. The diagram suggests that the inclination of the cloud to the ecliptic is equal to $1.49 \pm 0.07°$, and the longitude of ascending node is $58.4 \pm 2.3°$ (Dermott et al. 1996a).

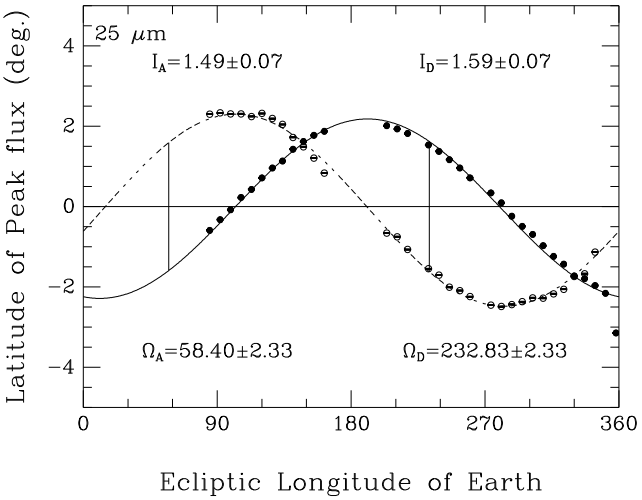

Figure 18. Variation of the latitude of peak flux of the zodiacal cloud with ecliptic longitude of Earth in the trailing (solid curve) and leading (dotted curve) directions derived from COBE observations in the 25 μm wave band. Reprinted with permission from Dermott et al. (1996a). Copyright 1996, American Institute of Physics.

Figure 19 (left) shows the variation of the brightnesses of the ecliptic poles with ecliptic longitude of the Earth (Dermott et al. 1999). The North and South polar brightnesses are equal when the Earth is at either the ascending ($70.7 \pm 0.4°$) or descending node of the local plane of symmetry (at 1 AU) of the cloud. This is in contrast to the result found earlier from the latitudes of peak intensity of the cloud in the trailing and leading directions, that gave a result of $58.4°$. Since the latter observations sample the cloud external to 1 AU, this implies that the plane of symmetry of the zodiacal cloud varies with heliocentric distance, i.e., that the zodiacal cloud is warped (shown schematically in Fig. 9).

Figure 19 (right) shows an attempt to model the variation in polar brightness using a purely asteroidal model for the background cloud (Dermott et al. 1996b). The source population for the model particles are the main belt asteroids, and the material is distributed through the inner Solar System as expected by Poynting-Robertson drag. The total surface area in the model is scaled such that the peak ecliptic brightness of the model matches the peak ecliptic brightness of the observations. It is evident that this model fails to account for the flux observed at 1 AU and falls short by a factor of ~ 2. This is another route (in addition to the dust bands) by which we can answer the question of the relative contribution of asteroidal and cometary material: by combining such asteroidal and cometary models we can discover which combination provides the best fit to the observations. Early attempts have been published (Liou et al. 1995) which suggest a cometary:asteroidal ratio of about 3:1, but these results suffer from the fact that the asteroidal and cometary models were extremely

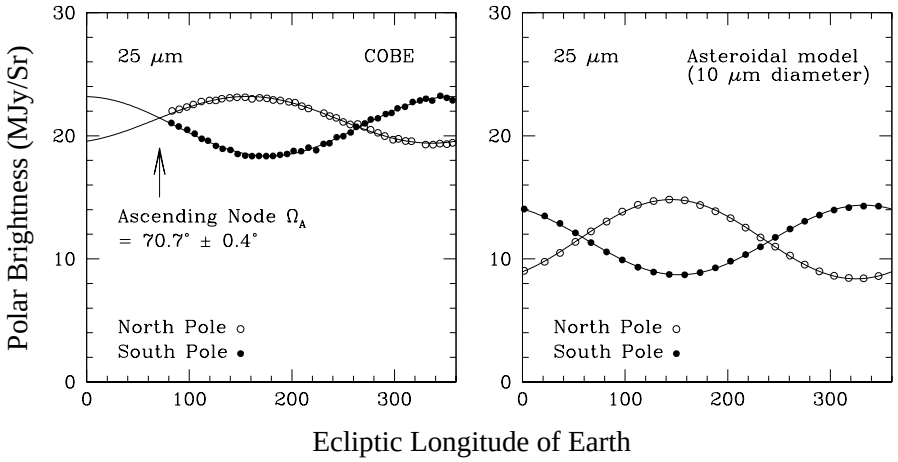

Figure 19. (Left) COBE observations of the North (open circles) and South (filled circles) polar fluxes obtained from observations in the 25 μm wave band. Reprinted from Dermott et al. (1999) with kind permission from Kluwer Academic Publishers. (Right) Polar flux predicted by an asteroidal model of the background zodiacal cloud based on single size astronomical silicate particles of diameter 10 μm. The model flux has been normalized to match the peak ecliptic flux observed in the leading direction with a solar elongation angle of 90°. Adapted from Dermott et al. (1996b) by kind permission of the Astronomical Society of the Pacific.

limited. The asteroidal model employed by Liou et al. (reproduced in Fig. 19), was composed only of 10 μm diameter particles, and we have shown that the distribution of the various size particles in the cloud varies significantly due to the secular perturbations (see Fig. 5). The amplitudes of the sinusoidal variations are also too large (once the absolute fluxes are scaled to the observations), suggesting that the 10 μm asteroidal model gives the incorrect mean forced inclination at 1 AU (the inclination of the plane of symmetry of the cloud with respect to the ecliptic). The distribution of material may also vary from the assumed $1/r$, for example, if additional surface area is produced by collisions in the inner Solar System then the asteroidal model would better describe the observations. In addition the sole source for the cometary model of Liou et al. was Comet P/Encke. We are working on producing a more complete description of the material originating from both asteroids (by increasing the range of particle sizes included) and from comets (by adopting a much more complete inventory of the cometary population).

In Table 1 we have summarized the results for the planes of symmetry with respect to the ecliptic for several features of the Solar System. In addition to the conclusions drawn about the structure of the background cloud from these results, the data provide support for the localized nature of the dust band material separated from the background by the Fourier filter. The observed

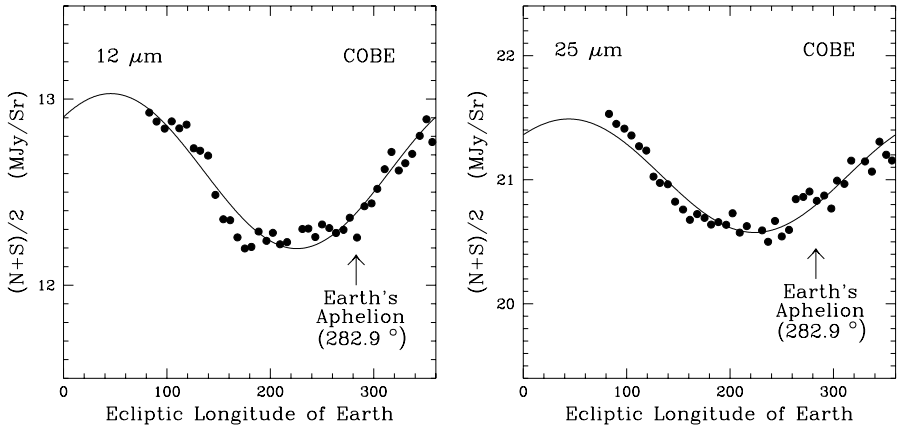

Figure 20. Variation of the mean polar brightness, (North + South)/2, as a function of ecliptic longitude of Earth, in both the 12 μm (left) and the 25 μm (right) COBE wave bands. Clearly, the minimum in the mean polar brightness does not occur at Earth's apocenter, indicating that the center of symmetry of the zodiacal cloud is offset from the Sun (Dermott et al. 1998, 1999; Holmes et al. 1998). Reprinted from Dermott et al. (1999) with kind permission from Kluwer Academic Publishers.

plane of symmetry of the ten degree band is quite distinct from that of the background cloud, but is closely similar to that of the asteroid families in the outer part of the main belt.

Figure 20 shows COBE observations of the sum of the brightnesses in the 12 and 25 μm wavebands at the North and South ecliptic poles, $(N+S)/2$ (Dermott et al. 1998, 1999; Holmes et al. 1998), where there is no contamination from the galactic plane. If the zodiacal cloud was rotationally symmetric with the Sun at the center, then the cross-sectional area density of particles in the near Earth region would vary according to $\sigma(r, \theta, \phi) \propto r^{-\gamma} f(\phi)$, where r is radial distance from the Sun, θ is azimuth, ϕ is latitude, and γ is a constant. Because the Earth's orbit is eccentric, geocentric observations sample the zodiacal cloud at different radial distances from the Sun. Thus, the minimum of the $(N+S)/2$ observation is expected to occur either at the Earth's aphelion, $\lambda_\oplus = 282.9°$, or perihelion, $\lambda_\oplus = 102.9°$, depending on whether $\gamma > 1$ or $\gamma < 1$, which is determined by the collisional evolution of particles in the near-Earth region (e.g., Leinert and Grün 1990, discuss the observational evidence and conclude that $\gamma \approx 1.3$ as found by the Helios zodiacal light experiment). However, the minimum in the 25 μm waveband observations occurs at $\lambda_\oplus = 224°$, and a similar result is found in the 12 μm waveband (the close similarity of these two curves is further evidence that the dominant particle diameter is large). This is expected only if the Sun is not at the center of symmetry of the zodiacal cloud. Parametric models of the zodiacal cloud have also shown the need for an offset to explain the observations (e.g., Kelsall et al. 1998).

Changes in the heliocentric distance of the Earth over the course of the year (due to its eccentric orbit) also provides an opportunity to compare the observed variation of the polar flux with heliocentric distance to theoretical values appropriate for asteroidal and cometary distributions (the polar flux gradient is a strong function of the eccentricity of the dust particle population at 1 AU, and can be observationally estimated from Fig. 20 by dividing the ratio of the amplitude to the mean of the sine curve by the Earth's eccentricity). Preliminary work (Dermott et al. 1999) showed that the observed polar flux gradient is indicative of a predominantly asteroidal distribution, but we have already shown that secular perturbations will strongly affect the distributions of both asteroidal (see Section III) and cometary material (see discussion in Section IV) at 1 AU. A more accurate qualitative result will follow from our ongoing investigation of the dynamical history of both asteroidal and cometary dust particles.

V.B. Physical Understanding of the Asymmetries

The effect of secular perturbations on the structure of a disk can be understood by considering the effect of the secular evolution of the constituent particles' orbits on the distribution of their orbital elements. The discussion in Section III shows that secular perturbations affect only the distribution of disk particles' complex eccentricities, $n(z)$, and complex inclinations, $n(y)$, while having no effect on their size distribution. However, secular changes in the eccentricity do affect the orbital decay rate (see Eq. 11) and this in turn affects the radial distribution of material.

In Section III, it was shown that the P-R drag affected particles in the zodiacal cloud have a distribution of complex eccentricities, $n(z)$, that lie on a circle. This means that the distribution of pericenters is biased towards the orientation in the disk that is defined by $\varpi_{\rm f}$. The consequence of this biased orbital element distribution on the spatial distribution of this family material is best described with the help of Fig. 21 (right). This shows a face-on view (i.e., perpendicular to the plane of symmetry), of the family material in orbit around a star S. The resulting disk is made up of particles on orbits that have the same a, $e_{\rm f}$, $\varpi_{\rm f}$, and $e_{\rm p}$, but random $\varpi_{\rm p}$. The contribution of each particle to the spatial distribution of material in the disk can be described by an elliptical ring of material coincident with the particle's orbit. These elliptical rings have been represented by uniform circles of radius a, with centers that are offset by ae in a direction opposite to the pericenter direction, ϖ (this is a valid approximation to first order in the particles' eccentricities); a heavy line is used to highlight the orbital ring with a pericenter located at P, and a displaced circle center located at D, where $DP = a$. The vector SD can be decomposed into its forced and proper components; this is shown by the triangle SCD, where $SD = ae$, $SC = ae_{\rm f}$, and $CD = ae_{\rm p}$ (there is a similar triangle in Fig. 21 (left)). Given that the distribution of $\varpi_{\rm p}$ is random, it follows that the distribution of the rings' centers, D, for the family disk are distributed on a circle of radius $ae_{\rm p}$ and center C. Thus, the family forms a uniform torus of inner radius $a(1 - e_{\rm p})$

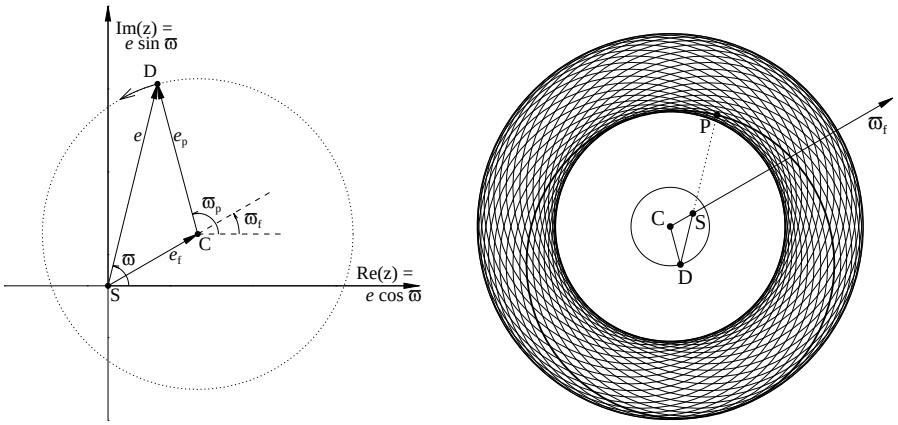

Figure 21. (Left) The osculating (instantaneous) eccentricity, e, of the orbit of a dust particle can be resolved vectorially into two components: a forced eccentricity, $e_{\rm f}$, imposed by the perturbers in the system; and a proper eccentricity, $e_{\rm p}$, that is determined by initial conditions. The corresponding osculating, forced and proper longitudes of pericenter, ϖ, $\varpi_{\rm f}$ and $\varpi_{\rm p}$ define the orientation of the orbit with respect to an arbitrary fixed direction. (Right) Shown here is an idealized disk of dust around a star S. The disk particles all have the same a, $e_{\rm f}$, $\varpi_{\rm f}$, $e_{\rm p}$ but random $\varpi_{\rm p}$ leading to variable osculating e, ϖ. To first order, the elliptical orbits can be represented by circles of radius a whose centers are offset by ae in a direction opposite to the pericenter direction, ϖ. A heavy line is used to highlight one orbit with pericenter P and displaced circle center D, where $DP = a$. The location of the center D can be decomposed into its two components shown by the triangle SCD with sides $SD = ae$, $SC = ae_{\rm f}$ and $CD = ae_{\rm p}$ correspond to a similar triangle in the panel on the left. Given that the distribution of $\varpi_{\rm p}$ is random, it follows that the points D for all the dust particles in this idealized disk will be distributed on a circle of radius $CD = ae_{\rm p}$ and center C. Thus, the disk forms a uniform torus of inner radius $a(1 - e_{\rm p})$ and outer radius $a(1 + e_{\rm p})$ centered on a point C displaced from the star S by a distance $ae_{\rm f}$ in a direction away from the forced pericenter, $\varpi_{\rm f}$ (Wyatt et al. 1999b). Adapted from Dermott et al. (1985) with kind permission from Kluwer Academic Publishers.

and outer radius $a(1+e_{\rm p})$ centered on a point C displaced from the star S by a distance $ae_{\rm f}$ in a direction away from the forced pericenter, $\varpi_{\rm f}$ (Dermott et al. 1985; Dermott et al. 1998).

The distribution of the complex inclinations, $n(y)$, of these particles, is also the distribution of their orbital planes. Changing the reference plane relative to which the particles' orbital inclinations are defined to that described by $y_{\rm f}$, shows that the secular complex inclination distribution of this family material leads to a disk that is symmetrical about the $y_{\rm f}$ plane; the opening angle of this disk is described by $I_{\rm p}$. If the $y_{\rm f}$ plane varies with heliocentric distance, as indeed it was shown to do in Section III, the resulting disk appears warped

(see Fig. 9). The distribution of nodes is biased towards the orientation in the disk that is defined by Ω_f.

V.C. Application to Circumstellar Disks

Observations of the disk of dust around HR4796A (Telesco et al. 2000) show a double-lobed feature, consistent with observations of a nearly "edge-on" disk of dust with a central clearing hole that is almost completely devoid of dust. The images obtained also show that the NE lobe is 5% brighter than the SW lobe; an asymmetry that could be due to gravitational perturbations by seen or unseen companions. Our modeling of the disk (Wyatt et al. 1999b), as well as accounting for the large-scale symmetrical structure, shows how a forced eccentricity imposed on all disk particles would be expected to produce the lobe brightness asymmetry. As outlined above, the center of symmetry of particles at the inner edge of the disk (those that contribute most to the flux) is offset, so that particles in the forced pericenter direction are closer to the star than those at the forced apocenter, so these particles are hotter and emit more flux. This is the so-called "pericenter glow" phenomenon, and reveals the presence of a perturbing body in the system. HR4796 is a binary system, but the orbit of the companion star is poorly constrained (the orbital period of the star is estimated at 7,000 years). Therefore we cannot definitively say whether the observed asymmetry is due to the companion or alternatively a planet or planets embedded in the disk. If the perturber in the system is a planet then depending on its location it would give rise to a detectable pericenter glow for even low eccentricity orbits. The only constraint on the planetary mass, $M_{\rm pl}$, is that the disk must be older than the time it takes for the secular perturbations to build up, an approximation for which is the precession period, $t_{\rm prec} = 2\pi/A \propto 1/M_{\rm pl}$. In this system we find that for secular perturbations to have built up at the edge of the disk, $M_{\rm pl} > 10\,M_\oplus$, where the mass of the Earth $M_\oplus = 3 \times 10^{-6} M_\odot$, but for older systems this mass limit would be lower. If there are two or more perturbers in the system then the forced element variation with semi-major axis will depend on both the mass of the perturbers and the orientation of their orbits. Such a variation could cause the disk to be warped, as discussed above.

The brightness asymmetry in HR4796A does not have high statistical significance, but we have shown here that if moderately sized planets in moderately eccentric orbits are present, then such asymmetries are to be expected. HR4796A was observed with the infrared imager OSCIR for only one hour on Keck II. Given that the significance level of any asymmetry will increase at a rate $\propto \sqrt{t}$, one good night on a 10 m telescope would settle the question of whether this asymmetry is real, and if so set some constraints on the planets that may be causing it. The measurement of such asymmetries and the detection of the presence of planets, even small planets, in circumstellar disks is clearly now within our reach. For a review of circumstellar disk structure see, for example, Beckwith (1999).

VI. RESONANT RING

Over the past 30 years or more, the possibility of resonant trapping of dust particles by the Earth and other planets has been discussed by several authors, including Schmidt (1967), Gold (1975) and Jackson and Zook (1989), but no observational evidence was found to support these discussions. In 1983, the IRAS spacecraft gave us our highest resolution data on the structure of the zodiacal cloud. Dermott et al. (1988a) analyzed these data and pointed out a marked but peculiar asymmetry, namely that the peak brightness of the cloud in the trailing direction, opposite to the Earth's orbital motion, is consistently greater than that in the leading direction. This finding was later confirmed by Reach (1991) who concluded that either there is a calibration inconsistency between the leading and trailing IRAS scans, or there is an enhancement in dust density that follows the Earth around the Sun, and that this could be related to the resonant trapping described by Jackson and Zook (1989), or could be due to gravitational focusing. In 1994, we showed that if asteroidal collisions are a significant source of zodiacal dust, then a trailing/leading asymmetry of the zodiacal cloud due to resonant trapping is to be expected, and that the asymmetry observed by IRAS is quantitatively consistent with predictions based on our numerical investigation of the resonant trapping of asteroidal dust particles, that is, particles with low orbital eccentricities (Dermott et al. 1994a).

Figure 22 shows the more complete COBE observations (in four infrared wavebands) of the peak, near-ecliptic flux of the smooth (filtered) zodiacal background at a constant solar elongation of 90°, as function of the ecliptic longitude of the Earth. There are at least three reasons why the peak brightness of the zodiacal cloud should vary with ecliptic longitude when viewed at a constant elongation angle. Variations are expected to arise from: the forced eccentricities of the dust particle orbits which produce a displacement of the Sun from the center of rotational symmetry (Fig. 20); from the inclination of the plane of symmetry of the cloud with respect to the ecliptic which produces a double sine variation (see Dermott et al. 1996a); and from the Earth's orbital eccentricity (Fig. 20). The curves fitted to the data in Fig. 22 are a combination of sine and double sine components only (Dermott et al. 1996a; Jayaraman and Dermott 1996a), and the mean difference between the two curves for the leading and trailing directions is a measure of the flux asymmetry. This asymmetry is present in all four wavebands, but is seen most clearly in the $25\,\mu$m waveband. In the $12\,\mu$m waveband, the peak-to-peak difference between the trailing and leading curves is as high as $\sim 10\%$. This fact, coupled with the large differences in the shapes of the curves seen in the four wavebands, makes it difficult to confirm the existence of a mean trailing brightness excess of $\sim 3\%$ by subtracting a simple model of the background cloud from the COBE data, as attempted by Reach et al. (1995). It is our opinion that, at present, we do not have a model of the background cloud in the various wavebands that is good at the $\sim 3\%$ level.

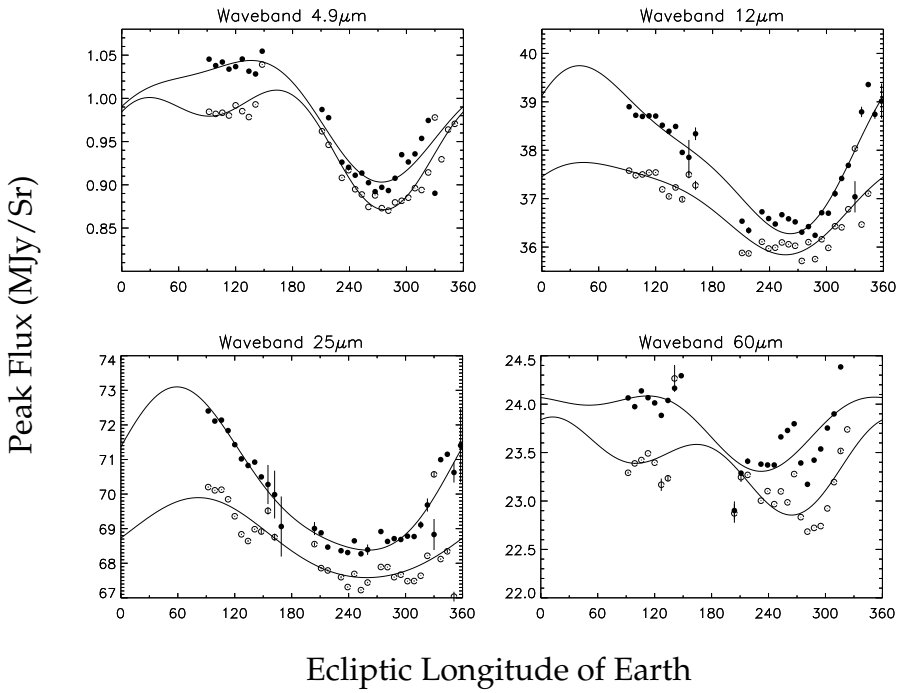

Figure 22. COBE observations of the peak flux of the smooth (filtered) zodiacal background as function of the ecliptic longitude of Earth at a solar elongation of 90° in four infrared wavebands. The flux in the Earth's trailing (filled circles) and leading (open circles) directions are fitted with independent sine curves. These curves are a combination of sine and double sine components only (Dermott et al. 1996a; Jayaraman and Dermott 1996a), and the mean difference between the two curves for the leading and trailing direction is a measure of the flux asymmetry (Jayaraman and Dermott 2001). Adapted with permission from Jayaraman and Dermott (1996a). Copyright 1996, American Institute of Physics.

Mean motion resonances occur at those heliocentric distances for which the ratio of the orbital periods of a particle and the planet are the ratio of two small integers, $p+q:p$. If we retain only the leading term in the disturbing function of the particle, then the equation of motion of the resonant argument, ϕ, defined by (Dermott et al. 1988b)

$$\phi = p\lambda - (p+q)\lambda' + q\varpi', \tag{32}$$

is that of a damped harmonic oscillator and the acceleration of ϕ, $\ddot{\phi}$, is given by

$$\ddot{\phi} = -(\mathcal{G}M_{\oplus}/a')f(\alpha)e'^{q}\sin\phi - (p+q)\dot{n}'_{\rm PR}, \tag{33}$$

where p and q are integers, λ is the mean longitude, ϖ is the longitude of perihelion, $\mathcal{G}M_{\oplus}$ is the gravitational mass of the Earth, a is the semi-major

axis, e the eccentricity, $\alpha = a/a'$, $f(\alpha)$ is a function of Laplace coefficients that increases markedly with increasing p, $\dot{n}'_{\rm PR}$ is the rate of change of the mean motion of the dust particle due to the action of Poynting-Robertson and solar wind drag, unprimed quantities refer to the orbit of the Earth and primed quantities refer to a dust particle on an orbit exterior to that of the Earth.

A particle is said to be "trapped" in a resonance with the Earth while the effect of P-R and solar wind drag acting on the particle is counterbalanced by resonant gravitational perturbations due to the Earth. In this case, we have

$$\frac{\langle \dot{e}' \rangle}{e'} \simeq -\frac{q}{2(p+q)e'^2} \left(\frac{\dot{a}'}{a'} \right)_{\rm PR}, \tag{34}$$

where $\langle \dot{e}' \rangle$ represents the rate of change of the dust particle's eccentricity averaged over the librational period of the resonant argument. Given that $\dot{a}' < 0$ and the orbit of the dust particle is *converging* on the orbit of the Earth, trapping into resonance results in a rapid increase in the particle's orbital eccentricity and a strengthening of the resonance (Dermott et al. 1988b). Paradoxically, this leads to resonance disruption on timescales $\sim 10^4$ yr — see Fig. 23. If the eccentricities are large, then the libration widths associated with the resonances are also large, and the dynamics may break down and become chaotic due to resonance overlap (Wisdom 1980). However, Marzari and Vanzani (1994) used a numerical approach to map the capture probability in the e–ϖ (eccentricity and longitude of perihelion) phase space of the particle. They found that the increase in the orbital eccentricity of the particles after resonant capture leads to Earth-crossing orbits and the particles eventually escape out of resonance due to close encounters with the Earth. Therefore, close encounters with the planet probably play a critical role in curtailing the lifetime of a particle in resonance. These encounters are not included in any theory of orbital evolution, although Beaugé and Ferraz-Mello (1994) have made an attempt in that direction.

We should note here that Eq. (34) also applies to the orbital evolution of cometary particles trapped in resonances interior to the orbit of Jupiter. But in this case, since the resonances are interior, the equation for $\dot{e}$ contains a sign change and because $\dot{a} < 0$ and the orbits are *diverging* from Jupiter, orbital evolution results in a decrease in the orbital eccentricity (Dermott et al. 1988b) — see Fig. 6 (Examples 4 and 5).

The paths of particles librating in the 4:3, 5:4, 6:5, and 7:6 mean motion resonances with the Earth are shown in Fig. 24. Without drag, these paths would have mirror symmetry about the Earth-Sun line. But drag introduces a phase lag into the equations of motion, with the result that the paths are asymmetric; as the particles pass through perihelion, they approach the Earth closer in the trailing direction (behind the Earth in its orbit) than in the leading direction. By setting the left-hand side of Eq. (33) to zero, we find that the phase lag is a maximum ($|\sin\phi| \approx 1$) when

$$|\left(\mathcal{G}M_{\oplus}/a'\right) f(\alpha) e'^q| = |(p+q)\dot{n}'_{\rm PR}|, \tag{35}$$

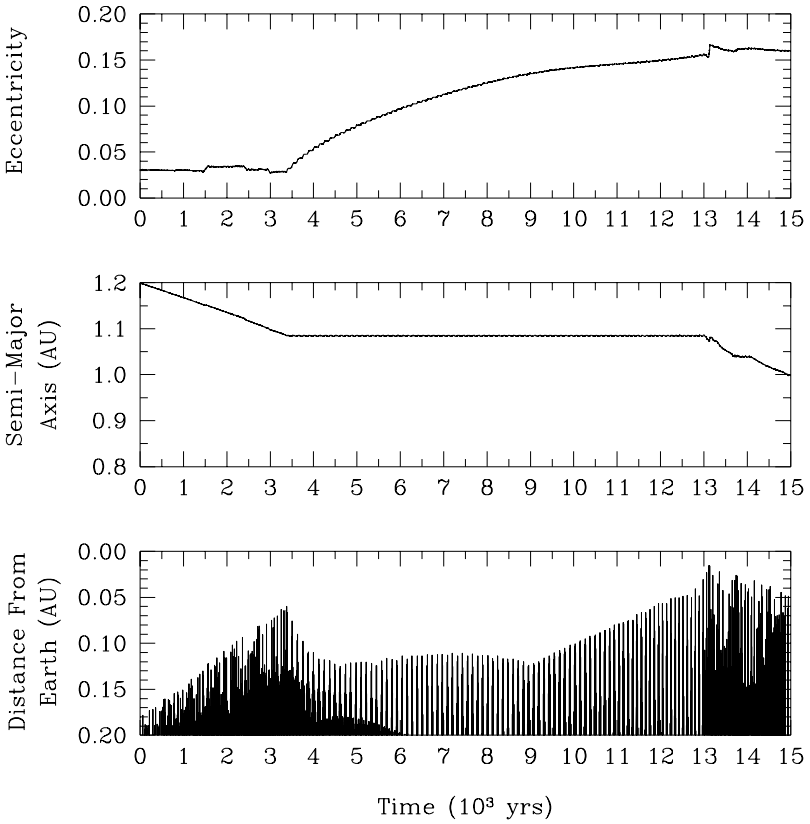

Figure 23. Orbital evolution of a 20 μm diameter dust particle. From left to right we see the semi-major axis (middle panel) of the particle orbit decay until, after about 3,500 years, it becomes trapped in a first-order exterior mean motion resonance with Earth. At this point the mean semi-major axis remains constant while the eccentricity (top panel) begins to increase. While the orbit is decaying the distance of closest approach of the particle from Earth (bottom panel) decreases. Upon capture into resonance the particle is initially kept away from Earth by the resonance. However, as the eccentricity increases the minimum gap between Earth and particle narrows until eventually the particle is released from the resonance, after being trapped for about 10,000 years (Kortenkamp and Dermott 1998a).

and the strength of the resonance is just sufficient to counteract the effect of drag on the particle's semi-major axis. Given that the P-R drag rate increases with decreasing diameter (see Eqs. 6 and 10), it follows that there is a lower limit to the size of the particles that can be trapped in a particular resonance. We have determined the capture probabilities of asteroidal particles composed of astronomical silicate with density 2,500 kg m^{-3}, and found numerically that the lower cut-off for resonance trapping with the Earth is $D \sim 5\,\mu$m (see Fig. 25).

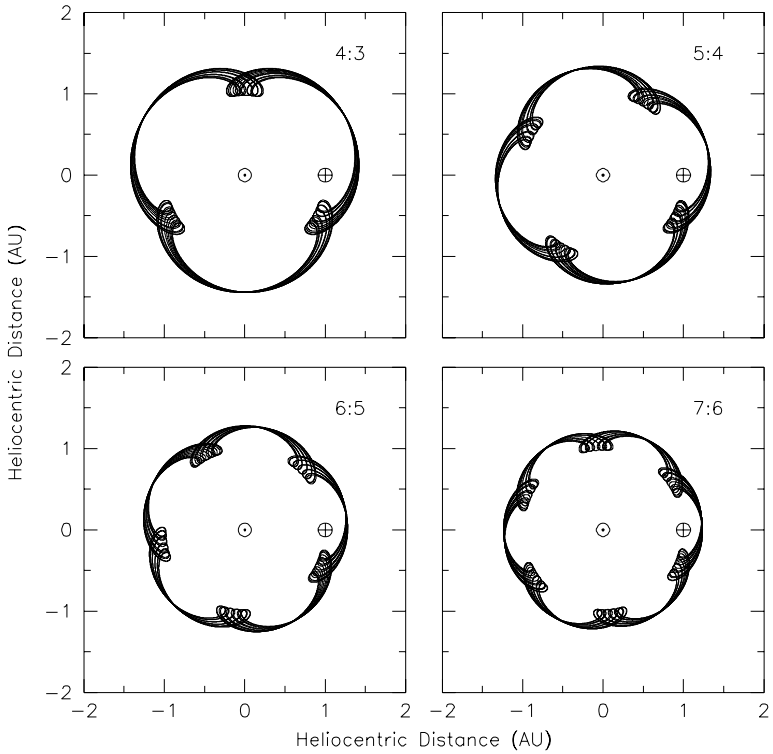

Figure 24. Illustrations showing the orbital paths traced out by asteroidal dust particles trapped in four different external mean motion resonances with Earth. The resonances occur in regions where the ratio of the orbital periods of the dust particle and the planet can be expressed as the ratio of two small integers, like the 4:3, 5:4, 6:5, and 7:6 resonances shown here. These paths are shown in a Sun-centered reference frame that is corotating with Earth's mean orbital motion. Earth ($\oplus$) is nearly stationary in this reference frame. Over many years the orbit of the dust particle librates about a quasi-stable resonant configuration. Because of the drag forces the paths of the dust particles are not symmetric about the Earth-Sun line. Different resonances cause a similar effect, but with differing numbers of lobes in the paths. Two common features of all resonant orbital paths are the cavity that Earth sits in and the proximity of the dust particles trailing behind the planet. The super-position of numerous resonances results in a circumsolar ring of asteroidal dust with Earth embedded in a cavity and followed in its orbit by a cloud of trailing dust particles. Adapted from Kortenkamp et al. (2001) with kind permission from Kluwer Academic Publishers.

Thus, the observed trailing/leading asymmetry of the zodiacal cloud must be produced by particles larger than 5 μm (unless, of course, they have lower densities, the lower limit is more correctly a lower limit on β – see Eqs. 6 and 10).

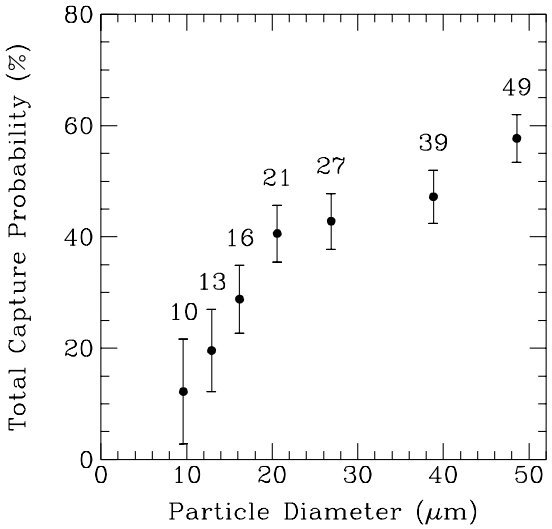

Figure 25. Capture probabilities of asteroidal dust particles into all first-order mean motion resonances of Earth between 2:3 and 15:16 as a function of particle diameter. For particle diameters less than $\sim 5\,\mu$m (which corresponds to $\beta = 0.1$ for a density of $2{,}500\,\mathrm{kg\,m^{-3}}$) the capture probability is zero, setting a lower limit to the diameters of particles trapped in the ring (Jayaraman and Dermott 2001). Adapted with permission from Jayaraman and Dermott (1996a). Copyright 1996, American Institute of Physics.

The structures of the rings produced by resonant trapping have been estimated from numerical integrations. In these investigations, we only considered main belt asteroidal particles, because the high orbital eccentricities of both cometary particles and particles originating from the disruption of near-Earth asteroids make resonant trapping improbable (Dermott et al. 1988b; Gomes 1995). The particles in the Earth's resonant ring must originate from a low eccentricity source in the zodiacal cloud, and this is most likely the main asteroid belt.

To obtain a detailed description of the structure of a resonant ring, the dynamics of a wide range of particle sizes needs to be considered. However, for heuristic purposes, it is instructive to compare the results of modeling rings of single-size particles with density $2{,}500\,\mathrm{kg\,m^{-3}}$ and diameters $13\,\mu$m and $39\,\mu$m, respectively. These ring structures were found by determining the fraction of particles trapped in each resonance (Fig. 25) and the average time spent by the particles in these resonances (Fig. 26). The trapping times decrease sharply with increasing p as the locations of the resonances get closer to the Earth and the probability of close encounters increases. The overall distribution of particles in a ring at any given time is a convolution of the quantities given in Figs. 25 and 26 with the distributions of the positions of the particles in the

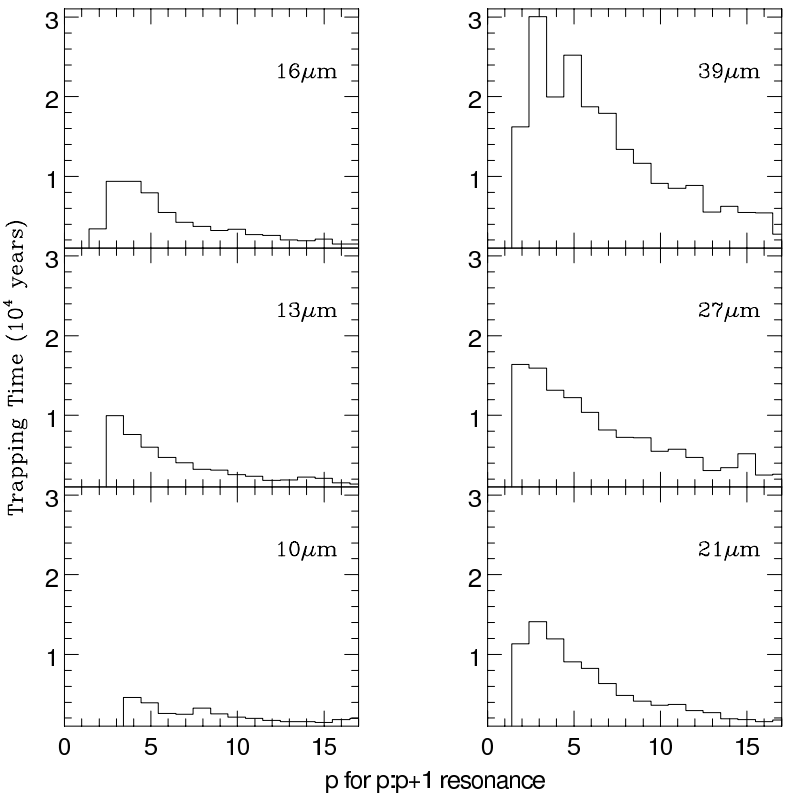

Figure 26. Average trapping lifetimes of particles in first order mean motion resonances between 2:3 and 15:16, determined empirically from numerical integrations for various particle diameters. The trapping lifetimes are longer for the larger particles and for those particles in resonances most distant from Earth's orbit (Jayaraman and Dermott 2001).

various resonances, as tracked in a reference frame centered on the Sun and rotating with the Earth from the time of capture to the typical time of release. Our final models are simulated "images" binned in pixels of $0.04 \times 0.04\,\mathrm{AU}$ (Jayaraman and Dermott 2001).

The 6:5 resonance shown in Fig. 24 has five lobes, with the Earth residing asymmetrically in one of those lobes. All the other possible resonances have similar structures, but different numbers of lobes. The resultant image obtained by the super-position of the various paths, weighted according to the probability of capture and the trapping times shows that, in a rotating reference frame, the trapped particles form a near-uniform ring around the Sun that corotates in inertial space with the Earth. The rings have two notable features. First, there is a cavity in the ring at the location of the Earth. Figure 27 also shows that apart from an asymmetry in the mean position of the Earth in the ring's

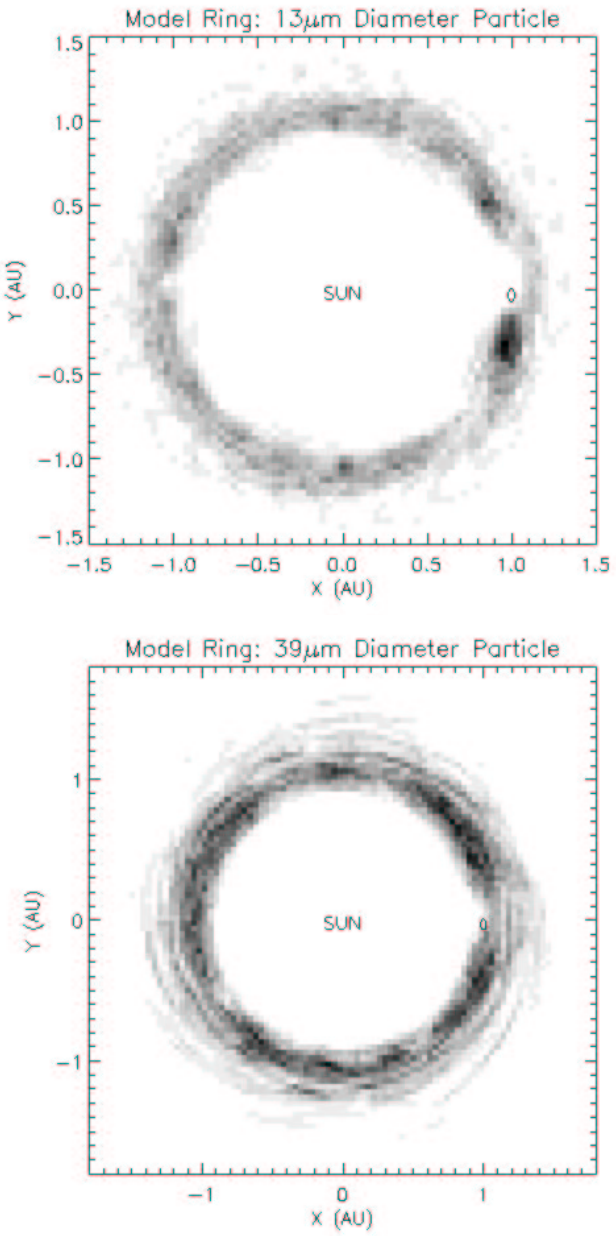

Figure 27. Simulated images of the variations in the particle number density in rings of asteroidal dust particles of diameters 13 μm (top) and 39 μm (bottom). The images are plotted in a rotating reference frame and have resolutions of 0.04×0.04 AU (Jayaraman and Dermott 2001). Adapted with permission from Jayaraman and Dermott (1996a). Copyright 1996, American Institute of Physics.

cavity, for the smaller particles alone there is also a marked asymmetry in the longitudinal variation of the particle number density. The increase in resonance strength, and the corresponding decrease in phase shift with increasing p value, disperses the longitudes of the perihelia of the particle paths in the rotating frame in the leading direction, while concentrating the longitudes of the perihelia in the trailing direction. For a ring of small particles that just satisfy the trapping criterion (Eq. 35), this results in a marked enhancement of particle number density behind the Earth in its orbit, as if the Earth had a trailing cloud of dust permanently in its wake. This trailing cloud is absent from the ring of larger particles. The probability of capture into resonance increases with increasing diameter (see Fig. 25), reaching a maximum that is determined by orbital eccentricity (Dermott et al. 1988b). However, simply because these particles are larger, their drag rates are smaller as are the phase shifts and asymmetries associated with resonant trapping. Thus, although large particles form resonant rings more easily than small particles, provided the trapping criterion is satisfied, resonant rings associated with large particles do not produce a trailing/leading asymmetry. While we expect resonant rings to be common in our Solar System, and in exosolar systems, trailing clouds are likely to be uncommon, only occurring where there is a near critical balance between the resonance force and the drag force. For example, almost all of the material that migrates out of the Kuiper Belt is expected to become trapped in resonances with Neptune forming a large irregular ring, but without a trailing cloud as the drag rates this far from the Sun are very small and the resonant phase lags are negligible. However, due to the multiple-lobed structure of resonant orbits detectable brightness asymmetries should still exist in Neptune's resonant ring (Liou and Zook 1999). Liou et al. (2000) argue that such a signature can be interpreted as evidence for a planetary system in the dust disk of ε Eridani.

Most of our work on the structures of resonant rings has been concerned with the dynamics of particles just larger than the lower limit of $D \sim 5\,\mu$m dictated by the trapping criterion (Eq. 35). It is a fact that only particles close to this limit can contribute to a marked trailing/leading asymmetry (Jayaraman and Dermott 1996a, 2001). However, we have argued here that the diameters of most of the particles that migrate from the asteroid belt to the Earth are probably $\sim 10^2\,\mu$m and much larger than this lower limit. This paradox may be resolved by allowing for the disintegration of large particles *while* they are trapped in resonance with the Earth. More work is needed on the dynamics of this problem. We also need to complete a more detailed analysis of the COBE data. Figure 28 shows a geocentric view of the trailing dust cloud obtained from line of sight integrations through a three dimensional model of the ring. The four lower panels show images of the trailing cloud as seen in the model at ecliptic longitudes $\lambda_\oplus = 0°$, $90°$, $180°$, $270°$. The plane of symmetry of this model is described by $I_\mathrm{f} = 3°$, $\Omega_\mathrm{f} = 50°$, which causes an apparent latitudinal oscillation of the trailing cloud. Although these oscillations are expected, they have yet to be detected in the COBE data and they will probably remain undetected until we have models accurate at the 1% level for both the background

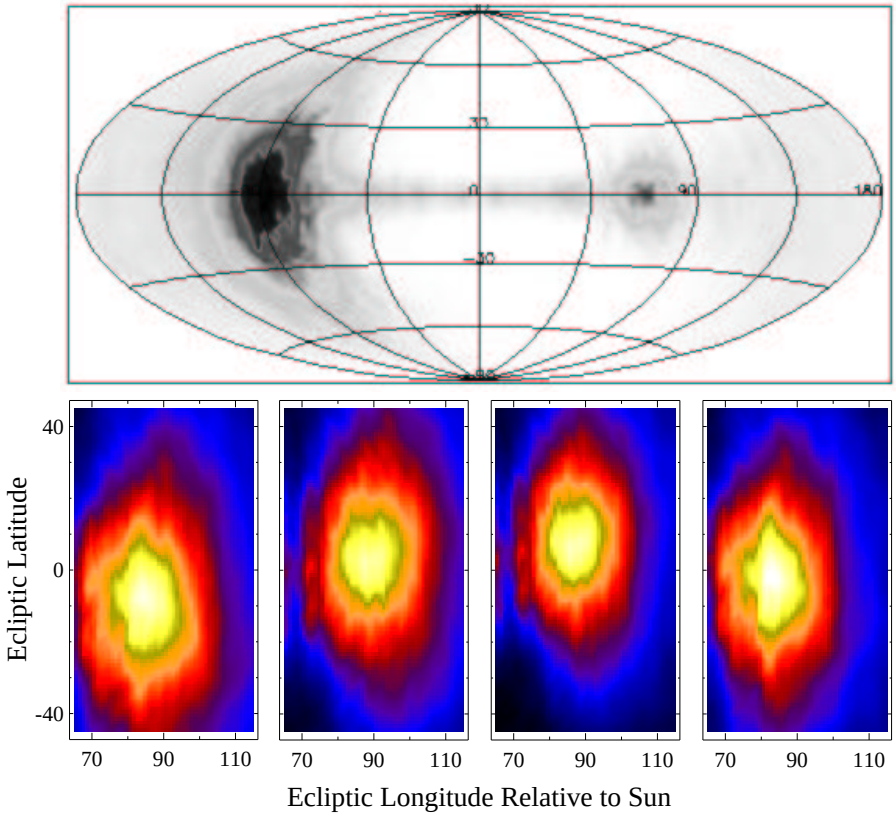

Figure 28. (Top) Geocentric view of the trailing dust cloud obtained from line of sight integrations through a three dimensional model of the ring. The longitude is defined to be zero in the direction opposite to the Sun and is measured in the clockwise direction as viewed from the North. This view of a ring of 13 μm diameter particles shows that the brightness of the trailing dust cloud (on the left) is much stronger than the leading cloud (on the right). Reprinted from Dermott et al. (1999) with kind permission from Kluwer Academic Publishers. (Bottom) Four panels showing images of the trailing cloud as seen in the model at ecliptic longitudes $\lambda_\oplus = 0°$, 90°, 180°, 270°. The plane of symmetry of this model is described by $I_{\rm f} = 3°$, $\Omega_{\rm f} = 50°$, which causes an apparent latitudinal oscillation of the trailing cloud. Reprinted from Wyatt et al. (1999a) by kind permission of the Astronomical Society of the Pacific.

cloud and the dust bands. Once we have these models to subtract from the COBE observations, the time-varying structure of the resonant ring should be revealed. The forthcoming launch of SIRTF (Space Infrared Telescope Facility) should also provide us with a wealth of data on the structure of the Earth's resonant ring as it drifts through the trailing cloud of dust in the wake of the Earth's orbit (Jayaraman and Dermott 1996b; Wyatt et al. 1999a).

VII. ACCRETION OF IDPs

The rate at which Earth captures dust particles from different sources is dependent on the average spatial density of particles near Earth and the geocentric encounter velocity of the particles. As particles approach Earth their heliocentric trajectories are deflected toward the planet by its gravitational field. Öpik (1951) showed that this deflection results in an effective "gravitational" capture cross-section of Earth given by

$$\sigma_{\rm c} = \sigma_{\oplus} \left(1 + \frac{v_{\rm e}^2}{v_0^2} \right), \tag{36}$$

where $\sigma_{\oplus}$ is the geometric cross-section of Earth (taken out to 100 km altitude), $v_{\rm e}$ is the escape velocity at the surface of the planet (at 100 km altitude, $v_{\rm e} \simeq 11.1\,{\rm km\,s^{-1}}$) and v_0 is the geocentric encounter velocity of the particle prior to its acceleration by the planet. To illustrate the importance of this gravitational focusing effect consider that a dust particle approaching Earth with $v_0 \approx 1\,{\rm km\,s^{-1}}$ will "see" the effective cross-sectional area of the planet as ~ 100 times greater than its actual physical cross-section. Wetherill and Cox (1985) have shown numerically that even for extremely low encounter velocities ($v_0/v_{\rm e} \leq 0.02$) Eq. (36) is still valid – albeit in a statistical sense – but approaches an upper limit of $\sigma_{\rm c}/\sigma_{\oplus} \simeq 3{,}000$.

Earth-crossing orbits of typical asteroidal and cometary dust particles have similar distributions in ecliptic inclination. The drag forces acting on dust particles that cause their semi-major axes to decay towards the Sun also act to reduce their eccentricities (Eqs. 10 and 11). Earth-crossing asteroidal dust particles have low orbital eccentricities, typically $e < 0.1$, while Earth-crossing cometary dust particles generally have considerably higher orbital eccentricities, reaching as high as $e \simeq 1$ (Flynn 1989; Jackson and Zook 1992; Kortenkamp and Dermott 1998a). The disparity in eccentricities results in lower geocentric encounter velocities for asteroidal dust particles and thus larger gravitational capture cross-sections of Earth compared to cometary particles. Flynn (1990) noted that this would result in a near-Earth enhancement of asteroidal over cometary dust. Flynn also showed that any low inclination asteroidal dust particles would encounter a gravitational capture cross-section as much as two orders of magnitude larger than the actual geometric cross-section of Earth. It was later suggested that two of the largest families in the asteroid belt — Themis and Koronis — which have low ecliptic inclinations and are known dust producers, may contribute significantly to the IDPs (Love and Brownlee 1992).

Kortenkamp and Dermott (1998a) studied the orbital evolution of $10\,\mu$m diameter dust particles released from: 797 members of the Eos, Themis, and Koronis asteroid families (orbital elements were obtained from the PDS Small Bodies Node at http://pdssbn.astro.umd.edu); 830 non-family asteroids (a bias-free set was obtained from the Small Bodies Node by selecting bright main belt asteroids with absolute visual magnitudes $H < 11$); and 175 short-period Jupiter family comets (a subset of the MPC catalog, Marsden 1995). Their evolution

was followed until the dust particles had decayed through the entire Earth-crossing region. The cometary dust particles were divided into two distinct populations — those that were temporarily trapped in Jovian mean motion resonances and those that were not, in order to properly take into account the effect of resonant capture on the dust particles. Distributions of semi-major axis (a), eccentricity (e), and inclination (I) were determined for the Earth-crossing orbits in each population. Using these orbital elements the average spatial density (Kessler 1981) at heliocentric distance R and latitude l, is given by

$$S(R,l) = \frac{1}{2\pi^3 Ra\left[\left(\sin^2 I - \sin^2 l\right)(R-q)(Q-R)\right]^{1/2}}, \tag{37}$$

where $q = a(1-e)$, $Q = a(1+e)$, $q < R < Q$ and $0 < l < I$. [$S(R,l)$ is used to create the schematic diagrams of the dust bands shown in Fig. 9]. If Earth is at position (R,l) then the fraction of dust particles captured per unit time (i.e., the capture rate for a given a, e, I) is

$$P = v_0 \sigma_c S(R,l). \tag{38}$$

Typical capture rates are quite low and usually expressed as the fraction of particles with the given a, e, I captured per 10^9 years (dimensionally, Gyr^{-1}). [For details on the implementation of $S(R,l)$ for each population see Kortenkamp and Dermott (1998a).]

Figure 29 shows the mean geocentric encounter velocity (v_0) plotted against mean values of σ_c, $v_0\sigma_c$, and $v_0\sigma_c S(R,l)$ for each of the six Earth-crossing populations. The mean σ_c values (top plot) for the low eccentricity, low inclination Themis and Koronis dust particles (labeled T and K) are about a factor of ten higher than for the cometary population not previously trapped in mean motion resonances with Jupiter (solid C) and five times the previously trapped cometary population (open C). The Eos (E) and non-family asteroidal (A) populations have similar mean σ_c values. In terms of the effective volume of each population swept out by Earth per unit time ($v_0\sigma_c$; middle plot), the enhancements of the Themis and Koronis populations are reduced to less than a factor of two over the cometary populations. The enhanced capture cross-sections associated with the low velocity encounters are significantly offset by the greater volume swept up in the high velocity encounters. However, in the total capture rate (bottom plot) the differences in σ_c and $v_0\sigma_c$ are dwarfed by the remarkable range in the average spatial densities of the six populations, which spans about two orders of magnitude.

Combining estimates of the contribution of each source to the zodiacal cloud with the average capture rates for each population yields the contribution of each source to the atmospheric IDPs. A wide range of these estimates can be accommodated by Fig. 30. The right-hand panel is for the case where only 5% of the population of all Earth-crossing dust particles is due to Eos, Themis and Koronis, a conservative estimate. Here cometary dust could possibly account for 0% to 95% with the complement of this range (95% to 0%) from other

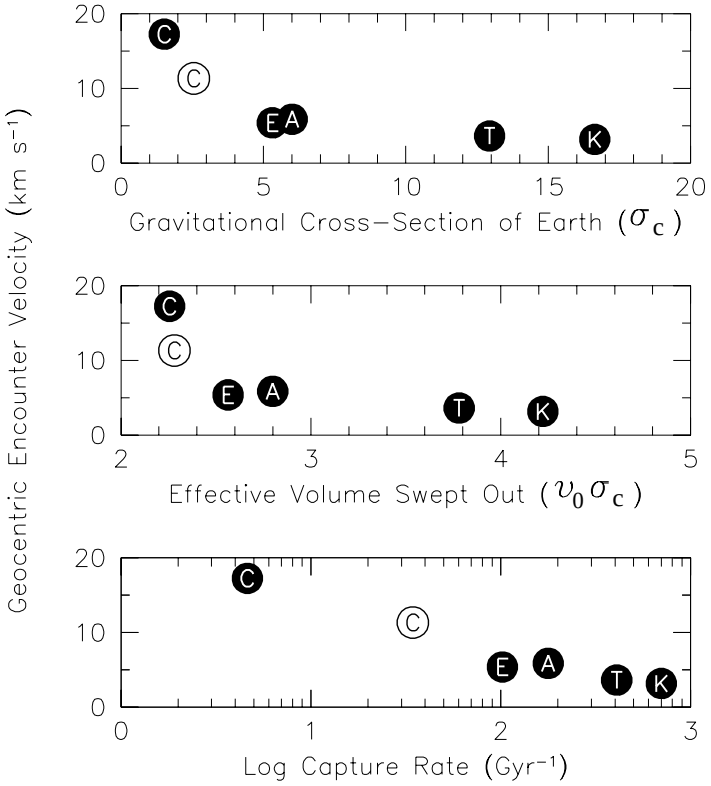

Figure 29. Mean geocentric encounter velocities (v_0 in text) for 10 μm diameter dust particles are plotted against mean gravitational capture cross-section of Earth (σ_c; top), mean effective volume of each population swept up by Earth each second ($v_0\sigma_c$; middle), and log of the mean capture rate ($v_0\sigma_c S(R,l)$; bottom). E, T, and K labels indicate the Eos, Themis and Koronis populations while A indicates other non-family asteroidal particles. Open points labeled C indicate cometary particles that were previously trapped in Jovian mean motion resonances. Solid points labeled C indicate cometary particles that were not previously trapped in Jovian mean motion resonances. Reprinted from Kortenkamp et al. (2001) with kind permission from Kluwer Academic Publishers.

asteroids. The left-hand panel is for the case where 25% of the population of all Earth-crossing dust particles is due to Eos, Themis and Koronis, a result of the dust band modeling presented earlier (Fig. 14). Cometary dust can then range from 0% to 75%, with the complement of this range (75% to 0%) being due to other asteroids. As an example, it has been suggested that the ratio of dust production by asteroid families to dust production by all asteroids is about 1:3 (Grogan et al. 2001). In this example, if dust from asteroid families contributes 25% to the population of all Earth-crossing dust particles then

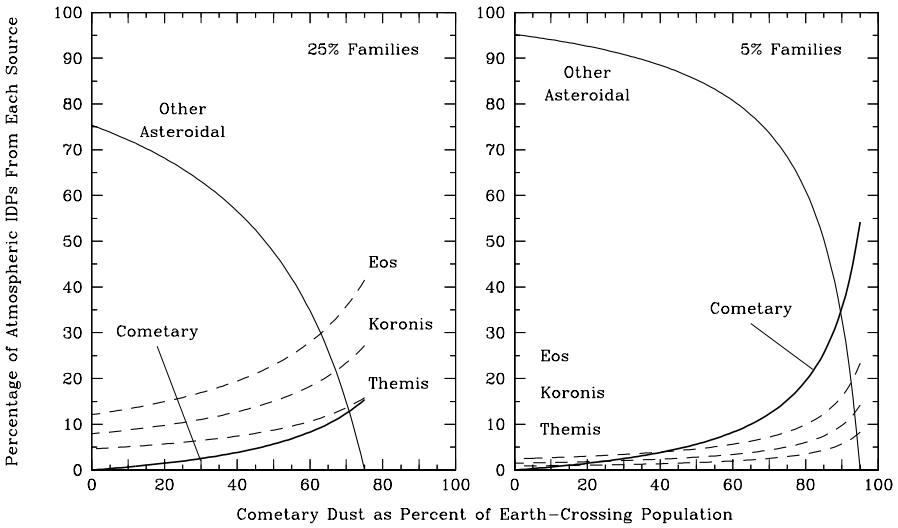

Figure 30. Based on the two dust band models of Grogan et al. (1997) these plots assume that the broad range of 5 to 25% offers a good estimate of the probable contribution of asteroid families to the population of all Earth-crossing dust particles. Using this range, we calculate the percentage of IDPs deposited in the atmosphere from each source as a function of the cometary contribution to the population of all Earth-crossing dust particles. The left-hand panel is for the case in which 25% of the dust comes from the Eos, Themis, and Koronis families. The cometary contribution can then range from 0 to 75%, with the complement of this range (75 to 0%) being due to other asteroidal dust. The three dashed lines represent Eos, Koronis, and Themis, respectively, in order of decreasing atmospheric percentages. The right-hand panel is for the case in which 5% of the dust comes from the Eos, Themis, and Koronis families. The cometary contribution can then range from 0 to 95%, again with the complement of this range (95 to 0%) being due to other asteroidal dust. Under most conditions shown in these two panels, asteroidal dust dominates the atmospheric IDPs. Only when cometary dust represents nearly 95% of the Earth-crossing population (far right, right-hand panel) does cometary dust represent more than half of the IDPs deposited in the atmosphere (adapted from Kortenkamp and Dermott 1998a).

all asteroids (non-family and family) contribute 75%. This leaves 25% to be supplied by comets. In the left-hand panel of Fig. 30 with cometary dust as 25% of the Earth-crossing population we see that Eos contributes about 17% to the IDPs, Themis and Koronis combine to provide another 18%, and nearly all of the remaining IDPs are due to other asteroids. In this example, cometary particles represent only about 2% of all IDPs.

From this figure certain conclusions are almost unavoidable, regardless of the cometary contribution to the zodiacal cloud. The existence of the dust bands and the evidence that asteroidal dust is transported to the inner Solar

System (Dermott et al. 1994a) implies that most IDPs are asteroidal. Also, it shows that even though the Themis and Koronis families may contribute only between 1% and 4% to the population of all Earth-crossing dust particles, these two families make a very significant contribution to the population of IDPs. What may be most striking is that only under the most extreme of circumstances does cometary dust represent more than 50% of the IDPs. A conservative estimate based on Fig. 30 and using a value between 5% and 25% dust from families is that probably fewer than 25% of the dust particles entering the atmosphere are cometary. Losses due to melting and vaporization during atmospheric entry of the higher velocity cometary particles will further reduce their contribution to collections of intact IDPs retrieved from the stratosphere. The conclusions from our work so far are clear, the Earth predominantly accretes low inclination and eccentricity particles, and a large — perhaps dominant — fraction of this dust comes from the three asteroid families Eos, Themis and Koronis. Samples of these known K-type (Eos), S-type (Koronis) and C-type (Themis) asteroids may already exist in our IDP collections. However, we have shown in Section III that the distributions of large asteroidal particles in the cloud are different to the distributions of smaller particles, and more work needs to be done to characterize the accretion rates of this larger size asteroidal dust population. We have also discussed (see Section III; Liou and Zook 1996) how cometary particles trapped into interior mean motion resonances with Jupiter can evolve onto lower eccentricity orbits and hence increase their rate of capture by the Earth.

VII.A. Long Term Variations

Muller and MacDonald (1997) have suggested that the accretion rate of IDPs might be variable and could be responsible for driving Earth's 100,000 year climate cycle (Rial 1999, raises serious questions about the validity of this hypothesis). They proposed that the accretion rate was linked to the varying inclination of Earth's orbit with respect to the invariable plane of the Solar System. This hypothesis has been tested for accretion of asteroidal IDPs from the dust bands and, in a preliminary fashion, from Earth's circumsolar resonant dust ring.

1 Accretion from the dust bands

A raw number representing the inclination of an orbital plane is meaningless if it is not accompanied by a description of the reference plane. Traditionally in Solar System astronomy this reference plane is the ecliptic (the plane of the Earth's orbit) at a specific date. Some astronomers prefer to use the invariable plane of the Solar System as a reference. Two different reference planes are used to determine the proper and forced inclination of the dust particle orbits in a dust band. Proper inclination is referred to the midplane of the dust band and is therefore a measure of the angular half-width of the dust band. The forced inclination indicates the tilt of the dust band midplane with respect to a designated reference plane. The first step in studying the accretion rate of dust

band material is the recognition that we must use Earth's orbital inclination measured with respect to the midplane of the dust bands at 1 AU, not with respect to the invariable plane.

As dust particles are produced by the gradual comminution of asteroid family members the resulting dust band takes on the orbital characteristics of the family. As the orbits of dust particles decay toward the Sun under the effect of Poynting-Robertson drag, secular gravitational perturbations due to the planets cause a variation in the forced inclination, essentially warping the dust band midplane (see Fig. 9). Furthermore, because the orbital decay rate (Eq. 12) is dependent, through β, on the physical properties of the dust particles (Eq. 4), dust bands composed of different sized dust particles will exhibit different warping (Fig. 5a).

Kortenkamp and Dermott (1998b) reconstructed the orientation of the Earth-crossing portion of the dust bands back to 1.2 million years ago. The simulations included gravitational interactions with seven planets (Mercury and Pluto were excluded), radiation pressure, P-R drag and solar wind drag. A wave of 10 μm diameter dust particles was released from the Eos asteroid family every 20,000 years and their orbits were allowed to decay into the inner Solar System. When each wave of dust particles became Earth-crossing (about 50,000 years after release) the eccentricity and inclination of Earth's orbit were determined (A and B of Fig. 31). The inclination was calculated with respect to the midplane of the Earth-crossing portion of the dust bands. The capture rate was then calculated using Eq. 38) and the average capture rates at each time step were normalized over the 1.2 million year period (solid lines in C and D of Fig. 31).

Several aspects of Fig. 31 deserve closer attention. First, from B, Earth's orbital inclination with respect to the Earth-crossing dust bands does not vary in a smooth periodic fashion. This fact alone argues against the idea of an inclination driven 100,000 year periodicity in the dust accretion rate, as suggested by Muller and MacDonald (1997), Farley and Patterson (1995), and Patterson and Farley (1998). Second, the accretion rate of Eos, Themis, and Koronis dust particles is strongly anti-correlated with Earth's orbital eccentricity. Third, when Earth's orbital inclination reaches or exceeds the mean proper inclination of the Themis and Koronis dust bands (dashed line in B) the planet is actually outside most of the dust band material for some period of time each year. During these years (e.g., near 0.5×10^5 and 9×10^5 years ago in C) the capture rate of Themis and Koronis material falls despite the fact that Earth's eccentricity may be near its minimum value. The higher proper inclination of the Eos dust band ensures that Earth is always deeply embedded within that dust band and so the capture rate of Eos dust particles does not show a correlation with Earth's orbital inclination (D). The transition from an inclination-driven to an eccentricity-driven accretion rate is complete for proper inclinations above 4° (Kortenkamp and Dermott 1998a). The mean proper inclination for the asteroid belt is about equal to that for the Eos family (about 10°), so variations in the accretion rate of most asteroidal dust particles will

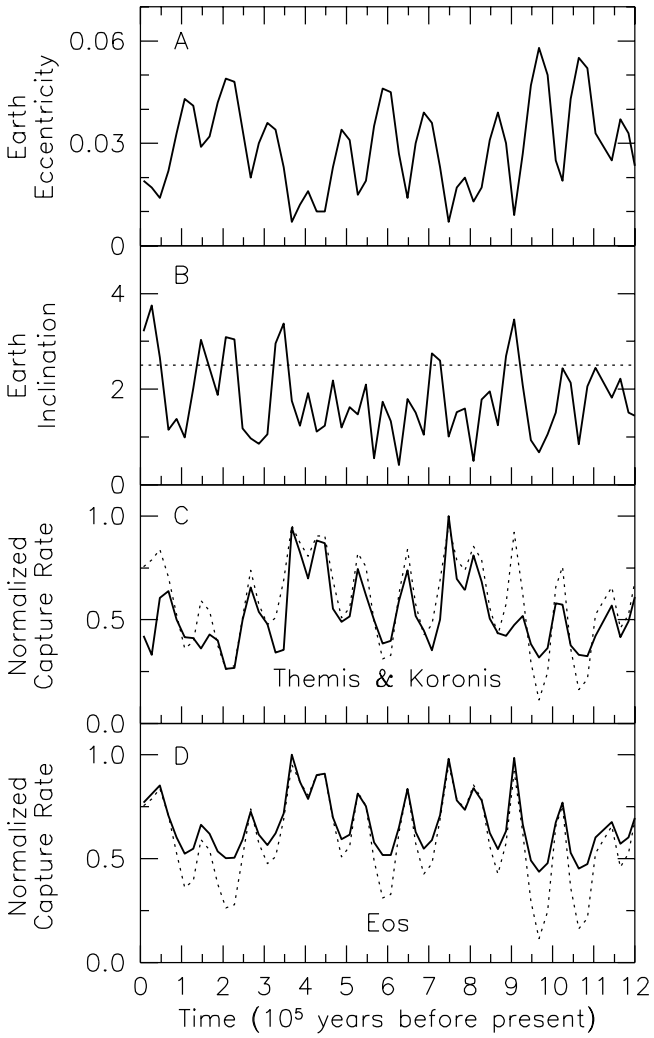

Figure 31. (A) Earth's orbital eccentricity. (B) Earth's orbit inclination with respect to the midplane of the Earth-crossing dust bands. The dashed line marks the mean proper inclination of Earth-crossing dust particles in the Themis and Koronis dust bands, which are indistinguishable at 1 AU. (C and D) Normalized average capture rate (solid lines) for 10 μm diameter dust particles from the Themis and Koronis families and the Eos family. In C and D the dashed line is Earth's orbital eccentricity plotted with the y-axis flipped from that in A. Reprinted from Kortenkamp et al. (2001) with kind permission from Kluwer Academic Publishers. [The capture rates shown in C and D are slightly different from those reported in Kortenkamp and Dermott (1998b) after correcting for a size-dependent term in the heliocentric velocity of the dust particles.]

also be anti-correlated with Earth's orbital eccentricity. Furthermore, because Earth's orbital eccentricity is not controlled by the dynamics of interplanetary dust particles, it follows that variations in the accretion rate of most asteroidal dust particles will be independent of the size of the particles. The long term accretion of asteroidal dust of all sizes should be anti-correlated with Earth's orbital eccentricity and varying with a 100,000 year periodicity.

The abundance of extraterrestrial ^{3}He in deep-sea sediments is indicative of the flux of IDPs to the sea floor, although opinions differ as to whether this amounts to a tracer of the actual accretion rate of IDPs (see Marcantonio et al. 1996, Farley and Patterson 1995). Analyses of sediment core samples do show a 100,000 year periodicity in the concentration of ^{3}He. However, the sea-floor ^{3}He periodicity is 50,000 years out of phase with the expected IDP accretion rate. Accretion from Earth's resonant ring of asteroidal dust is being investigated as a possible explanation of this 50,000 year phase lag.

2 Accretion from the resonant ring

We have numerically integrated the orbits of 40 μm diameter asteroidal dust particles from the main belt to the Earth, and divided them into those orbits that were temporarily trapped in mean motion resonances with the Earth and those that were not (Kortenkamp et al. 2001). The dust particles were assumed to be derived from the Eos asteroid family and were composed of astronomical silicate with density 2,500 kg m^{-3}. We then examined the total distribution of the minimum distances of these two populations from Earth, and also their relative velocities at close encounter, and found that the resonant particles (those that were trapped in resonance with Earth) do not have closer encounters than the non-resonant particles. However, they do tend to have higher geocentric encounter velocities (v_0) and so their capture probability is likely to be lower (see Eq. 38). There is one other consideration: when a particle escapes from resonance it is still in a near-resonant orbit and so may suffer further close encounters. The resonant population of particles may therefore undergo more close encounters with the Earth than the non-resonant particles, although our work to date indicates that this is not, in fact, the case. Hence, capture into resonance may ultimately hinder rather than aid accretion. These results are based upon integrations involving only $\sim 10^2$ dust particles of a single size, which is not sufficient to allow us to reach firm conclusions. We now need to repeat these simulations over a range of particle sizes and with a population of $\sim 10^5$ particles or more, to better determine their dynamical behaviour.

VIII. CONCLUSIONS

The motive for most of the work described in this review arises from the problem of determining the relative contributions of asteroidal and cometary material to the zodiacal cloud. Our approach to this problem is narrow, in that it is purely dynamical. We do not, for example, consider the physical properties of captured IDPs or their chemistry, even though these data may ultimately prove

to be pivotal. We choose instead to focus on a small number of well-determined features of the cloud that clearly demand a dynamical explanation. We consider that a detailed analysis of these features may also produce a solution to the question of origins; a question that otherwise may remain unresolved. However, our work on this subset of dynamical problems is far from complete and, at present, it is biased towards the dynamics of asteroidal rather than cometary dust. This bias exists partly because the dynamics of particles in low eccentricity and inclination orbits are more tractable, largely because the secular variations of the orbital eccentricities and inclinations are decoupled and thus easier to describe in a full and systematic manner. Thus, we study the dynamics of asteroidal dust because we are actually able to solve some of the problems presented by these particles. However, our bias also exists for a more positive reason, namely that there is one important feature of the zodiacal cloud that can only be accounted for in terms of asteroidal dynamics and that feature is the Solar System dust bands discovered by IRAS.

Our modeling and analysis of the collisional evolution of the dust bands demonstrates that large particles with diameters between 10^2 and 10^3 μm dominate the dust band structures. Numerical investigation of their dynamical history demonstrates that these bands have a natural inner edge just exterior to 2 AU, because the action of secular resonances at the inner edge of the main asteroid belt disperses the inclinations and nodes of the large dust band particles into the background cloud. This leads us to estimate that approximately 4% of the in-ecliptic infrared emission from the zodiacal cloud is produced by dust band particles that orbit exterior to 2 AU. This is clear, unambiguous evidence that asteroidal dust is a significant component of the zodiacal cloud, at least at the 4% level.

If we now make the assumption that some of these asteroidal particles migrate to the inner Solar System, where they must be both hotter and closer to Earth, then we conclude that infrared emission from the asteroidal dust associated with the dust bands alone is likely to be much greater than 4% of the total emission. If these asteroidal particles migrate to the inner Solar System without further breakup, we calculate that the contribution is 30%. If the particles are broken up and blown out of the Solar System before reaching the inner Solar System, then our estimate would, of course, remain closer to 4%. However, it is certainly possible and perhaps even more likely that particle breakup leads to an increase in the effective area of the dust in which case our estimate would be greater than 30%. Consider, for example, that if a 10^2 μm particle breaks up to produce 10^3 particles of diameter 10 μm, then the total effective surface area of the dust would increase by a factor of 10. Whether, the effective area of the dust actually increases or decreases is not known and thus 30% is, at present, our best estimate of the contribution of asteroidal dust, from the dust bands alone, to the zodiacal cloud.

But 30% must be an underestimate of the total asteroidal contribution. From a separate discussion of the ratio of the average rate of dust production in the asteroid belt as a whole to that due to those asteroids in the Eos, Themis

and Koronis families, which we estimate to be 3:1, we are led to conclude that asteroidal dust may constitute 90% of the zodiacal cloud. There are other large uncertainties here because of the stochastic nature of asteroidal collisions, and because we do not have a good estimate of the quantity of dust that would be liberated by the destruction of, for example, a single 15 km diameter rubble-pile.

Thus, we have strong, quantitative evidence that asteroidal dust exists in the asteroid belt, but this does not prove that asteroidal dust is transported to the inner Solar System. However, there are other, equally well-defined features of the zodiacal cloud that require a dynamical explanation. These include: the inclination and orientation of the plane of symmetry, as seen in a given waveband, and the variation of these parameters with waveband and heliocentric distance; the offset of the center of symmetry from the Sun; and the trailing/leading asymmetry. Given that the origin of the particles in the cloud is either asteroidal or cometary, the aim of the Florida group is to follow the orbital evolution of these two sets of particles from source to sink, and to compare the structures of the various possible clouds, which could be purely asteroidal, purely cometary, or some combination of the two, with the range of observations listed above.

We have accounted for the trailing/leading brightness asymmetry of the zodiacal cloud in terms of the resonant trapping of asteroidal particles with diameters between approximately 5 and 30 μm. We consider that the particles are asteroidal because the probability of capture into resonance decreases markedly with increasing orbital eccentricity and thus it is less likely that the dominant particles in the resonant ring are cometary. This may be evidence that asteroidal particles are actually transported from the asteroid belt to Earth. That the particles must be small is apparently at odds with other considerations that indicate that the asteroidal particles that migrate out of the asteroid belt are large, with diameters between 10^2 and 10^3 μm. However, these small particles may be formed by collisional processes within the resonant ring. Dust particles are also expected to be trapped in resonances external to the orbits of other planets, including those embedded in circumstellar disks. These rings will always have some structure due to the geometry of particles in resonant orbits, but trailing clouds of dust may be rare.

Using the numerical and analytical methods described in this review, it will be possible for us to address the other dynamical features of the cloud, namely, the parameters describing the planes of symmetry and the offset of the center of symmetry from the Sun. These features may well provide a clear answer to the problem of the asteroidal or cometary origin of the cloud. However, our work on these models is still incomplete. The asteroidal models need to be extended to include much larger diameter particles than those that have been included to date. The dynamics of these larger asteroidal particles will need to take account of particle breakup as these particles migrate to the inner Solar System. Their dynamics will also be strongly influenced by resonant trapping, certainly with Earth and Mars, but possibly also with Venus, and by point-mass gravitational scattering by these terrestrial planets.

The cometary models must also be extended to include a range of particle sizes. It may well be that we need a significant cometary component of the cloud to account for the dynamical features listed above, but, at this stage, we have no clear reason to invoke a cometary model to account for any of these observations. However, we have also pointed out that the distinction between the orbital elements of cometary and asteroidal dust particles may not be as sharp as that displayed by the orbits of their parent bodies. Cometary particles that are trapped in resonance with Jupiter can have their orbital eccentricities decreased to asteroidal values. On the other hand, the large asteroidal particles that migrate slowly through the secular resonances at the inner edge of the main belt can have their orbital elements increased to the low end of the cometary range. Caution may be in order when classifying orbits as asteroidal or cometary without an appreciation of their possible orbital history. What is clear is that accretion of particles by the Earth is strongly biased towards particles in low eccentricity and inclination orbits. If our arguments with respect to the dust bands are correct, and asteroidal particles constitute a significant, and possibly dominant fraction of the particles in the broad-scale, background zodiacal cloud, then it is unlikely that cometary particles constitute a significant fraction of the IDPs that are archived in our collections.

This surprising conclusion has now been presented, by us and by others, at several meetings including the recent meeting in Canterbury (IAU Colloquium 181) without gaining, shall we say, wide acceptance. Our final comment in this regard is that it will not be possible to settle the question of particle origin by considering the rates of supply from the two sources. We now know the numbers and orbits of nearly all the asteroids in the main belt with diameters greater than about 20 km. Thus, we have a very good estimate of the collision rates of asteroidal bodies. However, we do not have good estimates of the strengths of these bodies, we do not have good estimates of the quantity of dust that would be liberated from the disruption of a rubble-pile, and we do not have a good description of the size-frequency distribution of asteroidal dust and its variation with heliocentric distance. Thus, even in the case of an asteroidal source, although we can show that asteroids could be an adequate source, we cannot claim using this supply rate argument alone that asteroids must be the dominant source.

However, the supply argument for a cometary source is markedly less useful. We know very little about either the size-frequency distribution of comets or their strength. Cometary dust trails may be clear evidence that cometary dust is deposited in the zodiacal cloud, but these trails have never been used to make a useful, quantitative assessment of the overall contribution of comets to the broad-scale, background zodiacal cloud.

Acknowledgements

The other members of the Florida Solar System Dynamics Group whose work has contributed to this paper and who we would like to thank are J.-C. Liou, E.K. Holmes and D. Fogle.

REFERENCES

Artymowicz, P. 1997. Beta Pictoris: an early Solar System? *Ann. Rev. Earth Planet. Sci.* **25,** pp. 175–219.

Backman, D. E., Dasgupta, A., and Stencel, R. E. 1995. Model of a Kuiper Belt small grain population and resulting far-infrared emission. *Astrophys. J.* **450,** pp. L35–L38.

Beaugé, C., and Ferraz-Mello, S. 1994. Capture in exterior mean-motion resonances due to Poynting-Robertson drag. *Icarus* **110,** pp. 239–260.

Beckwith, S. V. W. 1999. Circumstellar Disks. In *The Origin of Stars and Planetary Systems*, eds. C. J. Lada and N. D. Kylafis (Dordrecht: Kluwer Acad. Publ.), pp. 579–612.

Bowell, E. L. G. 1997. The Asteroid Orbital Elements Database. Lowell Observatory, ftp://ftp.lowell.edu/pub/elgb/astorb.html.

Bottke, W. F., Jr., Rubincam, D. P., and Burns, J. A. 2000. Dynamical evolution of main belt meteoroids: Numerical simulations incorporating planetary perturbations and Yarkovsky thermal forces. *Icarus* **145,** pp. 301–331.

Brouwer, D., and Clemence, G. M. 1961. *Methods of Celestial Mechanics.* (New York: Academic Press).

Burns, J. A., Lamy, P. L., and Soter, S. 1979. Radiation forces on small particles in the Solar System. *Icarus* **40,** pp. 1–48.

Davis, D. R., Chapman, C. R., Weidenschilling, S. J., and Greenberg, R. 1985. Collisional history of asteroids: Evidence from Vesta and the Hirayama families. *Icarus* **62,** pp. 30–53.

Davis, D. R., Weidenschilling, S. J., Farinella, P., Paolicchi, P., and Binzel, R. P. 1989. Asteroid collisional history: Effects on sizes and spins. In *Asteroids II*, eds. R. P. Binzel, T. Gehrels and M. S. Matthews (Tucson: Univ. of Arizona Press), pp. 805–826.

Davis, D. R., Farinella, P., Paolicchi, P., and Bagatin, A. C. 1993. Deviations from the straight line: Bumps (and grinds) in the collisionally evolved size distribution of asteroids. *Lunar Planet. Sci.* **24,** pp. 377–378.

Dermott, S. F., Nicholson, P. D., Burns, J. A., and Houck, J. R. 1984. Origin of the Solar System dust bands discovered by IRAS. *Nature* **312,** pp. 505–509.

Dermott, S. F., Nicholson, P. D., Burns, J. A., and Houck, J. R. 1985. An analysis of IRAS' Solar System dust bands. In *Properties and Interactions of Interplanetary Dust*, ASSL Proc. **119,** eds. R. H. Giese and P. Lamy (Dordrecht: D. Reidel Publ. Co.), pp. 395–410.

Dermott, S. F., and Nicholson, P. D. 1986. Masses of the satellites of Uranus. *Nature* **319,** pp. 115–120.

Dermott, S. F., Nicholson, P. D., and Wolven, B. 1986. Preliminary analysis of the IRAS Solar System dust data. In *Asteroids, Comets, Meteors II*, eds. C.-I. Lagerkvist, B. A. Lindblad, H. Lundstedt and H. Rickman (Uppsala: Reprocentralen HSC), pp. 583–594.

Dermott, S. F., Nicholson, P. D., Kim, Y., Wolven, B., and Tedesco, E. F. 1988a. The impact of IRAS on asteroidal science. In *Comets to Cosmology*, ed. A. Lawrence, (Berlin: Springer-Verlag), pp. 3–18.

Dermott, S. F., Malhotra, R., and Murray, C. D. 1988b. Dynamics of the Uranian and Saturnian satellite systems: A chaotic route to melting Miranda? *Icarus* **76,** pp. 295–334.

Dermott, S. F., Nicholson, P. D., Gomes, R. S., and Malhotra, R. 1990. Modeling the IRAS Solar System dust bands. *Adv. Space Res.* **10,** pp. 171–180.

Dermott, S. F., Gomes, R. S., Durda, D. D., Gustafson, B. Å. S., Jayaraman, S., Xu, Y.-L., and Nicholson, P. D. 1992. Dynamics of the zodiacal cloud. In *Chaos, Resonance and Collective Dynamical Phenomena in the Solar System*, ed. S. Ferraz-Mello, (Dordrecht: Kluwer Acad. Publ.), pp. 333–347.

Dermott, S. F., Jayaraman, S., Xu, Y.-L., Gustafson, B. Å. S., and Liou, J.-C. 1994a. A circumsolar ring of asteroidal dust in resonant lock with the Earth. *Nature* **369,** pp. 719–723.

Dermott, S. F., Durda, D. D., Gustafson, B. Å. S., Jayaraman, S., Liou, J.-C., and Xu, Y.-L. 1994b. Zodiacal dust bands. In *Asteroids, Comets and Meteors 1993*, eds. A. Milani, M. Martini and A. Cellino (Dordrecht: Kluwer Acad. Publ.), pp. 127–142.

Dermott, S. F., Jayaraman, S., Xu, Y.-L., Grogan, K., and Gustafson, B. Å. S. 1996a. The origin and dynamics of the interplanetary dust cloud. In *Unveiling the Cosmic Infrared Background*, AIP Conference Proc. **348,** ed. E. Dwek, (New York: Woodbury), pp. 25–36.

Dermott, S. F., Grogan, K., Gustafson, B. Å. S., Jayaraman, S., Kortenkamp, S. J., and Xu, Y.-L. 1996b. Sources of interplanetary dust. In *Physics, Chemistry and Dynamics of Interplanetary Dust*, ASP Conference Series **104,** eds. B. Å. S. Gustafson and M. S. Hanner (San Francisco: Astron. Soc. of the Pacific Press), pp. 143–153.

Dermott, S. F., Grogan, K., Holmes, E. K., and Wyatt, M. C. 1998. Signatures of planets. In *Exozodiacal Dust Workshop Conference Proceedings*, eds. D. E. Backman, L. J. Caroff, S. A. Sanford and D. H. Woodford (Washington DC: NASA CP-1998-10155), pp. 59–84.

Dermott, S. F., Grogan, K., Holmes, E. K., and Kortenkamp, S. J. 1999. Dynamical structure of the zodiacal cloud. In *Formation and Evolution of Solids in Space*, eds. J. M. Greenberg and A. Li (Dordrecht: Kluwer Acad. Publ.), pp. 565–582.

Dohnanyi, J. S. 1969. Collisional model of asteroids and their debris. *J. Geophys. Res.* **74,** pp. 2531–2554.

Draine, B. T., and Lee, H. M. 1984. Optical properties of interstellar graphite and silicate grains. *Astrophys. J.* **285,** pp. 89–108.

Durda, D. D., and Dermott, S. F. 1997. The collisional evolution of the asteroid belt and its contribution to the zodiacal cloud. *Icarus* **130,** pp. 140–164.

Durda, D. D., Greenberg, R., and Jedicke, R. 1998. Collisional models and scaling laws: A new interpretation of the shape of the main-belt asteroid size distribution. *Icarus* **135,** pp. 431–440.

Everhart, E. 1985. An efficient integrator that uses Gauss-Radau spacings. In *Dynamics of Comets: Their origin and evolution*, eds. A. Carusi and G. B. Valsecchi (Dordrecht: D. Reidel Publ. Co.), pp. 185–202.

Farley, K. A., and Patterson, D. B. 1995. A 100-kyr periodicity in the flux of extraterrestrial ^{3}He to the sea floor. *Nature* **378,** pp. 600–603.

Flynn, G. J. 1989. Atmospheric entry heating: A criterion to distinguish between asteroidal and cometary sources of interplanetary dust. *Icarus* **77,** pp. 287–310.

Flynn, G. J. 1990. The near-Earth enhancement of asteroidal over cometary dust. In *Proceedings of the 20th Lunar and Planetary Science Conference*, (Houston: Lunar and Planet. Inst.), pp. 363–371.

Giese, R. H., Kneissel, B., and Rittich, U. 1986. Three-dimensional models of the zodiacal dust cloud — A comparative study. *Icarus* **68,** pp. 395–411.

Gold, T. 1975. Resonant orbits of grains and the formation of satellites. *Icarus* **25,** pp. 489–491.

Gomes, R. S. 1995. Resonance trapping and evolution of particles subject to Poynting-Robertson drag: Adiabatic and non-adiabatic approaches. *Celest. Mech. Dynam. Astron.* **61,** pp. 97–113.

Grogan, K., Dermott, S. F., and Gustafson, B. Å. S. 1996. An estimation of the interstellar contribution to the zodiacal thermal emission. *Astrophys. J.* **472,** pp. 812–817.

Grogan, K., Dermott, S. F., Jayaraman, S., and Xu, Y.-L. 1997. Origin of the ten degree dust bands. *Planet. Space Sci.* **45,** pp. 1657–1665.

Grogan, K., Dermott, S. F., and Durda, D. D. 2001. The size-frequency distribution of the zodiacal cloud: Evidence from the Solar System dust bands. *Icarus*, in press.

Grün, E., Zook, H. A., Fechtig, H., and Giese, R. H. 1985. Collisional balance of the meteoritic complex. *Icarus* **62,** pp. 244–272.

Gurnett, D. A., Ansher, J. A., Kurth, W. S., and Granroth, L. J. 1997. Micron-sized dust particles detected in the outer Solar System by Voyager 1 and 2 plasma wave instruments. *Geophys. Res. Lett.* **24,** pp. 3125–3128.

Gustafson, B. Å. S. 1994. Physics of zodiacal dust. *Ann. Rev. Earth Planet. Sci.* **22,** pp. 553–595.

Hirayama, K. 1918. Groups of asteroids probably of common origin. *Astron. J.* **31,** pp. 185-188.

Holland, W. S., Greaves, J. S., Zuckerman, B., Webb, R. A., McCarthy, C., Coulson, I. M., Walther, D. M., Dent, W. R. F., Gear, W. K., and Robson, I. 1998. Submillimetre images of dusty debris around nearby stars. *Nature* **392,** pp. 788–790.

Holmes, E. K., Dermott, S. F., Xu, Y.-L., Wyatt, M. C., and Jayaraman, S. 1998. Modeling the effects of an offset of the center of symmetry in the zodiacal cloud. In *Exozodiacal Dust Workshop Conference Proceedings*, eds. D. E. Backman, L. J. Caroff, S. A. Sanford and D. H. Woodford (Washington DC: NASA CP-1998-10155), pp. 272–273.

Housen, K. R., and Holsapple, K. A. 1990. On the fragmentation of asteroids and planetary satellites. *Icarus* **84,** pp. 226–253.

Jackson, A. A., and Zook, H. A. 1989. A Solar System dust ring with earth as its shepherd. *Nature* **337,** pp. 629–631.

Jackson, A. A., and Zook, H. A. 1992. Orbital evolution of dust particles from comets and asteroids. *Icarus* **97,** pp. 70–84.

Jayaraman, S., and Dermott, S. F. 1996a. COBE-DIRBE observations of the Earth's resonant ring. In *Unveiling the Cosmic Infrared Background*, AIP Conference Proc. **348,** ed. E. Dwek, (New York: Woodbury), pp. 47–52.

Jayaraman, S., and Dermott, S. F. 1996b. SIRTF: A unique opportunity for probing the zodiacal cloud. In *Physics, Chemistry and Dynamics of Interplanetary Dust*, ASP Conference Series **104,** eds. B. Å. S. Gustafson and M. S. Hanner (San Francisco: Astron. Soc. of the Pacific Press), pp. 159–162.

Jayaraman, S., and Dermott, S. F. 2001. Formation, structure and observations of the Earth's resonant ring. *Icarus*, submitted.

Jewitt, D. 1999. Kuiper Belt objects. *Ann. Rev. Earth Planet. Sci.* **27,** pp. 287–312.

Jones, M. H., and Rowan-Robinson, M. 1993. A physical model for the IRAS zodiacal dust bands. *Mon. Not. R. Astron. Soc.* **264,** pp. 237–247.

Kehoe, T. J. J. 1999. Long term dynamics of small bodies in the Solar System using mapping techniques. Ph.D. thesis, University of London.

Kehoe, T. J. J., Murray, C. D., and Porco, C. C. 2001a. A dissipative mapping technique for the N-body problem incorporating radiation pressure, Poynting-Robertson drag and solar-wind drag. *Astron. J.*, submitted.

Kehoe, T. J. J., Dermott, S. F., and Grogan, K. 2001b. A dissipative mapping technique for integrating interplanetary dust particle orbits. In *Dust in the Solar System and Other Planetary Systems*, ASP Conference Series, eds. J. A. M. McDonnell et al. (San Francisco: Astron. Soc. of the Pacific Press), submitted.

Kelsall, T., Weiland, J. L., Franz, B. A., Reach, W. T., Arendt, R. G., Dwek, E., Freudenreich, H. T., Hauser, M. G., Moseley, S. H., Odegard, N. P., Silverberg, R. F., and Wright E. L. 1998. The COBE diffuse infrared background experiment search for the cosmic infrared background. II. Model of the interplanetary dust cloud. *Astrophys. J.* **508,** pp. 44–73.

Kessler, D. J. 1981. Derivation of the collision probability between orbiting objects: The lifetime of Jupiter's outer moons. *Icarus* **48,** pp. 39–48.

Kortenkamp, S. J., and Dermott, S. F. 1998a. Accretion of interplanetary dust particles by the Earth. *Icarus* **135,** pp. 469–495.

Kortenkamp, S. J., and Dermott, S. F. 1998b. A 100,000 year periodicity in the accretion rate of interplanetary dust. *Science* **280,** pp. 874–876.

Kortenkamp, S. J., Dermott, S. F., Fogle, D., and Grogan, K. 2001. Sources and orbital evolution of interplanetary dust accreted by Earth. In *Accretion of Extraterrestrial Matter Throughout Earth's History*, eds. B. Peucker-Ehrenbrink and B. Schmitz (Dordrecht: Kluwer Acad. Publ.), pp. 13–30.

Leinert, C., and Grün, E. 1990. Interplanetary dust. In *Physics and Chemistry in Space: Physics of the Inner Heliosphere I*, Space and Solar Physics **20,** eds. R. Schween and E. Marsch (Berlin: Springer-Verlag), pp. 207–275.

Liou, J.-C., Dermott, S. F., and Xu, Y.-L. 1995. The contribution of cometary dust to the zodiacal cloud. *Planet. Space Sci.* **43,** pp. 717–722.

Liou, J.-C., and Zook, H. A. 1996. Comets as a source of low eccentricity and low inclination interplanetary dust particles. *Icarus* **123,** pp. 491–502.

Liou, J.-C., Zook, H. A., and Dermott, S. F. 1996. Kuiper Belt dust grains as a source of interplanetary dust particles. *Icarus* **124,** pp. 429–440.

Liou, J.-C., and Zook, H. A. 1999. Signatures of the giant planets imprinted on the Edgeworth-Kuiper Belt dust disk. *Astron. J.* **118,** pp. 580–590.

Liou, J.-C., Zook, H. A., Greaves, J. S., and Holland W. S. 2000. Does planet exist in ε Eridani? A comparison between obervations and numerical simulations. In *31st Annual*

Lunar and Planetary Science Conference, (Houston: Lunar and Planet. Inst.), abstract no. 1416.

Love, S. G., and Brownlee, D. E. 1992. The IRAS dust band contribution to the interplanetary dust complex: Evidence seen at 60 and 100 microns. *Astrophys. J.* **104,** pp. 2236–2242.

Love, S. G., and Brownlee, D. E. 1993. A direct measurement of the terrestrial mass accretion rate of cosmic dust. *Science* **262,** pp. 550–553.

Low, F. J., Beintema, D. A., Gautier, T. N., Gillet, F. C., Beichmann, C. A., Neugebauer, G., Young, E., Aumann, H. H., Boggess, N., Emerson, J. P., Habing, H. J., Hauser, M. G., Houck, J. R., Rowan-Robinson, M., Soifer, B. T., Walker, R. G., and Wesselius, P. R. 1984. Infrared cirrus: New components of the extended infrared emission. *Astrophys. J.* **278,** pp. L19–L22.

Malhotra, R. 1994. A mapping method for the gravitational few-body problem with dissipation. *Celest. Mech. Dynam. Astron.* **60,** pp. 373–385.

Marcantonio, F., Anderson, R. F., Stute, M. S., Kumar, N., Schlosser, P., and Mix, A. 1996. Extraterrestrial ^{3}He as a tracer of marine sediment transport and accumulation. *Nature* **383,** pp. 705–707.

Marsden, B. 1995. Catalogue of cometary orbits. Minor Planet Center, http://cfa-www.harvard.edu/iau/mpc.html.

Marzari, F., and Vanzani, V. 1994. Orbital evolution of dust particles near mean motion resonances with the Earth. *Planet. Space Sci.* **42,** pp. 101–107.

Muller, R. A., and MacDonald, G. J. 1997. Glacial cycles and astronomical forcing. *Science* **277,** pp. 215–218.

Murray, C. D., and Dermott, S. F. 1999. *Solar System Dynamics.* (Cambridge: Cambridge Univ. Press).

Neugebauer, G., Beichman, C. A., Soifer, B. T., Aumann, H. H., Chester, T. J., Gautier, T. N., Gillett, F. C., Hauser, M. G., Houck, J. R., Lonsdale, C. J., Low, F. J., and Young, E. T. 1984. Early results from the infrared astronomical satellite. *Science* **224,** pp. 14–21.

Öpik, E. J. 1951. Collision probabilities with the planets and the distribution of interplanetary matter. *Proc. R. Irish Acad.* **54,** pp. 165–199.

Patterson, D. B., and Farley, K. A. 1998. Extraterrestrial ^{3}He in sea floor sediments: Evidence for correlated 100 kyr periodicity in the accretion rate of interplanetary dust, orbital parameters, and Quaternary climate. *Geochim. Cosmochim. Acta.* **62,** pp. 3669–3682.

Reach, W. T. 1991. Zodiacal emission. II — Dust near ecliptic. *Astrophys. J.* **369,** pp. 529–543.

Reach, W. T. 1992. Zodiacal emission. III — Dust near the asteroid belt. *Astrophys. J.* **392,** pp. 289–299.

Reach, W. T., Franz, B. A., Weiland, J. L., Hauser, M. G., Kelsall, T. N., Wright, E. L., Rawley, G., Stemwedel, S. W., and Spiesman, W. J. 1995. Observational confirmation of a circumsolar dust ring by the COBE satellite. *Nature* **374,** pp. 521–523.

Reach, W. T., Franz, B. A., and Weiland, J. L. 1997. The three-dimensional structure of the zodiacal dust bands. *Icarus* **127,** pp. 461–484.

Rial, J. A. 1999. Pacemaking the ice ages by frequency modulation of Earth's orbital eccentricity. *Science* **285,** pp. 564–568.

Schmidt, H. 1967. The possibility of dust concentration near the Earth. In *The Zodiacal Light and the Interplanetary Medium*, ed. J. L. Weinberg, (Washington DC: NASA SP-150), pp. 333–336.

Standish, E. M., Newhall, X. X., Williams, J. G., and Yeomans, D. K. 1992. Orbital ephemerides of the Sun, Moon, and Planets. In *Explanatory Supplement to the Astronomical Almanac*, ed. P. K. Seidelmann, (Mill Valley: University Science Books), pp. 279–323.

Stern, S. A. 1995. Collisional time scales in the Kuiper Disk and their implications. *Astron. J.* **110,** pp. 856–868.

Stern, S. A., and Colwell, J. E. 1997. Collisional erosion in the primordial Edgeworth-Kuiper Belt and the generation of the 30–50 AU Kuiper Gap. *Astrophys. J.* **490,** pp. 879-882.

Sykes, M. V. 1988. IRAS observations of extended zodiacal structures. *Astrophys. J.* **334,** pp. L55–L58.

Sykes, M. V. 1990. Zodiacal dust bands: Their relation to asteroid families. *Icarus* **84,** pp. 267–289.

Sykes, M. V., and Greenberg, R. 1986. The formation and origin of the IRAS zodiacal dust bands as a consequence of single collisions between asteroids. *Icarus* **65,** pp. 51–69.

Sykes, M. V., and Walker, R. G. 1992. Cometary dust trails. I — Survey. *Icarus* **95,** pp. 180–210.

Telesco, C. M., Fisher, R. S., Piña, R. K., Knacke, R. F., Dermott, S. F., Wyatt, M. C., Grogan, K., Holmes, E. K., Ghez, A. M., Prato, L., Hartmann, L. W., and Jayawardhana, R. 2000. Deep 10 and 18 micron imaging of the HR 4796A circumstellar disk: Transient dust particles and tentative evidence for a brightness asymmetry. *Astrophys. J.* **530,** pp. 329–341.

Wetherill, G. W., and Cox, L. P. 1985. The range of validity of the two-body approximation in models of terrestrial planet accumulation II: Gravitational cross-sections and runaway accretion. *Icarus* **63,** pp. 290–303.

Wisdom, J. 1980. The resonance overlap criterion and the onset of stochastic behavior in the restricted three-body problem. *Astron. J.* **85,** pp. 1122–1133.

Wisdom, J., and Holman, M. 1991. Symplectic maps for the n-body problem. *Astron. J.* **102,** pp. 1528–1538.

Wyatt, S. P., Jr., and Whipple F. L. 1950. The Poynting-Robertson effect on meteor orbits. *Astrophys. J.* **111,** pp. 134–141.

Wyatt, M. C., Dermott, S. F., Grogan, K., and Jayaraman, S. 1999a. A unique view through the Earth's resonant ring. In *Astrophysics with Infrared Surveys: A prelude to SIRTF*, ASP Conference Series **177,** eds. M. D. Bicay, C. A. Beichman, R. M. Cutri and B. F. Madore (San Francisco: Astron. Soc. of the Pacific Press), pp. 374–380.

Wyatt, M. C., Dermott, S. F., Telesco, C. M., Fisher, R. S., Grogan, K., Holmes, E. K., and Piña, R. K. 1999b. How observations of circumstellar disk asymmetries can reveal hidden planets: Pericenter glow and its application to the HR 4796 disk. *Astrophys. J.* **527,** pp. 918–944.

Zappalà, V., Bendjoya, P. H., Cellino, A., Farinella, P., and Froeschle, C. 1995. Asteroid families: Search of a 12,487 asteroid sample using two different clustering techniques. *Icarus* **116,** pp. 291–314.

Zook, H. A., and Berg, O. E. 1975. A source for hyperbolic cosmic dust particles. *Planet. Space Sci.* **23,** pp. 183–203.